

**ELECTRICAL CONDUCTION AND DIELECTRIC BEHAVIOUR OF
THIN FILMS OF VACUUM EVAPORATED AMORPHOUS SILICON,
HYDROGENATED AMORPHOUS SILICON AND CHEMICALLY
DEPOSITED CADMIUM SULPHIDE**

K. RAJEEV KUMAR

**THESIS SUBMITTED TO
COCHIN UNIVERSITY OF SCIENCE AND TECHNOLOGY
FOR THE AWARD OF THE DEGREE OF
DOCTOR OF PHILOSOPHY**

**THIN FILM DIVISION
DEPARTMENT OF PHYSICS
COCHIN UNIVERSITY OF SCIENCE AND TECHNOLOGY
COCHIN - 682 022**

JUNE 1989

DEDICATED TO

MY PARENTS, BROTHER AND SISTER

DECLARATION

I hereby declare that the work presented in this thesis is based on the original work done by me under the guidance of Prof.K.Sathianandan at the Department of Physics, Cochin University of Science and Technology and has not previously formed the basis of any degree, diploma or any other recognition.

Cochin 682 022

20 June 1989




K.RAJEEV KUMAR.

CERTIFICATE

Certified that the work presented in this thesis is based on the bona fide work done by Shri K.Rajeev Kumar, under my guidance at the Department of Physics, Cochin University of Science and Technology and has not been included in any other thesis submitted previously for the award of any degree.

Cochin 682 022

20 June 1989



Dr.K.SATHIANANDAN
Professor of Physics
(Supervising Teacher)

ACKNOWLEDGEMENTS

I express my deep sense of gratitude to Prof. K.Sathianandan for his able guidance and valuable advices throughout the course of my research. His strong will, untiring patience and extremely understanding nature has really been the constant encouraging factor during the ups and downs of my student days in this department.

I thank Prof.K.Babu Joseph, Head of the Department of Physics and all other faculty members for the constant and continued encouragement during the course of this work.

I take this opportunity to express my great appreciation to Dr.K.Mohanachandran, Dr.S.Muraleedharan Pillai, Mr.P.K.Abraham, Mr.M.K.Jayaraj and Mr.R.Navil Kumar for all the help they have rendered during my research period. I also extend my sincere thanks to Dr.T.Ramachandran, Dr.S.Jayalakshmi and Dr.B.Pradeep for their help at various stages of my research. I owe much to the research scholars of the Laser division for the experimental assistances offered to me.

Mr. Boben Thomas has been closely associated with me during the initial stages of my research and has been assisting me in all the fabrications related to the experimental set-up. I take this opportunity to extend my thanks to him.

I acknowledge the immense help rendered by the staff of USIC and the administrative and library staff of the Physics department. I am also thankful to Mr. Sasi and Mr. Peter for the neat typing and binding of the thesis.

Finally, I would like to express my thanks to Prof. K.G. Nair, Head of the Department of Electronics and Prof. K.G. Balakrishnan of the same department for helping me in finding time to complete this work. I also extend my thanks to all my friends in the Electronics department for their encouragements.

Bearing in mind the inadequacy of words, I would like to mention two names--Mr. K.P.B. Moosad and Mr. Babu Anto--just for being around for so many years giving the emotional support.

PREFACE

Ever since the first successful doping of hydrogenated amorphous silicon (a-Si:H) thin films, this material has become a target of intense research. The main impetus for the interest is the possibility of fabricating low cost solar cells for the terrestrial applications. The band gap energy of amorphous silicon (1.6 eV) is well suited for this purpose. Initial investigations by various researchers have shown that this materials is also suitable for the fabrication of other electronic devices such as field effect transistors, photodiodes, image sensing devices etc. However, much of the work carried out in the field of a-Si:H thin films is still concerned with films prepared by glow discharge decomposition of silane. In this thesis preparation of a-Si:H thin films by vacuum evaporation using tungsten baskets is presented and their electrical and dielectric properties are reported.

The thesis is divided into seven chapters. Chapter 1 is the introduction to the subject. It starts with a few remarks on thin film physics followed by a thorough description of the amorphous materials with special reference to amorphous silicon. The two important energy

band models proposed for amorphous materials are also reviewed in this chapter.

In chapter 2 the general methods of thin film preparation along with the merits and demerits of each one are presented. It is followed by the special method adopted in the present study. The hydrogenation procedure employed in the present case is also discussed in detail.

Study on the electrical properties is the single most important tool for characterizing a semiconductor. Hence a detailed investigation on the d.c. and a.c. electrical properties of a-Si and a-Si:H is presented in chapter 3. The effect of different gas environments on the d.c. electrical characteristics of a-Si and a-Si:H thin films are also presented in this chapter.

Dielectric property of a-Si:H films is comparatively less studied. The details of an investigation conducted in this direction are presented in chapter 4.

The feasibility of producing electronic devices from a-Si:H thin films produced by the method adopted here has been tested by fabricating field effect transistors

using europium oxide as the gate insulator. The results are encouraging. An account of the fabrication procedure and analysis of the experimental results are presented in chapter 5.

In chapter 6 preparation and characterization of another semiconductor--cadmium sulphide--is presented. It is prepared by chemical bath deposition method and is characterized by studying the electrical and dielectric properties. From the a.c. conductivity studies the density of states at the Fermi level is calculated. The modifications adopted in the preparation technique enabled to reduce the sulphur deficiency and to prepare intrinsic films.

The concluding remarks and the directions for future work in this field are presented in chapter 7.

LIST OF PUBLICATIONS

1. "Preparation and characterization of amorphous silicon thin films" (16th Optical Society of India Symposium, January 1988).
2. "Studies on the a.c. and d.c. electrical conductivities of hydrogenated amorphous silicon thin films" (National Seminar on Physics and Applications of New Materials, 1988, Calcutta).
3. "Frequency dependence of the dielectric parameters of hydrogenated amorphous silicon thin films" (National Symposium on Crystallography, BHU, Varanasi, 1988).
4. "Switching properties of vacuum evaporated amorphous silicon thin films" (Solid State Symposium, BARC, Bombay, 1987).
5. "Fabrication and characterisation of a MOS field effect transistor using amorphous silicon as the active material" (National Symposium on Electrochemical Materials Science, Karaikudi, 1988).
6. "Effect of adsorbates on the electrical conductivity of amorphous silicon thin films" (XIXth Seminar on Crystallography, Changanacherry, 1987).

7. "Dielectric measurements of CdS prepared by chemical bath deposition" (XVIIIth National Seminar on Crystallography, Jammu, 1986).
8. "Studies on the a.c. and d.c. electrical conduction of hydrogenated amorphous silicon thin films prepared by vacuum evaporation", Indian Journal of Physics, 63A(5) (1989) 500.
9. "Conductivity and dielectric behaviour of cadmium sulphide thin films prepared by chemical bath method" (Communicated).

CONTENTS

	<u>Pages</u>
PREFACE	i
Chapter 1 INTRODUCTION	1
Chapter 2 METHODS OF THIN FILM PREPARATION AND PARAMETER MEASUREMENT TECHNIQUE ..	
Abstract ..	29
2.00 Introduction ..	30
2.10 Physical method ..	30
2.11 Vacuum evaporation ..	31
2.12 Reactive evaporation ..	34
2.13 Co-evaporation ..	35
2.14 Flash evaporation ..	36
2.15 Electron-beam gun evaporation ..	37
2.20 Sputtering ..	38
2.21 Glow discharge sputtering ..	38
2.22 Triode sputtering ..	39
2.23 R.F.sputtering ..	40
2.24 Ion-beam sputtering ..	42
2.25 Reactive sputtering ..	43
2.30 Chemical methods ..	43
2.31 Electrolytic deposition ..	44
2.32 Electroless deposition ..	45
2.33 Anodic oxidation ..	45
2.34 Chemical spray method ..	46
2.35 Chemical vapour deposition ..	46
2.36 Pyrolysis ..	47

		<u>Pages</u>
2.40	Sample preparation followed in the present work ..	47
	2.41 Hydrogenation of a-Si films ..	49
2.50	Measurement set-up ..	54
	2.51 Thickness measurement ..	54
	2.52 Electrical measurements ..	56
	REFERENCES ..	61
Chapter 3	ELECTRICAL CONDUCTION IN AMORPHOUS SILICON AND HYDROGENATED AMORPHOUS SILICON ..	
	Abstract ..	64
3.00	Introduction ..	65
	3.10 D.C.electrical conduction ..	66
	3.11 Theory of d.c.electrical conduction in amorphous semiconductor ..	66
	3.12 D.C.conduction in a typical unhydrogenated amorphous silicon film ..	68
	3.13 Effect of annealing temperature on Al-a-Si-Al planar structures ..	77
	3.14 Effect of annealing time on the electrical conduction in a-Si films ..	88
	3.15 Effect of substrate temperature on the electrical conduction in a-Si films ..	93
	3.16 Thickness dependence of conductivity ..	100
	3.17 Effect of hydrogenation temperature on the electrical properties of hydrogenated amorphous silicon films ..	104
	3.18 Effect of hydrogen partial pressure ..	109

		<u>Pages</u>
3.20	A.C.conduction in a-Si and a-Si:H thin films ..	113
	3.21 Introduction and theory ..	113
	3.22 Experimental ..	122
	3.23 Results and discussion ..	122
3.30	Adsorbate induced conductivity changes..	132
	3.31 Introduction ..	132
	3.32 Experimental ..	135
	3.33 Results and discussion ..	137
	REFERENCES ..	150
Chapter 4	DIELECTRIC PROPERTIES OF a-Si AND a-Si:H THIN FILMS ..	
	Abstract ..	154
4.00	Introduction ..	155
4.10	Theory ..	158
4.20	Experimental ..	162
4.30	Results and discussion ..	163
	4.31 Unhydrogenated amorphous silicon ..	163
	4.32 Hydrogenated amorphous silicon ..	165
4.40	Conclusion ..	176
	REFERENCES ..	178
Chapter 5	FABRICATION AND CHARACTERIZATION OF METAL-OXIDE-SEMICONDUCTOR FIELD EFFECT TRANSISTORS ..	
	Abstract ..	180

			<u>Pages</u>
5.00	Introduction	..	181
5.10	Theory of the conductance modulation by field effect	..	185
5.20	Structure of thin film FETs	..	189
5.30	Experimental	..	191
5.40	Results and discussion	..	193
	REFERENCES	..	209
Chapter 6	CHARACTERIZATION OF CADMIUM SULPHIDE THIN FILMS PREPARED BY CHEMICAL BATH DEPOSITION METHOD	..	
	Abstract	..	212
6.00	Introduction	..	213
6.10	Method of preparation of cadmium sulphide	..	217
6.20	Experimental details and measurement techniques	..	220
6.30	Results and discussion	..	221
	6.31 D.C.conduction		221
	6.32 A.C.conduction	..	224
	6.33 Dielectric measurements	..	228
6.40	Conclusion	..	231
	REFERENCES	..	232
Chapter 7	CONCLUSIONS AND SUGGESTIONS FOR FUTURE RESEARCH	..	236

Chapter 1

INTRODUCTION

The impact of thin film technology on the spectacular developments in the field of microelectronics during the last two decades had been tremendous. This was one of the most stimulating factors which helped the efforts to increase the understanding of thin films and to improve the level of sophistication of their deposition techniques. The recent discovery of the possibility of the production of p-n and p-i-n junctions using hydrogen passivated amorphous silicon thin films, coupled with mass producibility of large area non-epitaxial growth on any substrate material, match very timely with the strong current need for the development of a low cost solar cell as a new energy resource for terrestrial applications. Along with this, the increasing requirement of the optical industry and magnetic information storage devices also boosted the interest in the field of thin films.

A thin film is defined as a thin layer of a material whose one dimension is negligibly small compared to the other two dimensions and is created by the condensation process of atoms or molecules. Depending upon how the atoms or molecules are created from the bulk material for the condensation

process, the methods of depositing thin films are termed physical vapour deposition (PVD) or chemical vapour deposition (CVD) [1]. A brief review of this is given in Chapter 2.

If we go through the early history of thin films, it can be seen that during the ancient periods thin films were used for decorative purposes. Over three centuries back itself non-solid films were studied to explain the interference colours associated with thin oil layers on water surfaces. But the first solid films were obtained by Bunsen and Grove in 1852 by means of chemical reaction and by glow discharge sputtering respectively [2]. In the post war period, it was the boom in the use of silicon based microelectronic devices that gave a respectable position to thin film technology. In a sense we can say that the development of thin films was directly connected with the growth of semiconductor industry. Since the work presented in this thesis is centred around the preparation and characterization of amorphous silicon thin films, it is important to review the developments in this field over the last few decades.

Semiconductors are materials whose electrical resistivity at room temperature is in the range 10^{-2} to 10^9 ohm cm (which is between that of a metal and an insulator) in which the electrical charge concentration increases with increase of temperature over some temperature range [3]. The

important semiconductors are elemental ones like silicon, germanium and selenium and compounds such as gallium arsenide, cuprous oxide, lead telluride and lead sulphide. Semiconductors are of three types according to their structure. They are crystalline, polycrystalline and noncrystalline. A crystalline semiconductor is characterized by the presence of long range periodicity. In other words, in a crystalline semiconductor, the surroundings of an atom will be exactly the same whatever be the position of the atom inside the crystal. This is because the atoms are arranged in an ordered lattice and the order extends throughout the crystal. A polycrystalline material is composed of many very small crystallites. In a noncrystalline material there is only short range order (SRO). That is, the immediate surroundings of an atom will be the same as that in a crystal. But as we go away from the reference atom, the very small deviations in the bond lengths and bond angles become appreciable and at a distance of the order of the tenth neighbour or so, the atoms are located essentially at random. Since noncrystalline semiconductors are predominantly covalently bonded, the lowest energy local configuration of each atom is almost always one in which its chemical valence requirements are fulfilled.

There are two main classes of noncrystalline semiconductors, the glasses and the amorphous films. Glasses are

those materials which can be quenched from the supercooled melt and usually exhibit a glass transition. The melts of most crystalline solids have viscosities less than 1 poise near the melting temperature T_m . Some of these melts can be supercooled by nearly 10-20 degrees below T_m without crystallization. Their viscosity increases rapidly with decreasing temperature [4]. It reaches a value of 10^7 poise near T_m . The viscosity continues to increase with decreasing temperature, and when it becomes 10^{14} poise the supercooled liquid becomes a solid glass. The process of glass transition which leads to the freezing of a supercooled liquid at $T = T_g$ (glass transition temperature) into a noncrystalline solid (glass) is still an actively investigated theoretical problem [5]. Eventhough glasses were known for over thousands of years, the beginning of the systematic study of the noncrystalline materials started only in 1950's when Kolomiets showed that the chalcogenide glasses behave like intrinsic semiconductors and that their electrical conductivity could not be altered by adding dopants [6].

Usually the term amorphous materials are restricted to those noncrystalline materials which can normally be prepared only in the form of thin films by deposition on substrates which are kept sufficiently cool to prevent crystallization. Amorphous films, in contrast to glasses, can exist in many different configurational states depending upon the

preparation techniques and upon a variety of substrate parameters. Annealing can lower the energy of a given amorphous film.

Although many defects common in crystalline solids like vacancies, interstitials, dislocations and grain boundaries are not likely to be found in the absence of periodicity, chemical defects such as undercoordinated or overcoordinated atoms and wrong bonds are quite possible. All glasses have intrinsic defects defined as the deviations from the lowest energy bonding arrangements [7,8]. Of all possible deviations from the ideal bonding configuration, the one that requires the least amount of energy will naturally be present at the highest concentration. The least energy requiring defects in chalcogenide glasses are the valence-alternation pairs (VAP). VAPs are two defects simultaneously created, one due to a positively charged overcoordinated atom and the other due to a negatively charged undercoordinated atom. They are known as VAPs because the valence or coordination is altered for the defect atoms. This never happens in a tetrahedrally bonded solid, since four is the maximum possible covalent coordination using 's' and 'p' orbitals. However large defect densities can exist in this material in the form of two fold and three fold coordinated atoms.

Experimental data on electrical transport properties can only be properly interpreted if a model for the electronic structure is available. For crystalline semiconductors, the main features of the energy distribution of the density of electronic states are the sharp structure in the valence and conduction bands and the abrupt terminations at the valence band maximum and the conduction band minimum. The sharp edges in the density of states produce a well defined forbidden energy gap. These specific features of the band structure are consequences of the long range and short range order. Since the short range order is present, the concept of the density of states is applicable to noncrystalline solids also.

In 1970 Mott argued that the spatial fluctuations in the potential caused by the configurational disorder in amorphous materials can create localized states in the form of a tail above and below the normal bands [10]. This argument was based on a theory by Anderson [11]. The states are called localized in the sense that an electron placed in a region will not diffuse at zero temperature to other regions with corresponding potential fluctuations.

Two most important band models for amorphous semiconductors are due to Cohen, Fritzsche and Ovshinsky (CFO model) and Davis and Mott [12,13]. The former describes a

simple band model based on the common features of the covalent amorphous alloys. It assumes that the tail states extend across the gap in a structureless distribution. This gradual decrease of the localized states destroys the sharpness of the conduction and valence band edges. The tails overlap at the centre. CFO model was specifically proposed for the multi-component chalcogenide glasses. Since in these materials, most atoms satisfy their valence requirements, there must be a valence band of extended states despite the randomly differing valencies and an energy band corresponding roughly to an energy for breaking valence bonds. However there will be mobility edges above and below the valence and conduction bands. At these mobility edges the mobility of the charge carriers change abruptly. The empty valence band tail states give rise to a random distribution of localized positive charges neutralized on the average by a corresponding distribution of an equal number of localized negative charges which are associated with the occupied conduction band tail states. These charged states above and below the Fermi level (E_F) act as efficient trapping centres for electrons and holes respectively. If we consider that the transition from the extended states to the localized states occur at energies E_v for the valence band and E_c for the conduction band, then we can expect a sharp drop in the mobility of the carriers at these energies as we pass from the extended states to the

localized states. The presence of the mobility edges explain why a well defined activation energy (ΔE) is observed for conductivity (σ) despite the lack of sharp band edges.

According to Davis and Mott model, the tails of localized states should be rather narrow and should extend a few tenths of an electron volt into the forbidden gap. Generated due to the defects in the random network, like dangling bonds and vacancies, a band of compensated levels exist near the mid gap according to this model. This band may be split into a donor and an acceptor band which will also pin the Fermi level. Mott suggested that at the transition from extended to localized states the mobility drops by several orders of magnitude producing a mobility edge. The energy interval between the two mobility edges acts as a pseudogap and is defined as the mobility gap.

The first proposal of a model showing bands of donors and acceptors in the upper and lower half of the mobility gap was introduced by Marshall and Owen in 1971 [14]. It is clear now that the density of states of an amorphous semiconductor does not decrease monotonically into the gap, but shows many peaks which can be well separated from each other. The position of the Fermi level is largely determined by the charge distribution in the gap states.

On the basis of Davis-Mott model there can be three processes leading to conduction in amorphous semiconductors. Their relative contribution depends upon the ambient temperature. At very low temperatures, conduction can occur by thermally assisted tunnelling between states at the Fermi level. At higher temperatures, charge carriers are excited into the localized states of the band tails. This conduction is by hopping. At still higher temperatures, carriers are excited across the mobility edge into the extended states. The mobility in the extended states is much higher than that in the localized states.

Now let us go a bit deep into the problem of amorphous silicon. Since the material has only one component, there is no question of compositional disorder. In amorphous silicon almost every atom is surrounded by four neighbouring atoms 2.35 \AA away, exactly the same atomic separation as in the crystal. Even the second neighbours are essentially at the same distance as in the crystal, but there is a spread in the separations which reflect bond-angle deviations of about $\pm 10^\circ$ [4]. This spread becomes more and more significant as we go away from the reference atom and the order is lost roughly at the distance of the tenth neighbour. Thus in pure amorphous silicon, strictly speaking, there is a short range order only upto about 5 \AA [5]. It is known that properties

of solids on an atomic scale whether crystalline or amorphous should be dominated by local chemical valence considerations as in the chemistry of molecules [13]. However, specifications of the short range order does not fully determine the structure of an amorphous semiconductor. One must also determine the distribution of ring sizes which can have important consequences on electronic states [14]. Ideal geometrical model of amorphous silicon historically is divided into two classes: microcrystalline and random network [15]. In the microcrystalline model, regions of crystalline-like order are connected by disordered boundaries, while in the random network model, there are no regions of crystalline order. For microcrystallites smaller than a few lattice constants in size, the structure is essentially a random network.

There are experimental evidences for the existence of large concentrations of spinless defects in amorphous silicon films. The observed spin density is almost always several orders of magnitude lower than the density of localized states in the gap [6]. When atomic hydrogen is introduced into pure silicon films, approximately hundred times as much hydrogen enters than the unpaired spin density suggests [7]. These unpaired silicon bonds are the most important defects in amorphous silicon films. They are also known as the dangling bonds. They occur with a density of 10^{18} - 10^{20} per c.c. in nominally pure amorphous silicon. The higher

concentrations occur in sputtered, evaporated, or ion-bombarded layers that are prepared below 200-300°C. Higher temperature deposits, most notably chemical vapour depositions by the pyrolysis of silane near 600°C, have spin densities at the lower end of the observed range. This is because in this case the unpaired silicon bonds are passivated by hydrogen atoms. For the point of illustrating the microscopics of hydrogenation, it is enough to consider the idealized planar representation of a trivacancy as shown in Figure 1.10. When the material is hydrogenated not only the dangling bonds but the adjacent back bonds are also likely to pick-up H atoms, since they tend to be weaker than the typical Si-Si bonds within an ideal Si network. It is seen that many hydrogen atoms can be incorporated in the vicinity of a single paramagnetic defect. A paramagnetic site is composed of two aligned but unpaired bonds. In fact hydrogen can also be taken up by the nonparamagnetic multivacancies as well. It therefore explains why more hydrogen atoms are present in hydrogenated amorphous silicon than the number of paramagnetic centres in pure amorphous silicon [8]. Furthermore, due to the nature of the disorder itself there can be other weak bonds (Si-Si bonds with bond lengths other than the ideal 2.35 Å) within the random network and these bonds may also be easily broken apart and then terminated by hydrogen atoms [9].

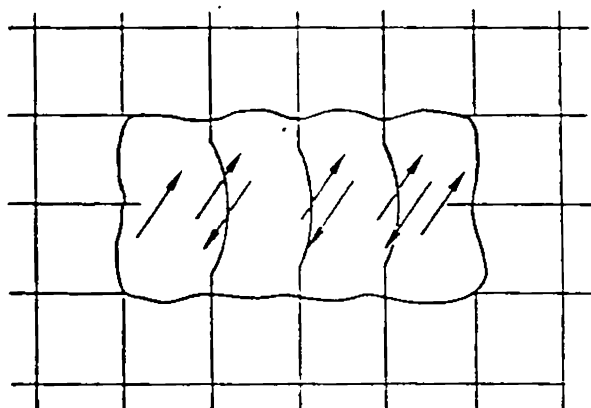
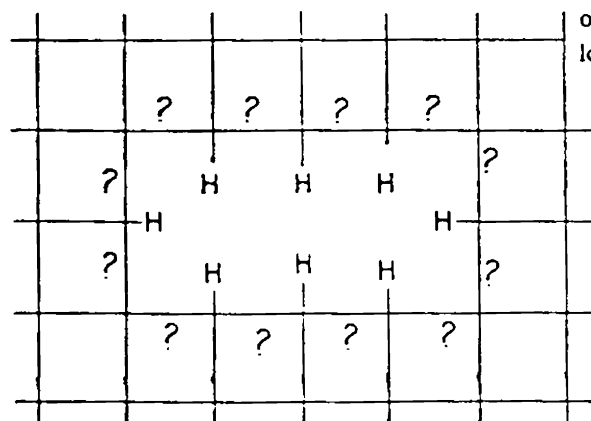


Fig.1.10

Idealized planar representation
of a tri-vacancy: upper) In pure Si.
lower) In hydrogenated Si.



Early theoretical work suggested that the addition of hydrogen to the amorphous silicon matrix would remove states from the top of the valence band [16]. In the case of crystalline silicon it was observed that electronic energy levels of the dangling and weak bonds lie within the band gap. Hydrogenation of crystalline silicon surfaces removes gap states and replaces them with Si-H bonding levels deep down in the valence band and antibonding levels in or near the conduction band [8]. Thus the effect of hydrogenation of amorphous silicon is the removal of states from within the band gap [10]. Early theoretical work suggested that the addition of hydrogen to the amorphous silicon matrix would remove states from the top of the valence band [16]. This work suggested that the observed widening of the gap with increasing hydrogen content occurs primarily by depletion of states from the valence band edge [17-19]. The Si-H energy levels lie away from the band gap and hence do not interfere with the near band gap transport and optical phenomena which are of prime importance to the semiconductor physicists.

It was Sterling and his collaborators at the S.T.L. Laboratories who first prepared thin films of amorphous silicon and amorphous germanium by the decomposition of the hydride in an r.f. glow discharge in the mid sixties [28-30]. Towards the end of 1968 a group at the University of Dundee

in U.K. started working in amorphous semiconductors [31]. Their aim was to provide some reasonably conclusive experimental tests of the proposed models and transport mechanisms. In the early stages of their work they found that thin films of amorphous silicon and amorphous germanium produced by the glow discharge technique were the most promising ones in which the basic properties of the amorphous phase were not obscured by a high density of defect states. In 1970 they published the first electron drift mobility results on glow discharge a-Si [31]. The first experimental information on the density of states in the energy gap was published by Spear and LeComber in 1972 [32]. During 1973 and 1974 a fairly detailed study of the optical and photoconductive properties of glow discharge produced silicon was carried out at Dundee, in which it was attempted to correlate the photoconductive behaviour with transport results and the density of state distribution [33,34].

In 1975 LeComber and Spear showed that the electronic properties of a-Si and a-Ge prepared by the glow discharge method could be controlled by substitutional doping in a systematic way over a wide range [35,36]. This was a remarkable step forward in the development of a-Si and it was quickly followed by the fabrication of the first a-Si p-n junction [37]. Soon after this, development of a-Si photovoltaic

devices was reported from the RCA laboratories [38]. This caused an explosion in the number of research papers coming out on the preparation and characterization of a-Si:H thin films and solar cells. Most of the research groups concentrated on the glow discharge method of film production while a relatively few groups worked on sputtered and evaporated amorphous silicon in an atmosphere of hydrogen [39,40]. It was soon established that post hydrogenated amorphous silicon films have certain advantages over the conventional glow discharge produced ones. They are the absence of the so called Staebler-Wronski effect (which is a light induced instability), reduction in the amount of hydrogen going into the interstitial positions and the better control over the amount of hydrogen incorporated into the film [41-43]. However, this method is the least investigated one. This is probably due to the early success of the glow discharge method.

During the past decade considerable efforts have been expended in attempts to characterize and understand the electronic properties of amorphous silicon films. Electrical conductivity studies are very important among them. The d.c. electrical characteristic of a-Si and a-Si:H films are carried out by many groups of researchers [44-49]. Due to Si-H bond formation the electrical conductivity and the density of gap states decreases. Also, due to hydrogenation, the Fermi level

shifts towards the conduction band and the extended state conduction becomes dominant at room temperature [43].

Just like the d.c. conductivity, the frequency dependent conductivity (a.c. conductivity) is also an important parameter to characterize an amorphous material. Under favourable circumstances the a.c. conductivity studies can be used to make an estimation of the density of states of amorphous materials [50-52]. Many reports have appeared on the a.c. conductivity of different amorphous materials [53-56] but that of a-Si:H is extremely rare. Mott [52] has shown that all the three conduction mechanisms that contribute to the d.c. conduction can contribute to the a.c. conduction also. They are the conduction through the extended states, conduction by carriers excited into the localized states at the edges of the valence or conduction band and hopping transport by carriers with energies near the Fermi level.

The change in the d.c. conductivity of a-Si and a-Si:H thin films due to exposure to different gas ambients is a rarely investigated but nevertheless a very important study. It gives information on the conductivity type of the film. This study also gives an explanation to the inconsistencies in the reported values of various electrical parameters of a-Si:H films prepared in different laboratories. Tanielian et al. have carried out such an investigation on a-Si:H thin

films prepared by glow discharge [57] and have found that different gas ambients have profound effects on the electrical characteristics of these films.

Due to these reasons a systematic study was carried out on the d.c. and a.c. electrical properties of a-Si and a-Si:H films prepared by vacuum evaporation. It was observed that various preparation parameters like substrate temperature, annealing temperature, annealing time, film thickness, hydrogenation temperature and hydrogen partial pressure play very important roles in shaping the electrical characteristics of these films.

The first major application of amorphous semiconductors was in the field of Xerography. This process utilizes the photoconductivity of certain high resistivity amorphous semiconductors containing selenium. The photoconductive properties of chalcogenide glasses are used in an image pick up tube known as saticon developed by Hitachi and the Japan Broadcasting Corporation for use in small colour television cameras [58]. Memory switching has been observed in many amorphous semiconductors including a-Si:H [59]. This phenomenon is used by many companies for developing an electrically alterable, read-only computer memory. Hydrogenated amorphous silicon films are widely used in the fabrication

of photoconductivity cells. These cells are used as light sensing elements in certain types of light meters and light activated switches. It is found that rectifying junctions could be fabricated by sputtering amorphous silicon into crystalline silicon substrates [60]. In certain cases when such a a-Si:H diode is forward biased, it emits light due to electroluminescence [61] with a peak photon energy of $\sim 1.2-1.3$ eV. However, as discussed earlier, the most important application of a-Si:H has been in the low cost solar cells [62]. Band gap of a-Si:H is ideal for solar energy conversion. Another very important application of amorphous silicon is in the fabrication of thin film field effect transistors. In 1976 itself there were proposals for the use of amorphous silicon field effect devices in the addressing of liquid crystal matrix displays as an alternative to thin film CdSe transistors. It was Neudeck and Malhotra [63] who have first fabricated thin film field effect transistors using evaporated amorphous silicon. They have made use of thermally grown SiO_2 as the gate insulator and photolithography techniques to define the shape of the aluminium source and drain electrodes. At present the main application of amorphous silicon FETs is in the liquid crystal display devices. The transient behaviour of an FET in the liquid crystal matrix is mainly determined by the capacitive loading of the liquid crystal element. It is possible, even with the present amorphous silicon

devices, to address about 1000 lines in 40 ms which is the charge retention time of the elementary liquid crystal capacitor in the off state of the FET. Recently it was shown that an integrated inverter circuit [64] and an image sensor [65] can be fabricated from amorphous silicon FETs. It is also reported that the fabrication of NAND and NOR gates is also possible with amorphous silicon FETs. The main limitation of the present devices is their low value of gain-bandwidth product. Attempts to improve this are carried out by many research groups.

In order to check whether the vacuum evaporated and post hydrogenated amorphous silicon films prepared in the present case can be used to fabricate electronic devices, elementary field effect transistors were fabricated in the coplanar structure and is discussed in detail in this thesis. The experiment was reasonably successful and indicated that optimization of preparation parameters and film thickness would yield better devices.

If a-Si:H is a new comer in the field of electronic materials, cadmium sulphide is one of the oldest and extensively investigated semiconducting materials. Relatively early in the research of photovoltaic effect and the development of solar cells, II-VI compounds have played an important role. Almost at the same time as the silicon solar cells were first

described [66], the photovoltaic effect in CdS/Cu₂S was reported [67]. A variety of II-VI based solar cells are known and actively investigated. It can be seen that the most prominently researched II-VI based solar cells are CdS/Cu₂S cells, CdS/CuInSe₂ cells or those with Cd_xZn_{1-x}S. A large number of techniques are employed for the deposition of CdS films, prominent among them are evaporation, spray pyrolysis and screen printing. Each of these methods has its own advantages and disadvantages [68-70]. Technologists are therefore on the lookout for newer methods in order to tailor the properties of the films to suit their needs. Of the several methods available, chemical methods have certain advantages for the fabrication of CdS thin films, since they are cheaper and easier compared with the physical methods. These very reasons will give chemical methods an upper hand in the future, at least as far as solar cells are concerned, if large scale manufacturing of thin film solar cells is to be a reality for terrestrial applications. Eventhough the structure, d.c. conduction, photoconduction and photovoltaic effects of this material are well studied [68,70-73], its a.c. conduction mechanisms and dielectric properties are not so extensively investigated. Even, parameters which are well studied should be subjected to reinvestigation when the film is produced by a new method or by a modified form of one of the well known methods. Elliott's theory [51] is ideal for interpreting

the results of the a.c. conduction experiments in CdS, since the theory is originally developed for II-VI compounds. It can be used to calculate the density of states of CdS at the Fermi level which is a very important parameter for any semiconductor.

In this thesis the d.c. and a.c. electrical characteristics and dielectric properties of CdS thin films prepared by chemical bath deposition technique are presented. By slightly modifying the preparation method it was found possible to decrease the sulphur deficiency and as a result nearly intrinsic films were obtained.

The investigation presented in this thesis therefore covers detailed studies on the dielectric properties and a.c./d.c. conduction of a-Si and a-Si:H thin films prepared by vacuum evaporation. The influence of the various gas ambients has also been investigated in detail. Using these films a field effect transistor is fabricated and characterized. In the case of CdS, by modifying slightly the chemical bath deposition method, very nearly intrinsic films were obtained and characterized. These investigations in general results in obtaining important informations.

REFERENCES

1. K.L.Chopra and S.R.Das, "Thin Film Solar Cells", Plenum Press, New York (1983) 7.
2. K.L.Chopra, "Thin Film Phenomena", Robert E.Krieger Publishing Co., New York (1979) 1.
3. Leo A.Aroian et al. "Van Nostrand Scientific Encyclopedia", D.Van Nostrand Co.Inc., Princeton (1968) 1598.
4. J.P.deNeufville and H.K.Rockstad, "Amorphous and Liquid Semiconductors", J.Stuke and W.Brenig (Ed.), Taylor and Francis, London (1974) 419.
5. M.H.Cohen and G.S.Grest, Phys.Rev.B. 20 (1979) 1077.
6. B.T.Kolomiets, "Proc.Intl.Conf.on Semiconductor Physics", Prague (1960) 884.
7. M.Kastner, D.Adler and H.Fritzsche, Phys.Rev.Lett., 37 (1976) 1504.
8. M.Kastner and H.Fritzsche, Phil.Mag.B. 37 (1978) 199.
9. W.E.Spear, "Amorphous and Liquid Semiconductors", J.Stuke and W.Brenig (Ed.), Taylor and Francis, London (1974) 1.
10. N.F.Mott, Phil.Mag. 22 (1970) 7.

11. P.W.Anderson, Phys.Rev., 109 (1958) 1492.
12. Morrel H.Cohen, H.Fritzsche and S.R.Ovshinsky, Phys.Rev. Lett., 22 (1969) 1065.
13. E.A.Davis and N.F.Mott, Phil.Mag., 22 (1970) 903.
14. J.N.Marshall and E.A.Owen, Phil.Mag., 24 (1971) 1281.
15. S.C.Moss and J.F.Graczyk, "Proc. Tenth Inter.Conf. on Phys. of Semicond.", USA, E.C., Washington (1979) 658.
16. David Adler, "Fundamental Physics of Amorphous Semiconductors", F.Yonezawa (Ed.), Springer-Verlag, New York (1981) 15.
17. F.Yonezawa and M.H.Cohen, "Fundamental Physics of Amorphous Semiconductors", F.Yonezawa (Ed.), Springer-Verlag, New York (1981) 71.
18. J.D.Joannopoulos and M.H. Cohen, Solid State Phys., 31 (1976) 71.
19. G.Lukovsky and T.M.Hayes, 'Amorphous Semiconductors', "Topics in Applied Physics", Vol.36, M.H.Brodsky (Ed.), Springer-Verlag, New York (1981) 215.
20. N.Sol, D.Kaplan, D.Dieumegard and D.Dubreuil, J.Non-Cryst. Solids, 35/36 (1980) 291.

21. W.Y.Ching, D.J.Lam and S.C.Lin, *Phys.Rev.Lett.*, **42** (1979) 805.
22. M.H.Brodsky and D.Kaplan, *J.Non-Cryst.Solids*, **32** (1979) 431.
23. J.D.Joannopoulos, *J.Non-Cryst.Solids*, **32** (1979) 241.
24. M.H.Brodsky, R.S.Title, K.Weiser and G.D.Pittit, *Phys.Rev.B.* **1** (1970) 2632.
25. D.J.Chadi, *Phys.Rev.Lett.*, **41** (1978) 1062.
26. D.J.Chadi, *J.Vac.Sci.Technol.*, **16** (1979) 1290.
27. J.D.Joannopoulos, *J.Non-Cryst.Solids*, **32** (1979) 241.
28. H.F.Sterling, R.C.G.Swan, *Solid State Electron.*, **8** (1965) 653.
29. R.C.Chittie, J.H.Alexander and H.F.Sterling, *J.Electrochem. Soc.*, **116** (1969) 77.
30. R.C.Chittie, *J.Non-Cryst.Solids*, **3** (1970) 255.
31. P.G.LeComber and W.E.Spear, *Phys.Rev.Lett.*, **25** (1970) 509.
32. W.E.Spear and P.G.LeComber, *J.Non-Cryst.Solids*, **8-10** (1972) 727.

33. R.J.Loveland, W.E.Spear and A.Al-Sharbaty, *J.Non-Cryst.Solids*, 13 (1973/74) 55.
34. W.E.Spear, R.J.Loveland and A.Al-Sharbaty, *J.Non-Cryst. Solids*, 15 (1974) 410.
35. W.E.Spear and P.G.LeComber, *Solid State Commun.*, 17 (1975) 1193.
36. W.E.Spear and P.G.LeComber, *Phil.Mag.*, 33 (1976) 935.
37. W.E.Spear, P.G.LeComber, S.Kinmond and M.H.Brodsky, *Appl.Phys. Lett.*, 28 (1976) 105.
38. D.E.Carlson and C.R.Wronski, *Appl.Phys.Lett.*, 29 (1976) 602.
39. Akio Hiraki, Yoshito Fukushima, Takeshi Sato, Hideki Kiyono, Hitoshi Terauchi and Takeshi Imura, *J.Non-Cryst.Solids*, 59 & 60 (1989) 791.
40. B.Y.Tong, P.K.John, S.K.Wong and K.P.Chik, *Appl.Phys.Lett.*, 38 (1981) 789.
41. P.K.John, S.K.Wong, P.K.Gogna, B.Y.Tong and K.P.Chik, *Journal de Physique*, 34 (1981) C4.
42. T.Nakashita, M.Hirose and Y.Osaka, *Jpn.J.Appl.Phys.*, 23 (1984) 146.

43. Toshio Nakashita, Kenji Kohno, Takeshi Imura and Yukio Osaka, *Jpn.J.Appl.Phys.*, 23 (1984) 1547.
44. David Emin, "Polycrystalline and Amorphous Thin Films and Devices", Lawrence L.Kazmerski (Ed.), Academic Press, New York (1980) 17.
45. M.J.Thompson, "Topics in Applied Physics, Hydrogenated Amorphous Silicon 1", Vol.55, J.D.Joannopoulos and G.Lucovsky (Ed.), Springer-Verlag, Berlin (1984) 161.
46. P.Dellafera, R.Labusch and H.H.Roscher, *Phil.Mag.B*, 45 (1982) 607.
47. G.Muller, H.Mannsperger and S.Kalbitzer, *Phil.Mag.B*, 53 (1986) 257.
48. Motoharu Yamazaki, Hideki Ohagi, Jun-ichi-Nakata, Shozo Imao, Junji Shirafuji, Keiji Fujibayashi and Yoshio Inuishi, *Jpn.J.Appl.Phys.*, 27 (1988) L1739.
49. J.C.Delgado, J.Andreu, G.Sardin, J.Esteve and J.L.Morenza, *Appl.Phys.A*, 46 (1988) 207.
50. M.Pollak, *Phil.Mag.*, 23 (1971) 519.
51. S.R.Elliott, *Phil.Mag.*, 36 (1977) 1291.
52. N.F.Mott and E.A.Davis, "Electronic Processes in Non-Crystalline Materials", Clarendon Press, Oxford (1971) 211.

53. A.E.Owen and J.M.Robertson, *J.Non-Cryst.Solids*, **2** (1970) 40.
54. H.K.Rockstad, *J.Non-Cryst.Solids*, **2** (1970) 192.
55. S.K.Bahl and K.L.Chopra, *J.Appl.Phys.*, **41** (1970) 2196.
56. G.S.Linsley, A.E.Owen and F.M.Hatyatee, *J.Non-Cryst.Solids*, **4** (1970) 208.
57. M.Tanielian, H.Fritzsche, C.C.Tsai and E.Symbalisky, *Appl. Phys.Lett.*, **33(4)** (1978) 353.
58. N.Goto, Y.Isozaki, K.Shidara, E.Maruyama, T.Hirai and T.Fujita, *IEEE Trans.Electron Devices*, **ED-21** (1974) 662.
59. S.R.Ovshinsky, *Phys.Rev.Lett.*, **21** (1968) 1450.
60. L.Mei and J.E.Greene, *J.Vac.Sci.Technol.*, **11** (1974) 145.
61. J.I.Pankove and D.E.Carlson, *Appl.Phys.Lett.*, **29** (1976) 620.
62. D.E.Carlson and C.R.Wronski, *Appl.Phys.Lett.*, **28** (1976) 671.
63. G.W.Neudeck and A.K.Malhotra, *Solid State Electron.*, **19** (1976) 721.

64. M.Matsumura and H.Hayama, Proc. IEEE, 68 (1980) 1349.
65. M.Matsumura, H.Hayama, Y.Nara and K.Ishibashi, IEEE EDL 1 (1980) 182.
66. P.Rappoport, Phys.Rev., 93 (1954) 246.
67. D.C.Reynolds, G.Leies, L.L.Antes and R.E.Marburger, Phys.Rev., 96 (1956) 533.
68. K.L.Chopra and S.R.Das, "Thin Film Solar Cells", Plenum Press, New York (1983).
69. H.Iwanaga and T.Yoshiie, Solid State Phys.(Japan), 18 (1983) 265.
70. N.R.Pavaskar, C.A.Menezes and A.P.B.Sinha, J.Electrochem. Soc., 24 (1977) 249.
71. G.Berote, D.Cossement, E.Orben de Xevry and J.M.Streydio, Conf.Record of the 16th IEEE Photovoltaic Specialists Conference, 1982, San Diego, CA, USA, 27-30 Sept. 1982, 872.
72. V.A.Shalpak, Sov.Phys-Semicond.(USA), 16 (1982) 785.
73. E.Vateva and D.Nesheva, J.Non-Cryst.Solids, 51 (1982) 381.

Chapter 2

METHODS OF THIN FILM PREPARATION AND PARAMETER MEASUREMENT TECHNIQUE

Abstract

A brief account of the several methods used for the production of thin films is presented in this Chapter. The discussions stress on the important methods used for the fabrication of a-Si:H thin films. This review also reveals that almost all the general methods, like vacuum evaporation, sputtering, glow discharge and even chemical methods are currently employed for the production of a-Si:H thin films. Each method has its own advantages and disadvantages. However, certain methods are generally preferred. Subsequently a detailed account of the method used here for the preparation of amorphous silicon thin films and their hydrogenation is presented. The metal chamber used for the electrical and dielectric measurements is also described. A brief mention is made on the electrode structure, film area and film geometry.

2.00 Introduction

The electronic properties of a semiconducting thin film depend largely upon the method of preparation. There are a large number of methods for thin film preparation. They can be broadly classified into physical and chemical methods. Physical methods include vacuum evaporation, sputtering and glow discharge while chemical methods normally cover electro deposition and chemical vapour deposition. Each of these deposition techniques is discussed briefly in the following with special reference to the preparation of hydrogenated amorphous silicon.

2.10 Physical method

Physical method of thin film preparation is the most widely used for industrial applications. Be it electronic, optical, opto-electronic or protective application, physical method is preferred over other techniques of thin film preparation. The reasons for this are the following. In the industrial production of low cost solar cells or electronic devices, production on a continuous basis is more easily accomplished by physical methods. Fabrication of multilayer structures like interference filters and multilayer antireflection coatings are easier by physical methods. In the physical methods, since all the coatings are done in a high vacuum or ultra high vacuum chamber, very clean production environment can be maintained. Such controlled conditions are very much essential

in the fabrication of electronic devices. Finally, physical deposition is a 'clean method' of film preparation, in the sense that no chemical solutions are used.

2.11 Vacuum evaporation

The deposition of thin films by vacuum evaporation involves several steps [1] and they are broadly brought under three as follows:-

1. Transition of condensed phase into a gaseous state.
2. Vapour traversing the space between the evaporation source and the substrate at reduced gas pressure and
3. Condensation of the vapour at reduced gas pressure on the substrate.

For evaporating most materials, the temperature of the source must be between 1000 and 2000°C [1]. To avoid contamination of the deposit, the filament material itself must have negligible vapour and dissociation pressures at the operating temperature. Suitable materials are refractory metals and oxides. There must not be any alloying or chemical reaction between the evaporant and the source material [2,3]. In order to evaporate a material from a filament, the following conditions must be fulfilled.

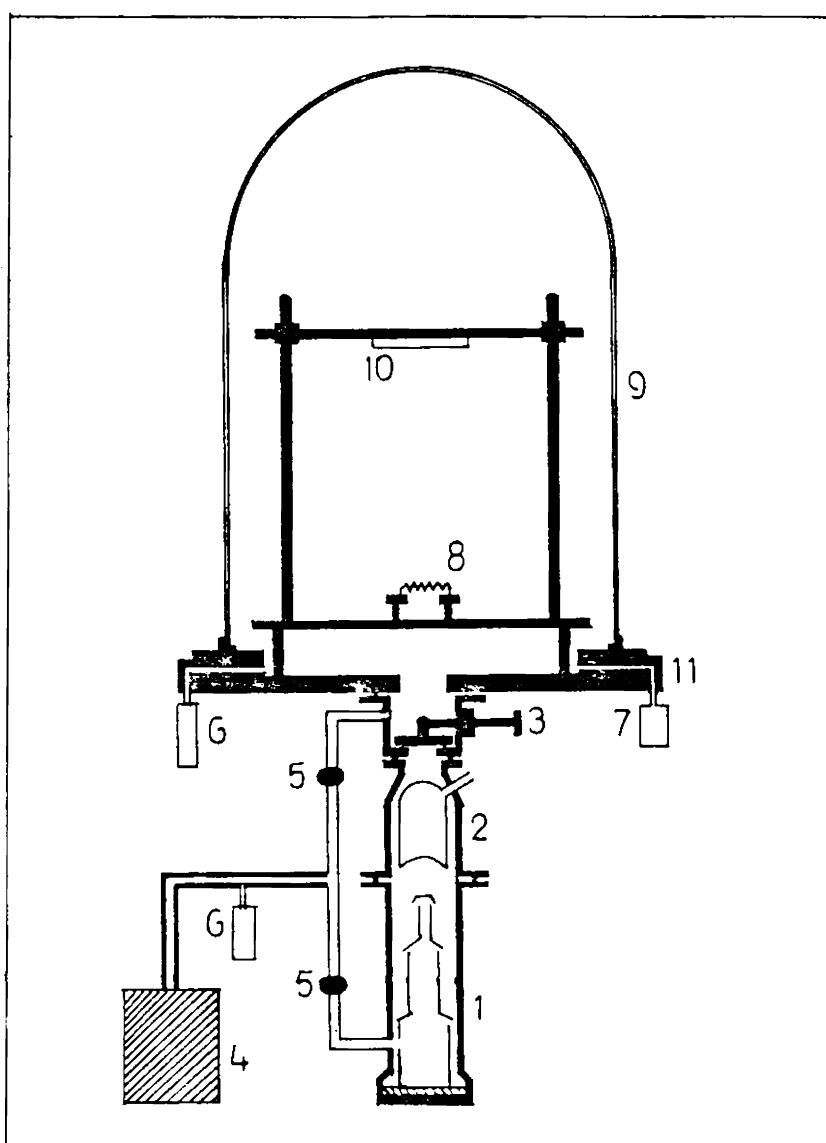
1. The material must adhere to the filament.
2. The melting point of the filament must be higher than that of the evaporant.
3. The filament and the evaporant must not form an alloy which has a melting point below that of the evaporant.

The alloy formation and filament failure will be more rapid if the evaporant is allowed to accumulate into isolated droplets over the heater surface. It was shown that a molten evaporant which wets refractory metal spirals could be made to flow as a uniform coating over the surface of the heater provided several strands of the wire twisted together are used instead of a single core spiral. Such sources have a maximum value of molecular radiation to heat radiation.

Schematic diagram of a vacuum coating system is shown in Figure 2.10. It consists of a bell jar evacuated using a diffusion pump and a rotary pump. The sizes of the pumps in the pumping line affect the pump down time, the steady state throughput and the ultimate pressure. In a system designed for evaporation, estimation of the throughput in advance is very difficult. It depends on many factors like purity of the material, outgassing, evaporation rate, the filament design, and the maximum permissible pressure rise during film formation.

Fig.2.10

Schematic diagram of a vacuum coating system



- | | |
|-----------------------|-------------------------|
| 1. Diffusion pump | 2. Liquid nitrogen trap |
| 3. Baffle valve | 4. Rotary pump |
| 5. Diaphragm valve | 6. Pirani gauge head |
| 7. Penning gauge head | 8. Tungsten filament |
| 9. Glass bell jar | 10. Substrate |
| 11. Base plate | |

However, the outgassing and leak rates play important roles in achieving the ultimate pressure.

Depending upon the materials to be deposited, different modifications are adopted in the vacuum evaporation technique and these are summarised in the following sections.

2.12 Reactive evaporation

For the deposition of metal and elemental semiconductor films, the background pressure is usually kept as low as possible, because the interaction of residual gases with the evaporant has adverse effects on the film properties [4]. In reactive evaporation, gases like oxygen or hydrogen at high pressure (10^{-5} to 10^{-2} torr) are deliberately maintained to produce fully oxidized or hydrogenated films. A controlled leak of the required gas is generally used to provide the desired atmosphere. Since the mean free path of vapours is very large at lower pressures, the probability of forming metal-oxide molecules by collision in the gas phase is very small. Instead, recombination takes place on the substrate surface. The formation of the oxide film by reactive evaporation begins with the impingement of metal atoms and oxygen molecules on the substrate surface. Some of these are adsorbed. The adsorbed vapours must then react to form the metal oxide. This reaction is essentially an ordering process, whereby an adsorbed particle

diffuses across the surface until they fall into the potential wells represented by the regular lattice sites [1]. The reactive evaporation of metals or lower metal oxides into substrates at moderate temperatures produces amorphous or poorly crystallized films whose stoichiometry is largely determined by the impingement rates of the constituents [5].

It had been shown by several workers that the dangling bonds in amorphous germanium and amorphous silicon could be saturated by depositing them in an atmosphere of hydrogen [6]. Hydrogen prevents the formation of dangling bonds as these provide favourable bonding sites for hydrogen atoms. The removal of the dangling bond states by hydrogen is manifested in the drastic reduction in the spin density and in the possibility of substitutional doping [7]. The increase in photoconductivity and the shift in the optical absorption edge to higher energies also demonstrate the removal of the dangling bond [8-14].

2.13 Co-evaporation

By operating two evaporation sources simultaneously in the same vacuum chamber, it is possible to deposit multi-constituent films which are not amenable to direct evaporation [1]. This method eliminates problems like fractionation and decomposition inherent in the evaporation of compound semi-

conductors. It is also possible to co-deposit materials which form neither compounds nor solid solutions. The control of the condensation rates in the exact constituent ratio is the main problem in co-evaporation. These rates are determined by the equilibrium pressure of the evaporant at the same temperature. The film composition can be controlled by direct measurements of the particle density in the vapour stream. The source temperatures can be adjusted to get pre-determined condensation rates. The problem of preferential condensation of compounds from binary vapours has been solved by developing three temperature method. This method exploits the fact that the free energies required for the dissociation of compounds are greater than the free energies of evaporation of the constituents.

2.14 Flash evaporation

Flash evaporation is another technique for producing films whose constituents have different vapour pressures [15-17]. In contrast to the two source evaporation, it does not require provisions to monitor the vapour density. Film composition is controlled by evaporating to completion small quantities of the constituents in the desired ratio. Fractionation of particles during evaporation can be minimized by dispensing the evaporant in a steady trickle. The net result of these simultaneous discrete evaporations is a vapour stream whose

composition is uniform and identical to the source material. The technique is applicable for evaporation of alloys, metal-dielectric mixtures and compounds. The proper choice of the material and the design of the flash evaporation filament are of considerable importance [1]. The filament must be capable of attaining temperatures as high as 2000°C without volatilization or heavy reaction with the evaporant. Tungsten or tantalum strips are most commonly used. The temperature of the substrate determines the degree of order and crystallinity of the films.

2.15 Electron-beam gun evaporation

In this method, a stream of electrons is accelerated through fields of 5 to 10 KV and focused onto the evaporant surface [18-21]. Upon impingement, most of the kinetic energy is converted into heat and a temperature exceeding 3000°C is obtained. Since the electron beam can be concentrated on the evaporating surface, other portions of the evaporant are maintained at lower temperatures. Thus interactions between evaporant and support material are greatly reduced.

A small tungsten helix or hair-pin filament constitutes the electron source. The filament is kept at a high negative voltage (usually -10KV) with respect to the ground, so that the electrons emanating from it are accelerated away

from it [22]. This accelerated electron beam then passes through a strong transverse magnetic field which focuses and bends the beam to a particular point where the evaporant is placed. In a straight beam gun the substrates must be mounted off to the side. By bending the beam using a magnetic field this restriction can be overcome. 180° and 270° bent beam guns are now commercially available. Models with powers between 3 to 10 KW and water cooled copper hearth to support the evaporant are common. Most of them are bakeable and can attain temperatures upto 3500°C.

2.20 Sputtering

When a material is bombarded with electrons of sufficient energy, the atoms of the lattice are pushed into new positions creating surface migration of atoms. When the energy of the impinging electrons exceeds four times the heat of sublimation of target material, the target atoms get ejected. This process is known as sputtering [23].

2.21 Glow discharge sputtering

A glow discharge produced by an applied electric field between two electrodes in a gas at a low pressure is a convenient and simple source of ions for sputtering [17]. Most of the applied voltage is dropped across the cathode

dark space. Ions and electrons produced are accelerated across the region. The energetic electrons produce more ions by collision with the atoms in the negative glow, and the energetic ions strike the cathode to produce sputtering and emit secondary electrons. The optimum condition for deposition with a uniform deposit extending to about half the area of the target is obtained when the cathode-anode distance is about twice the length of the cathode dark space. The sputtering rate is proportional to the current for a constant voltage which is thus a very convenient control parameter. Glow discharge sputtering is also known as diode sputtering. One of the main advantages of this method is that the rate of deposition remains constant with time, provided, the current density and voltage do not vary [17].

2.22 Triode sputtering

Triode sputtering is one form of low pressure sputtering. Controlled direction and higher mean energy of the ejected atoms striking the substrate owing to smaller collision losses are some of the desirable features of low pressure sputtering [17]. The sputtering rates at low pressures can be increased by increasing the ionization of the sputtering gas. Additional electrons may be supplied thermionically from a filament. Both the total ionization and the ionization efficiency are increased by accelerating the electrons by means

of a third electrode, and injecting them into the plasma. A magnetic field inclined to the lines of force between the cathode and anode enhances triode sputtering.

2.23 R.F. sputtering

High ionization yield of the sputtering gas can be obtained by the use of a radio frequency (r.f.) of several mega cycles. The r.f. power may be applied directly to the anode through a capacitor or via a high frequency coil inside or outside the discharge vessel. An applied magnetic field assists in supporting and stabilizing the high frequency discharge and makes the operation possible at low pressures of a few milli torr. R.F. sputtering is a versatile technique and has several other useful applications. Since insulators can be R.F. sputtered, the technique is ideally suited for high rate reactive sputtering. R.F. sputtering may be used to etch metals, semiconductors and insulators.

Amorphous Si:H can be produced by sputtering silicon target in a partial pressure of hydrogen. Doped targets are used to produce n-type or p-type films. Doping can also be done by introducing hydrides of phosphorus or boron into the chamber during the sputtering process. It was shown that a deposition temperature of $\sim 200^\circ\text{C}$ and a hydrogen partial

pressure of 5 milli torr are the optimum values for obtaining good quality a-Si:H films by r.f. sputtering. Several methods were devised to prepare r.f. sputtered a-Si:H films with low density of gap states, but the most successful method was sputtering under a higher partial pressure of argon of ~ 30 milli torr.

For preparing polymer films the monomer vapour is introduced into the chamber through a control valve, so that the required pressure is reached inside the chamber. The pumping rate and the rate of flow of the monomer vapour are adjusted to keep the pressure at the required value. The discharge is produced by applying a d.c. or r.f. power. If r.f. power is applied, the frequency range is 0.5-13.5 MHz. When the glow discharge is produced, free radicals are formed in the system and they recombine among themselves to form a large polymeric chain. The polymer thus formed get deposited on the cleaned substrate as well as on the walls of the chamber.

For producing a-Si:H films silane (SiH_4) gas is introduced into the chamber. The operating frequency range remains the same but 13.5 MHz is usually chosen. The silane pressure in the chamber range from 5 to 250 milli torr. When using

capacitive coupling with a superimposed d.c. bias, the properties of the films deposited on the two electrodes may differ.

The advantages of the glow discharge method of film preparation are many. Simple set-up, ease of preparation, better control over the film parameters and the superior electrical and dielectric properties of the polymer films are the most important among them. However the fact that only a few materials, in the liquid form, can be deposited by glow discharge method is a serious limitation [8,17].

2.24 Ion-beam sputtering

The diode, triode and r.f. sputtering techniques are all ineffective below 10^{-3} torr, because of the scarcity of ions. By producing ions in a high pressure chamber, and then extracting them into a differentially pumped vacuum chamber through suitable apertures and focusing the beam using suitable electron or ion optics, a beam of ions can be obtained for sputtering in vacuum. This arrangement is known as duoplasmatron. Ion sources capable of yielding a current of ~ 500 mA and a beam size of ~ 1 cm² have been developed by Chopra and Randlett [27]. Using this, metal semiconductor or insulator targets can be sputtered.

2.25 Reactive sputtering

The high chemical reactivity of the atomic form of stable diatomic gases can be used advantageously to produce thin film carbides, nitrides, oxides, hydrides and sulphides. This is achieved by introducing a mixture of the inert sputtering gas and a small quantity of reactant in gas form in the glow discharge or r.f. sputtering system. R.F. plasma can be used to promote a reaction for example, between SiH_4 and H_2O vapours to deposit silicon and between SiH_4 and NH_3 to form durable and insulating Si_3N_3 films [28]. The major problem associated with the reactive sputtering is the difficulty in controlling the stoichiometry of the products. However, the method is very promising for producing dielectric films.

2.30 Chemical methods

Eventhough evaporation and sputtering are preferred for thin film preparation, chemical methods are also used for certain applications because they offer cheaper methods. An example is the large scale production of solar cells for terrestrial applications, where chemical spray, chemical dipping etc., are widely used. Also, in certain cases, best films are obtained by chemical methods such as the spray pyrolysis for the preparation of transparent conducting indium tin oxide films. All chemical methods depend upon a definite

chemical reaction for the formation of the film. It can be due to an electrical separation of ions or thermal effects. Depending upon this, chemical methods are broadly classified into electro deposition and chemical vapour deposition. Electrolytic deposition, electroless deposition and anodic oxidation come under the former while pyrolysis, hydrogen reduction and polymerization are the main methods which come under the latter. Each of these methods are discussed briefly below [8,17,23].

2.31 Electrolytic deposition

According to the laws of electrolysis, the weight of the material deposited is proportional to the amount of electricity passed. The metallic ions in the electrolyte migrate towards the cathode under the influence of the applied electric field. The cation crosses the double layer, loses part of its water of hydration, and then becomes adsorbed on the metal surface as an adion. The adion which corresponds to the adatom in vapour deposition diffuses over the surface, loses the rest of its water of hydration and is finally incorporated as an ion into the metal lattice. The structure that is obtained can vary from single crystals, crystalline aggregates unoriented deposits of very fine grain size and disordered structures. Single crystal films grown by this

method are found to be highly perfect upto 1000 Å. The films are continuous even at a thickness of 50 Å.

2.32 Electroless deposition

Electrolytic action may be achieved by a chemical reduction process without the use of an external potential source. This technique is known as 'electroless deposition' [24]. This method can be used to deposit Ni, Co and Pb films by reduction of their chlorides by sodium hypophosphite. For non-metallic surfaces it may be necessary to use a sensitizer [8]. The rate of film growth is dependent on the reaction temperature and is difficult to control.

2.33 Anodic oxidation

A large number of metals called 'valve metals' tend to form very thin oxide films when exposed to oxygen. But by anodic polarization of these metals in a suitable aqueous solution, a high resistance film can be grown. The anodization process involves the migration of ions of oxygen, metal or both through existing oxide film. Growth rate of an anodic film depends on the current density and the temperature of the electrolyte. If the current is kept constant the growth increases linearly with time. The maximum value of thickness

depends on the anodization voltage, the electrolyte and its temperature. The anodic films are generally amorphous and under certain conditions crystalline films are also formed. The application of the method comes in the production of ultra thin and thick oxide films for tunnel devices, capacitors and protective layers. A disadvantage of anodization in aqueous solutions is the incorporation of water and OH ions into the films producing adverse effects on their dielectric properties [25].

2.34 Chemical spray method

Photoconducting and electroluminescent films of II-VI compounds can be prepared by a chemical spray method. Reagents such as thiourea, selenourea and thioacetamide interact with salt solutions of heavy metals and form precipitates of II-VI compounds when heated. Films upto 20 μm can be prepared by this method.

2.35 Chemical vapour deposition (CVD)

In this method a volatile compound of a substance is vapourized and the vapour is thermally decomposed or reacted with other gases, vapours or liquids at the substrate to yield a non-volatile reaction product. This product deposits atomistically on the substrate [8,23]. CVD is a versatile and

flexible technique and can be employed to produce films of pure metals, semiconductors and insulators. Single crystal metal oxides can also be prepared by this method. The application of a transverse electric field to the substrates during deposition will increase the growth rate of substances like silicon, germanium and gallium arsenide.

2.36 Pyrolysis

The thermal decomposition of a compound to yield a deposit of the stable residue is called pyrolysis [17]. Pyrolysis of silane (SiH_4) and germane (GeH_4) is employed to produce epitaxial layers of silicon and germanium. Silane at a pressure of 8 torr decomposes completely at about 777°C . The silicon deposit can be grown epitaxially on single crystal silicon wafers. The reaction is very slow below 800°C [26]. Films of SiO_2 can be prepared by passing an inert carrier gas carrying vapour from the silicates over a heated substrate. Deposition of Al_2O_3 films have been obtained by pyrolysis of aluminium triethoxide in vacuo at 550°C [17].

2.40 Sample preparation followed in the present work

Thin films of amorphous silicon of thickness ranging from 250 \AA to 1500 \AA were prepared in a conventional vacuum coating unit. The system was pumped down to $\sim 10^{-5}$ torr

using a 6" diffusion pump backed by a 500 l/min. rotary pump. Tungsten basket was used as the evaporation source. It was made from multistranded tungsten wire of diameter 0.5 mm. Prior to silicon evaporation, the basket was fired in vacuum at a temperature greater than the melting point of silicon several times. The silicon used for evaporation was 99.999% pure polycrystalline granules supplied by Balzers.

Optically flat glass slides of dimension 2.5x7.5 cm were used as the substrates [supplied by Blue Star Co.]. They were first cleaned using a soap solution and were then immersed in potassium dichromate solution for one hour. Subsequently the plates were cleaned using distilled water and subjected to ultrasonic cleaning. After these steps, the slides were dried slowly without any water mark and were loaded in the vacuum chamber. The chamber is pumped and when the pressure reaches $\sim 10^{-2}$ torr the slides are subjected to ion bombardment (IB) cleaning for 15 to 30 minutes by applying a voltage of ~ 1 KV to the aluminium electrodes of the IB cleaning set-up. After this the chamber is pumped down to $\sim 10^{-5}$ torr and silicon taken in the tungsten basket is evaporated. It was found that a single basket can be used only for three or four coatings after which blisters appeared on the baskets, probably due to the silicon-tungsten reaction, and eventually they broke.

The shape and size of the silicon films were defined by means of suitable masks made using mica. For electrical measurements films of 2.5x1.5 cm area were prepared. Over this aluminium or silver electrodes were deposited in the planar structure with a gap between the electrodes. For dielectric studies, films were sandwiched between the electrodes. For MOSFET fabrication the area of the film was chosen to be 1 cm².

There was a substrate heater mounted inside the vacuum chamber using which the substrate temperature during deposition could be varied. Films were prepared at substrate temperatures varying from 300K to 573K. The structure of the device is as shown in Figure 2.40.

2.41 Hydrogenation of a-Si films

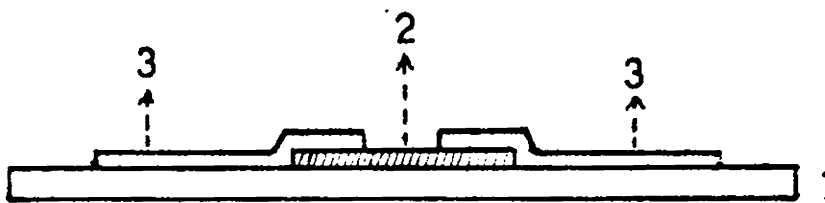
For hydrogenation, the as-deposited amorphous silicon films were transferred to another chamber. The hydrogenation set-up is shown schematically in Figure 2.41. It consists of a 40 cm long glass tube with a diameter of 6 cm. One end of the tube has a demountable vacuum joint. The other end is connected to a 6" diffusion pump backed by a rotary pump, through a two way valve. The chamber could be evacuated to 10⁻⁵ torr. Pure hydrogen was prepared in a Kipp's apparatus using dilute HCl and Zn granules. The hydrogen was collected

Fig. 2.40

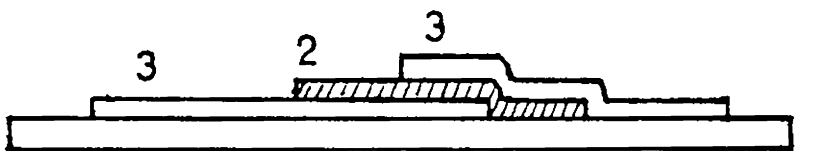
Two types of the electrode structures used in the present study

(a) Planar structure

(b) Sandwich structure



(a)

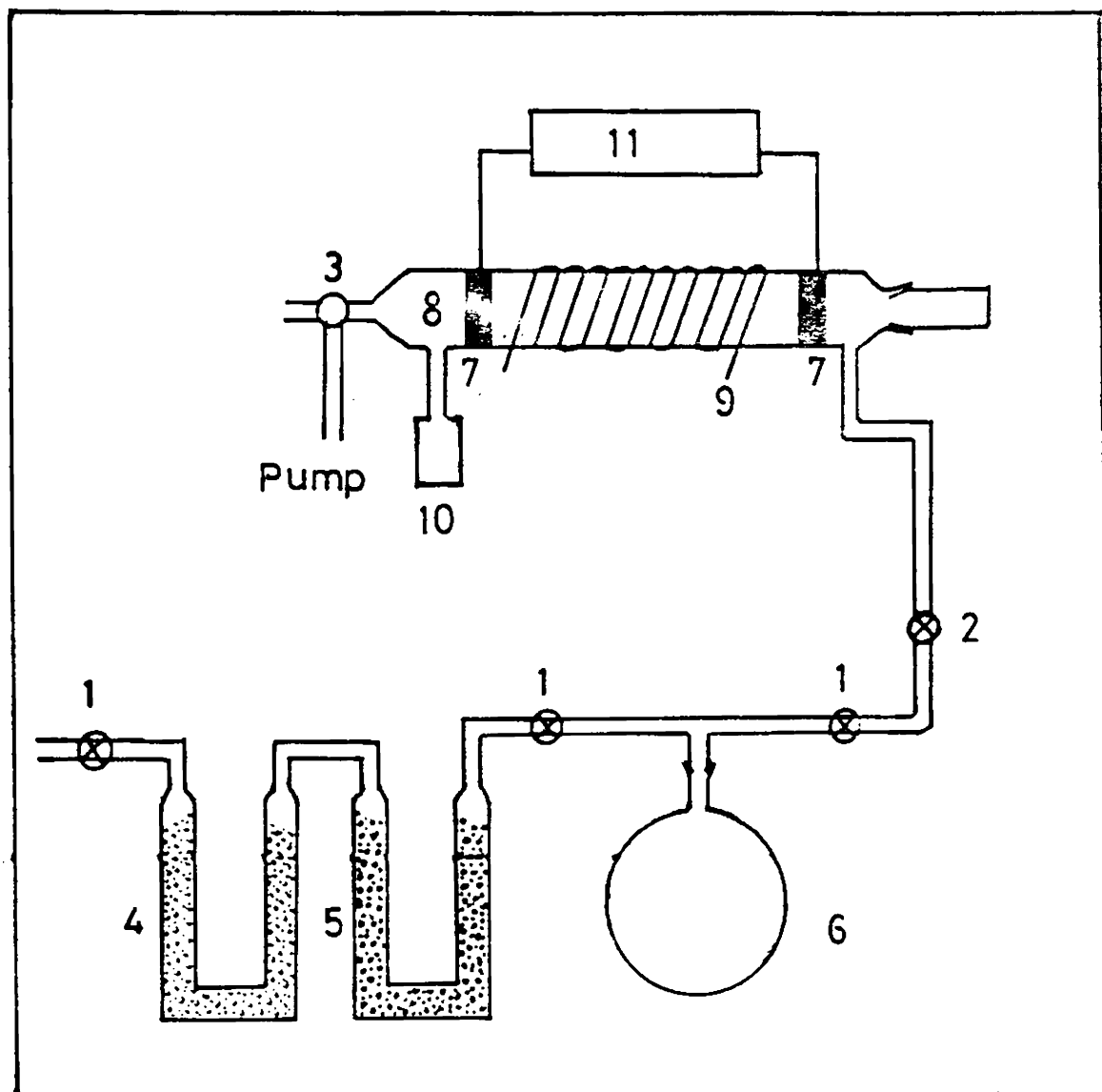


(b)

- 1) Substrate
- 2) Semiconductor
- 3) Electrodes

Fig.2.41

Schematic diagram of the hydrogenation set-up



- | | |
|--------------------------|--|
| 1. Glass valve | 2. Needle valve |
| 3. Two-way valve | 4. U-tube containing CaCl ₂ |
| 5. U-tube containing KOH | 6. Round bottom flask |
| 7. Metal electrodes | 8. Glass chamber |
| 9. Heating tape | 10. Pirani gauge head |
| 11. R.F.generator | |

in a three litre bottle by the downward displacement of water. A part of the hydrogen thus prepared was passed through a U-tube containing CaCl_2 for removing water vapour and another U-tube containing KOH pellets for removing acid vapours. The dry hydrogen is finally collected in a two litre round bottomed flask. From the flask it could be introduced into the hydrogenation chamber through the needle valve. The temperature of the chamber could be varied using a heating tape wound over it. A chromel-alumel thermocouple was used to measure the temperature inside the chamber. A plasma could be generated inside the chamber by applying r.f. (35W at 4.5 MHz) from a generator through two capacitively coupled electrodes. The electrodes consist of two 1" strips of aluminium foils wound at the two ends of the chamber at a distance of 25 cm. The sequence of hydrogenation is as follows:-

1. Substrates coated with a-Si films are placed at the centre of the glass chamber.
2. The thermocouple is made to touch a glass slide placed adjacent to the a-Si film.
3. The glass chamber is made vacuum tight by closing the open end using the metal lid in which an O-ring is properly placed.

4. The chamber is then pumped down to 10^{-5} torr using the 6" diffusion pump backed by a 500 l/min. rotary pump.
5. The baffle valve of the diffusion pump is closed and the chamber is flushed with dry hydrogen by opening the needle valve.
6. After one or two minutes the needle valve is closed and the system is again pumped down to 10^{-5} torr.
7. Flushing of the chamber with dry hydrogen is repeated three times to ensure the absence of oxygen in the chamber.
8. After the third flushing the chamber is again pumped down to 10^{-5} torr.
9. When the pressure inside the chamber is 10^{-5} torr, the needle valve is slowly opened and hydrogen is admitted into the chamber so that the pressure inside the chamber reaches a pre-determined value.
10. By adjusting the rate of introduction of hydrogen and the pumping rate a steady state is maintained in the chamber.
11. By switching on the heater the temperature of the a-Si film is rised to the desired value.
12. When the temperature has reached the desired value the r.f. generator is switched on and a hydrogen plasma is generated in the chamber.

13. The a-Si film is annealed in this high temperature plasma for a desired duration of time.
14. After annealing, the heater is switched off and the plasma is maintained till the temperature falls below 373K.
15. When the chamber reaches the room temperature the a-Si:H films are taken out, given proper electrodes and subjected to measurements.

Films were annealed in hydrogen plasma at various hydrogen pressures, temperatures and duration. No visible changes were observed in the hydrogenated films.

2.50 Measurement set-up

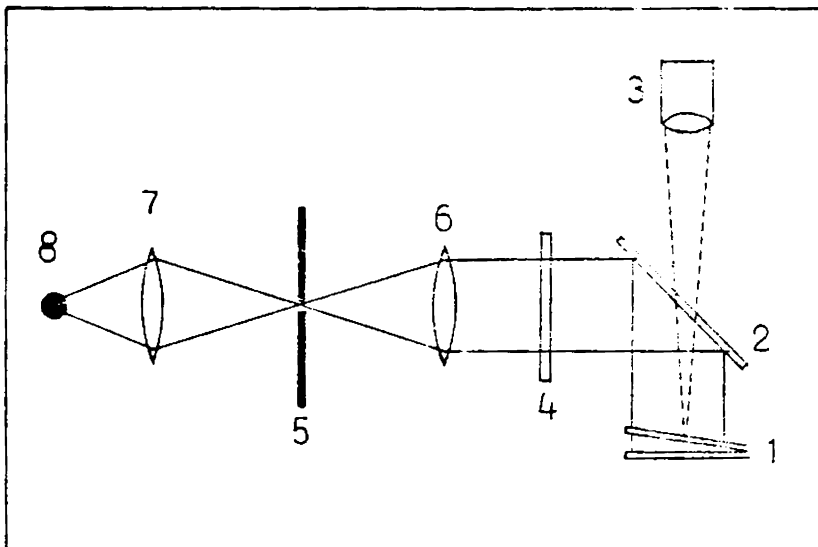
2.51 Thickness measurement

For measuring the thickness of the films Tolanky's interference method was used.

When two reflecting surfaces are brought into close proximity interference fringes are produced, the measurement of which makes possible a direct determination of the film thickness. These fringes are known as Fizeau fringes of equal thickness and are obtained in an optical apparatus shown in Figure 2.50. It consists of two slightly inclined optical flats, one of them supporting the film. The film forms a sharp

Fig.2.50

Schematic diagram of thickness measurement set-up



1. Sample covered with semi-silvered glass plate
2. Beam splitter
3. Microscope
4. Filter
5. Slit
- 6.) Lenses
- 7.)
8. Light source

step on the substrate. When the second optical flat is brought in contact with film surface and the interferometer is illuminated with a parallel monochromatic beam at normal incidence and viewed with a low power microscope, dark fringes can be observed, which trace out points of equal air-gap thickness. By adjusting the relative positions of the flats to form a wedge shaped air gap, the fringes can be made to run in straight lines perpendicular to the step on the opaque film. The fringes show a displacement as they pass over the film step-edge. By measuring the fringe shift and fringe spacing (distance between two adjacent fringes) the thickness of the film (t) can be calculated using the equation

$$t = \frac{\text{Fringe shift}}{\text{Fringe spacing}} \times \frac{\lambda}{2} \quad (2.10)$$

where λ is the wavelength of the monochromatic light used [5460Å in the present case].

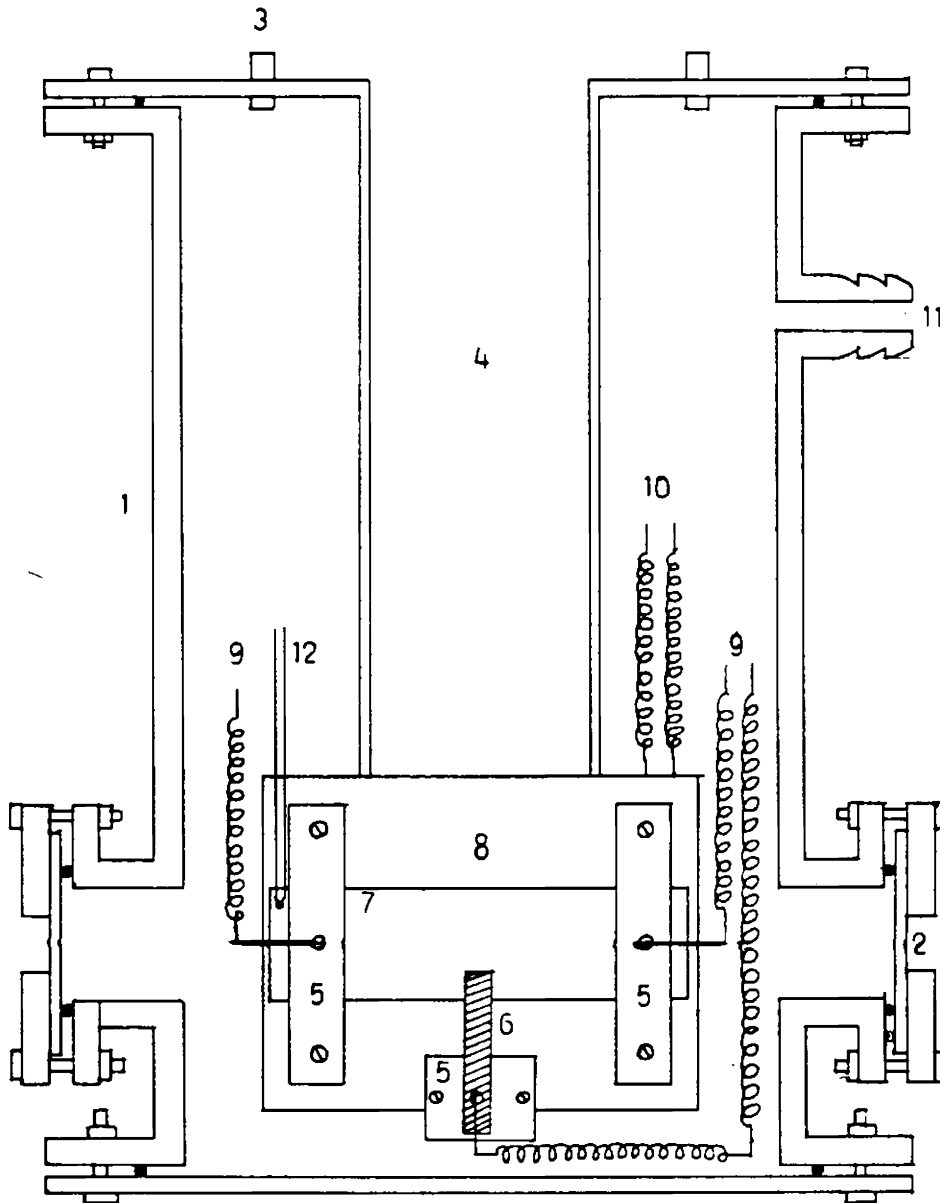
2.52 Electrical measurements

Since all the current measurements were done in the vderly low range ($\sim 10^{-8}$ to 10^{-10} A), there was disturbance from external electrical noises. Eventhough the room was well dehumidified, problems of humidity persisted in the current measurements. These external electrical pick-ups and varying humidity in the laboratory affected the reproducibility of

the measurements. These problems were minimized by holding the films inside a metal chamber (Figure 2.51). The chamber was well grounded and could be evacuated to 10^{-2} torr so that it acted as a shield to the electrical pick-ups and ambient humidity. The chamber had a metal cylindrical body of height 30 cm and diameter 10 cm. Four glass windows were provided at 90° to each other for photoconductivity measurements. It also had a pumping port, which could be connected to a rotary pump. One of the ports was used as a special threaded coupler to hold a pirani vacuum gauge head, so that the pressure inside the cell could be monitored. The top of the cell was closed vacuum tight using a circular metal plate, from which a liquid nitrogen cooled cold finger was introduced into the cell. At the end of the cold finger a film holder was connected by welding. This holder was provided with a heater ($\sim 40W$) in order to vary the temperature of the film for measurement purposes. All insulations of the holder were made from teflon. The heater could go upto $\sim 200^\circ C$. An iron-constantan thermocouple was used to measure the temperature. The electrodes of the holder were copper blocks mounted on teflon strips. The holder was provided with three separate electrodes in order to investigate three terminal devices like a field effect transistor. The electrical connections were taken out through BNCs. Shielded cables were used outside the metal cell, to make connections to d.c. power supply and electrometer.

Fig.2.51

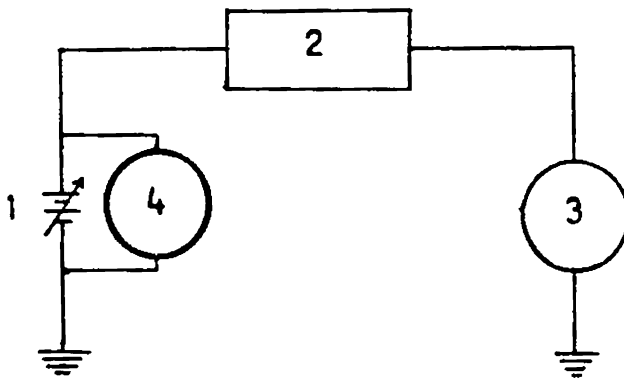
Schematic diagram of the metal chamber used for conductivity measurements



- | | |
|-----------------------------------|--|
| 1. Metal cylinder | 2. Glass window |
| 3. B.N.C. | 4. LN ₂ chamber |
| 5. Teflon blocks | 6. Copper electrode |
| 7. Substrate with film | 8. Heater/Substrate holder |
| 9. Electrode-BNC interconnections | 10. Electrical connections to the heater |
| 11. Pumping ports | 12. Thermocouple |

Fig.2.52

Electrical circuit for conductivity measurements



A steady d.c. power supply (2-24V) was used as the voltage source. For measurements below 2V another stable low voltage power supply was used. The current through the film was measured using an electrometer amplifier (Model EA 815, ECIL). The electrical circuit for conductivity measurements is shown in Figure 2.52. For electrical conductivity measurements the electrodes were deposited in the planar structure with a gap in between them. The d.c. voltage was applied across the film. The voltage was measured using a high impedance digital voltmeter. The electrometer was connected in series with the power supply and the film. For dielectric measurements the films were sandwiched between the electrodes with definite electrode crossover areas.

The details of the electrical and dielectric measurements, are discussed in detail in the respective chapters.

REFERENCES

1. L.I.Maissel and R.Glang, "Handbook of Thin Film Technology", McGraw-Hill Book Company, New York (1970) 1-7, 1-81, 1-85, 1-92.
2. L.Holland, "Vacuum Deposition of Thin Films", John Wiley and Sons Inc., New York (1961) 108.
3. K.H.Behrndt, "Techniques of Metal Research", Vol.I, Pt.3, Interscience Publishers Inc., New York (1968) 1225.
4. H.L.Caswell, "Physics of Thin Films", G.Hass (Ed.), Vol.I, Academic Press Inc., New York (1963) 1.
5. E.Ritter, J.Vacuum Sci.Technol., 3 (1966) 225.
6. P.Dellafera, R.Labusch and H.H.Roscher, Phil.Mag.B, 45 (1982) 607.
7. W.E.Spear and P.G.LeComber, Solid State Commun., 17 (1975) 1193.
8. K.L.Chopra and S.R.Das, "Thin Film Solar Cells", Plenum Press, New York (1983) 427, 204, 211, 214, 265.
9. W.E.Spear, "Fundamental Physics of Amorphous Semiconductors", F.Yonezawa (Ed.), Springer-Verlag, New York (1981) 40.

10. P.G.LeComber and W.E.Spear, "Topics in Applied Physics", Vol.36, M.H.Brodsky (Ed.), Springer-Verlag, New York (1979) 251.
11. W.E.Spear and P.G.LeComber, "Topics in Applied Physics", Vol.55, Springer-Verlag, New York (1984) 63.
12. Masataka Hirose, "Amorphous Semiconductor--Technologies and Devices", Vol.16, Y.Hamakawa (Ed.), OHM, Tokyo and North-Holland, Amsterdam (1984) 67.
13. L.Ley, "Topics in Applied Physics", Vol.56, J.D.Joannopoulos and G.Lucovsky (Ed.), Springer-Verlag, New York (1984) 61.
14. David Emin, "Polycrystalline and Amorphous Thin Films and Devices", Lawrence L.Kazmerski (Ed.), Academic Press, New York (1980) 17.
15. L.Harris and B.M.Siegel, J.Appl.Phys., 19 (1948) 739.
16. W.R.Beam and T.Takhashi, Rev.Sci.Instr., 35 (1964) 1623.
17. K.L.Chopra, "Thin Film Phenomena", Robert E.Krieger Publishing Company (1979) 18,23,29,34,36,43,47,49.
18. G.Siddall and B.A.Probyn, "Trans. 8th National Vacuum Symposium", Pergamon Press, New York (1961) 1017.
19. O.S.Heavens, J.Sci.Instr., 36 (1959) 95.

20. K.L.Chopra and M.R.Randlett, *Rev.Sci.Instr.*, **37** (1966) 1421.
21. D.H.Blackburn and W.Haller, *Rev.Sci.Instr.*, **36** (1965) 901.
22. B.A.Unvala and G.R.Booker, *Phil.Mag.*, **9** (1964) 691.
23. R.W.Berry, P.M.Hall and M.T.Harris, "Thin Film Technology",
Van Nostrand Reinhold Co., New York (1968) 191,255,266.
24. F.A.Lowenheim, "Modern Electroplating", John Wiley & Sons,
Inc., New York (1963).
25. D.A.Vermilyea, "Non Crystalline Solids", V.D.Frechette
(Ed.), John Wiley & Sons, Inc., New York (1958) 328.
26. B.A.Joyce and R.R.Bradley, *J.Electrochem.Soc.*, **110** (1963)
1235.
27. K.L.Chopra and M.R.Randlett, *Rev.Sci.Instr.*, **33** (1962) 905.
28. H.F.Sterling and R.C.G.Swan, *Solid State Electron.*, **8** (1965)
653.

Chapter 3

ELECTRICAL CONDUCTION IN AMORPHOUS SILICON AND HYDROGENATED AMORPHOUS SILICON

Abstract

The d.c. and a.c. electrical properties of hydrogenated and unhydrogenated amorphous silicon (a-Si:H and a-Si) films are studied. The effects of annealing temperature, annealing time, substrate temperature and thickness on the d.c. electrical properties of a-Si films and the role of hydrogenation temperature and hydrogen partial pressure in determining the d.c. electrical properties of a-Si:H films are investigated in detail. It is found that intrinsic films with conductivity $\sigma_{d.c.} = 4 \times 10^{-8} \Omega^{-1} \text{cm}^{-1}$ and activation energy $E_a = 0.76 \text{ eV}$ are obtained at a hydrogenation temperature of 573K and a hydrogen partial pressure of 0.05 torr. The a.c. conduction studies included the frequency and temperature dependence of conductivity in the range 10 kHz to 1 MHz and 300K to 398K respectively. $\sigma_{a.c.}$ is found to vary with frequency (ω) as $\omega^{1.4}$ to $\omega^{1.67}$. The effect of various gas ambients like CO_2 , NH_3 , H_2O etc. on the d.c. conduction were investigated for these films. In the case of a-Si films exposure to CO_2 caused a decrease in $\sigma_{d.c.}$ while exposure to NH_3 and H_2O vapour caused an increase. But in the case of a-Si:H films exposure to CO_2 caused an initial decrease followed by a gradual increase in $\sigma_{d.c.}$ while exposure to NH_3 and H_2O vapour caused an initial increase followed by a decrease. Suitable explanations are attempted for this behaviour.

3.00 Introduction

Study of the transport properties is one of the important ways of characterizing a semiconductor film. In this chapter a detailed analysis of the d.c. and a.c. electrical conduction in hydrogenated and unhydrogenated amorphous silicon films prepared by vacuum evaporation is given. The variation of conductivity with temperature is studied for all films and the activation energy is calculated in each case. The dependence of the conductivity and activation energy on film thickness, substrate temperature, annealing temperature and annealing time is studied for unhydrogenated samples. The effects of hydrogen annealing temperature, hydrogen annealing time and hydrogen partial pressure in the hydrogenation chamber are studied for the hydrogenated samples. Investigations are also carried out on the d.c. conduction in the hydrogenated and unhydrogenated films. A.C. conduction studies in favourable circumstances can be used to calculate density of defect states at the Fermi level [1-3]. The effect of certain gases adsorbed by the films, on its electrical conduction is presented subsequently. These investigations yield informations like the conductivity type (whether n-type or p-type) and the band bending at the surface of the film [4]. The present studies would form the starting point to a more systematic study on the feasibility of gas sensing thin film devices using amorphous silicon.

3.10 D.C. electrical conduction

3.11 Theory of d.c. electrical conduction in amorphous semiconductors

From Davis and Mott model for the density of states in a noncrystalline system [5], we know that there is a fairly narrow (< 0.1 eV) band of localized states exist near the middle of the mobility gap which effectively pins the Fermi level. So, electrical conduction is extrinsic rather than intrinsic. According to this model for the density of states and mobilities, three mechanisms of electrical conduction are identified in an amorphous semiconductor [5]. They are briefly discussed below.

(a) Conduction due to carriers excited beyond the mobility shoulders into extended states. For an n-type material the conductivity σ is given by

$$\sigma = \sigma_0 \exp \left[-(E_c - E_F)/kT \right] \quad (3.10)$$

where E_c is the mobility edge at the conduction band, E_F the Fermi level, k Boltzmann constant and T the absolute temperature.

The pre-exponential factor σ_0 lies between 100 and $500 \Omega^{-1} \text{cm}^{-1}$ in most materials.

(b) Conduction due to carriers excited into the localized states at the band edges. This is called hopping conduction. For an n-type material the conductivity is given by

$$\sigma = \sigma_1 \exp -(E_A - E_F + \Delta W_1)/kT \quad (3.11)$$

where E_A is the energy at the edge of the conduction band tail and ΔW_1 is the activation energy for hopping. σ_1 is expected to be less than σ_0 by a factor of 10^2 to 10^4 . This is mainly due to the lower mobility of the carriers in the localized states and partly due to the low effective density of states in these levels.

(c) Conduction due to carriers hopping or tunnelling between localized states near the Fermi energy. The process is analogous to the impurity conduction in heavily doped semiconductors. Conductivity in this case, can be written as

$$\sigma = \sigma_2 \exp (-\Delta W_2/kT) \quad (3.12)$$

where $\sigma_2 \lesssim \sigma_1$ and ΔW_2 is the hopping energy. ΔW_2 is of the order of half the width of the band at the mid gap which pins the Fermi level. It will be considerably less than half of the band gap. As the temperature is lowered ΔW_2 will

drop and finally $\ln \sigma$ behaves like $A-BT^{-\frac{1}{4}}$ [7]. Usually this type of conduction will be dominant at very low temperatures [5].

It may be noted that if the room temperature conduction is mainly due to type (a), then the range of the localized states must be less than $kT \ln(\sigma_0/\sigma_1)$ which is ≈ 0.2 eV [5]. The total conductivity of all processes is given by the integral over all available energy states. Thus for states above E_F we have,

$$\sigma = e \int N(E) \mu(E) f(E) dE \quad (3.13)$$

where $f(E)$ is the Boltzmann distribution function, $N(E)$ is the density of states and $\mu(E)$ is the mobility of the carriers. At a particular temperature any one of the three mechanisms discussed above will dominate the conduction process.

3.12 D.C.conduction in a typical unhydrogenated amorphous silicon film

The d.c. conduction studies in a typical unhydrogenated amorphous silicon are presented. The dark d.c. conductivity, activation energy for conduction, pre-exponential factor and the temperature coefficient of resistance are

calculated from experimental data. A detailed discussion of the results is also presented.

(a) Fabrication of metal-a-Si-metal structures

Thin films of unhydrogenated amorphous silicon of thickness 834 \AA and area $2.5 \times 1.5 \text{ cm}$ were prepared on optically flat and thoroughly cleaned glass plates as described in Chapter 2. Films were brown in colour and were fairly transparent. The adhesion of the films to the glass substrates was excellent. These films were annealed in a vacuum of $\sim 10^{-5}$ torr at 373K for 30 minutes and allowed to cool to room temperature slowly before taking measurements. Silver or aluminium electrodes ($\sim 1000 \text{ \AA}$) were then deposited over the amorphous silicon films in another chamber, in the planar structure. Electrodes usually had a width of 1 cm or 0.5 cm and had a separation of 0.5 cm or 0.3 cm between them as shown in Figure 2.40a. The area and shape of the a-Si and metal films were defined using mica masks. The films were then mounted inside the measuring chamber, pumped down to $\sim 10^{-2}$ torr and were subjected to the various measurements.

(b) Current-voltage characteristics of Ag-a-Si-Ag planar structure

The current-voltage characteristics of a Ag-a-Si-Ag structure was carried out. This study was mainly

intended to establish the ohmic nature of amorphous silicon-silver contacts. So many materials like molybdenum [8,9], aluminium [10-12], nickel-chromium [13,14] and gold [15] were used as ohmic contacts to hydrogenated amorphous silicon. For the present investigation Al and Ag were used for ohmic contacts. As a first step a study was made on silver-amorphous silicon contacts to establish its ohmic character.

The current-voltage characteristics of the annealed films were investigated by applying a d.c. voltage across the film and measuring the current through it, as described in Chapter 2. The voltage was varied from 0.2 V/cm to 50 V/cm. Measurements were carried out at room temperature (~ 26 C).

(c) Dependence of electrical conductivity on the temperature

To find out the temperature dependence of the conductivity, current through the film was measured at different temperatures by applying a constant voltage. For this the film was kept at different temperatures in the range from 300K to 423K. The temperature was monitored using an iron-constantan thermocouple. Measurements were taken at intervals of 5K. The temperature was kept steady for 5 minutes before applying the voltage. The voltage

applied was 40 V/cm. Two to three minutes after the application of the voltage, current was measured. Then the voltage was switched off and the temperature of the film was raised to another value and the experiment repeated.

All the current-voltage measurements were carried out with electrodes in the planar structure as shown in Figure 3.10. The sandwich configuration often showed diode and carrier-injection properties [16]. Moreover, in the sandwich structure, since the distance between the two electrodes is very small, there is a chance for the film to exhibit electrical switching properties [17].

(d) Results and discussion

From the current-voltage measurement at room temperature (Figure 3.11), it is found that, the silver amorphous silicon contact is ohmic in the voltage range 0.8 V/cm to 50 V/cm. The slope of the region BC in figure 3.11 is 0.97 which demonstrates a good ohmic contact.

Three sets of current-voltage measurements were carried out at room temperature. The average value of the electrical conductivity $\sigma = 6.15 \times 10^{-6} \Omega^{-1} \text{cm}^{-1}$. The temperature dependence of σ is shown in Figure 3.12 in

Fig.3.11

In I vs In V curve of
Ag- a-Si - Ag system

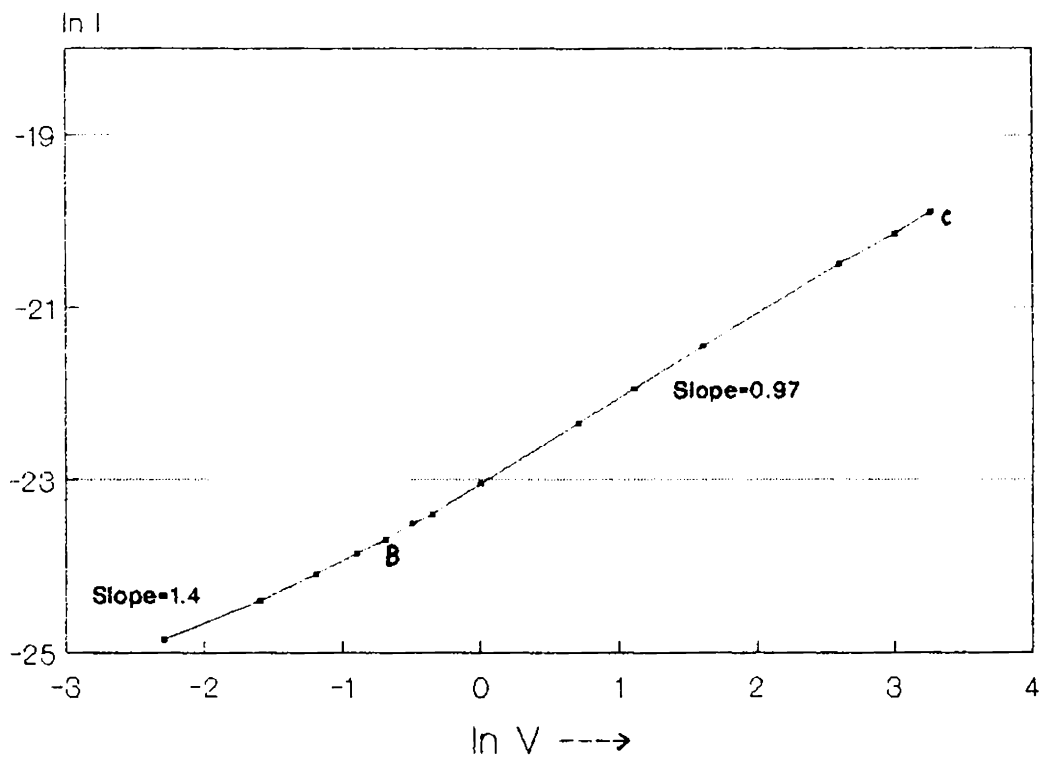


Fig.3.12

$\ln \sigma$ vs $10^3 / T$ curve for
Ag - a-Si - Ag system

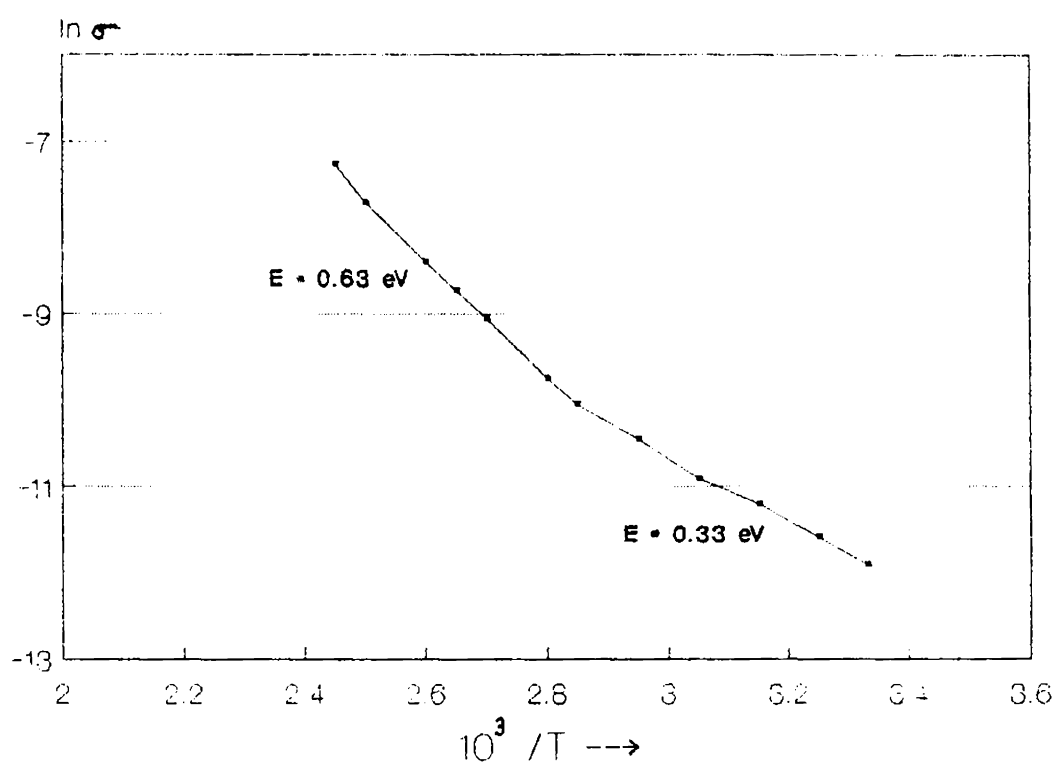


Fig.3.13

Resistance vs temperature for
Ag- a-Si - Ag structure

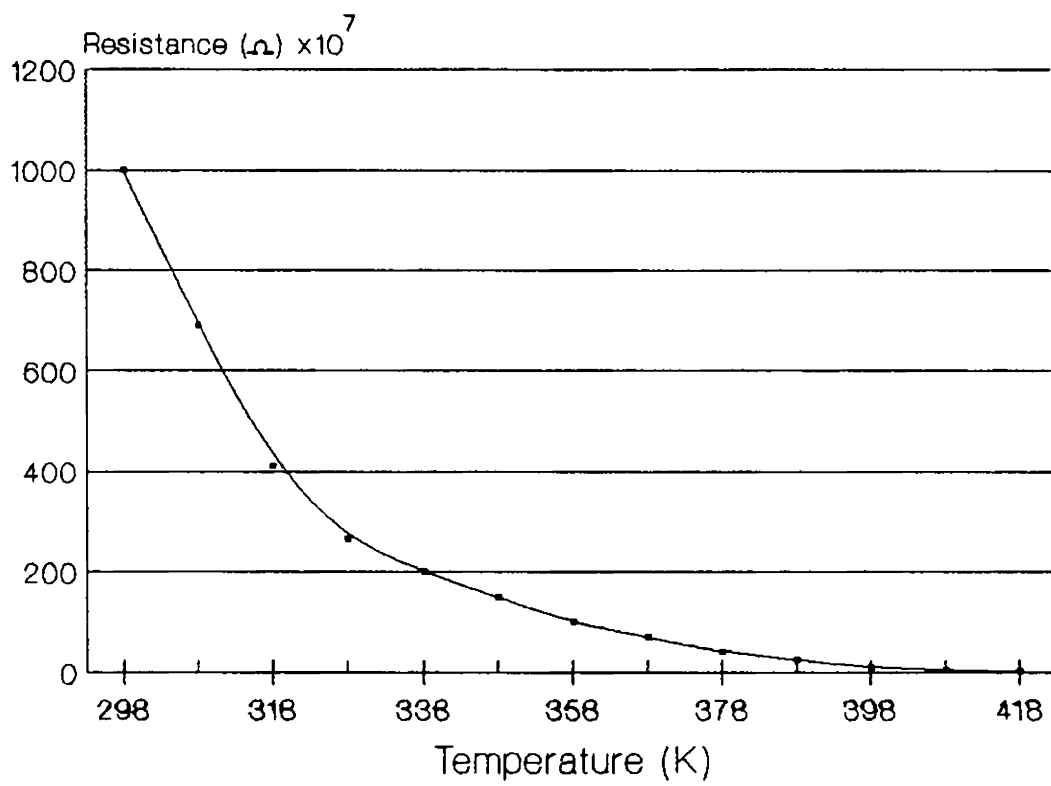
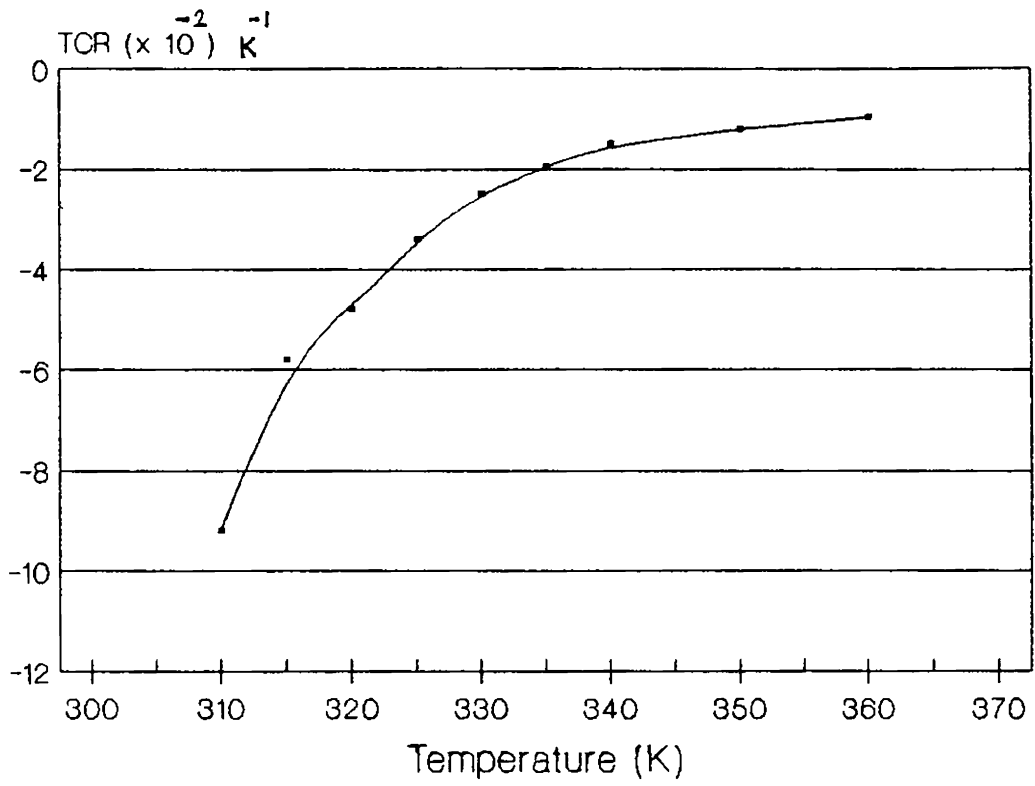


Fig.3.14

Temperature coefficient of resistance vs
Temperature for Ag- a-Si - Ag structure



which $\ln \sigma$ is plotted against $10^3/T$ in the temperature range 300K to 423K. Two distinct slopes are observed. The activation energy is 0.33 eV below 351K and 0.63 eV above this temperature. The pre-exponential factor σ_0 is found to be 195 at higher temperatures which indicates that the dominant conduction is through extended states [5] at elevated temperatures. The ratio of the localized state conductivity to extended state conductivity β can also be estimated from this plot. The high temperature part of the $\ln \sigma$ vs $10^3/T$ curve is extended to room temperature. The ratio of conductivity measured at room temperature to the value at the projected point gives β at room temperature [12] as 5.75. This establishes that at room temperature the conduction through localized states is dominant.

In Figure 3.13 the resistance R of the film is plotted against the absolute temperature T. As the temperature increases from 300K to 418K the resistance of the film decreases by three orders of magnitude. Temperature coefficient of resistance (TCR) calculated at various temperatures is plotted in Figure 3.14. Figure shows that TCR also decreases as the temperature increases.

3.13 Effect of annealing temperature on Al-a-Si-Al planar structures

Since aluminium is already reported as a very good ohmic contact to hydrogenated amorphous silicon [10-12], it is used here as the ohmic contact for the investigations on the amorphous silicon and hydrogenated amorphous silicon thin films. This has also helped in identifying the influence of hydrogenation (by r.f. plasma annealing) on the electrical properties of the amorphous silicon. The experimental details and results are discussed below.

(a) Experimental

Films of amorphous silicon with thickness 510 \AA were prepared as described in Chapter 2. These films were then annealed, at temperatures 383K, 423K, 474K and 523K for 30 minutes at $\sim 10^{-5}$ torr. Over these annealed films aluminium electrodes were deposited in the planar structure by vacuum evaporation. The breadth of the electrodes was 0.5 cm while the separation between them 0.3 cm. The films were mounted inside the measurement cell and were subjected to current-voltage measurements at different temperatures ranging from room temperature to 378K. The dependence of electrical conductivity on temperatures was determined for each film by applying four biasing voltages (5,10,15 and 20V). The results are discussed below.

(b) Results and discussion

(1) Films annealed at 383K

The current-voltage characteristics of the film annealed at 383K and measured at different temperatures are shown in Figure 3.15. The slope of the curve is 1 or very nearly 1 at all the temperatures. This means that Al-a-Si contact is ohmic in the temperature range at which measurements are carried out. The room temperature conductivity is $\sigma = 1.5 \times 10^{-7} \Omega^{-1} \text{cm}^{-1}$. The temperature dependence of the conductivity is given in Figure 3.16. Measurements are taken with applied voltages of 5, 10, 15 and 20V. For each applied bias there is only a single slope for the $\ln \sigma$ vs $10^3/T$ plot. The corresponding activation energy E_a is calculated in each case and there is only a very small difference in the value of E_a between the different plots. Since the conductivity is singly activated in the temperature range studied $\beta = 1$.

Resistance R is plotted against absolute temperature in Figure 3.17. TCR is calculated for different temperatures and is also plotted against temperature in the same figure.

(2) Films annealed at 423K

Current-voltage characteristics is given in Figure

Fig. 3.15

ln I vs ln V curves of a-Si film
annealed at 383 K

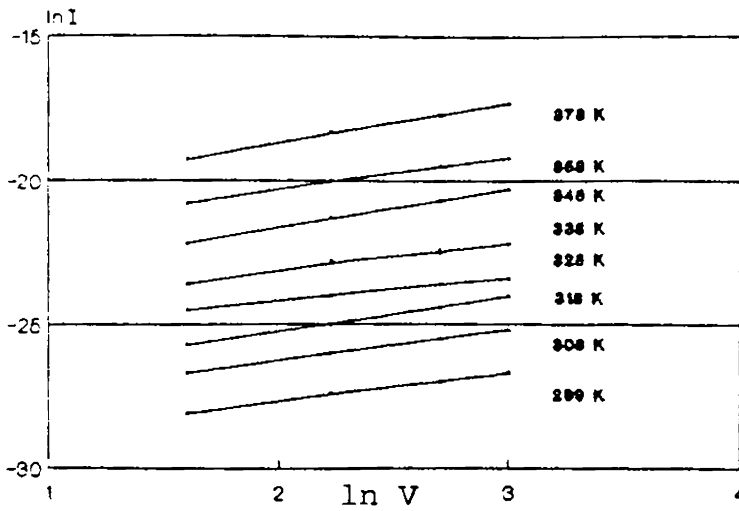


Fig. 3.16

ln I vs $10^3/T$ curve of a-Si
film annealed at 383 K

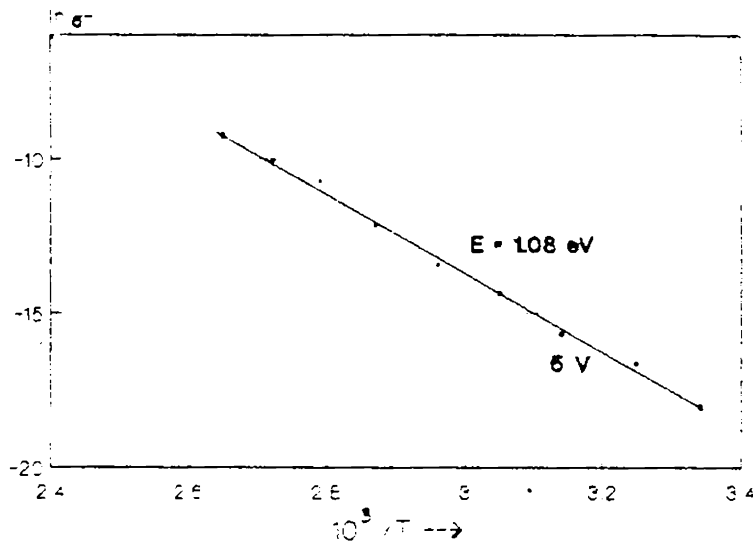
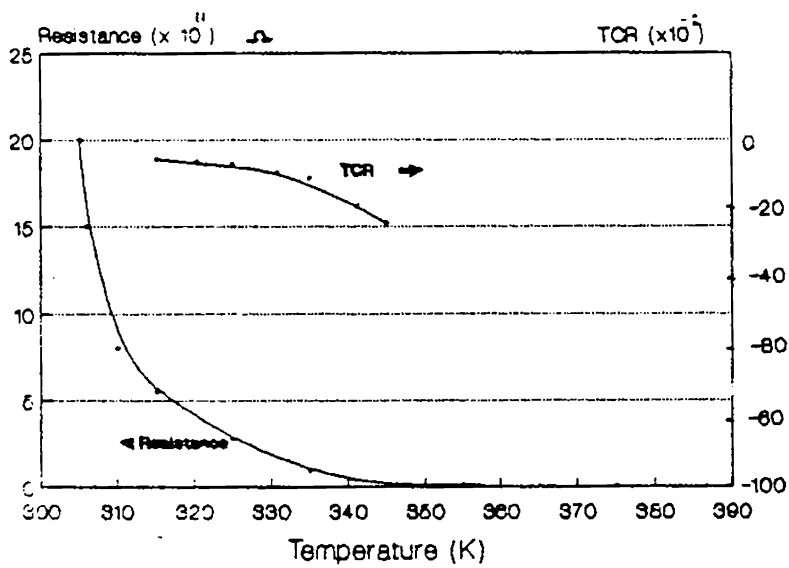


Fig. 3.17

Resistance & TCR vs Temperature curves
of a-Si film annealed at 383 K



3.18. The slope is 1 at all temperatures at which measurements were carried out indicating ohmic conduction. In Figure 3.19 $\ln \sigma$ vs $10^3/T$ is given for this film. Unlike in the previous case, here two distinct slopes are observed instead of one. From room temperature to 328K the activation energy is 1.31 eV and above this temperature it is 0.99 eV. β was found to be 0.37.

Resistance and TCR vs Temperature curves are given in Figure 3.20.

(3) Films annealed at 474K

The current-voltage characteristics and $\ln \sigma$ vs $10^3/T$ curves are given in Figures 3.21 and 3.22 respectively. As in the earlier cases the contact is ohmic at all temperatures. In Figure 3.22 the curves have two slopes as in the case of films annealed at 423K. The activation energies deduced from these slopes are $E_1 = 1.29$ eV below 328K and $E_2 = 1.02$ eV above this. β is equal to 0.45. Resistance and TCR vs Temperature curves are given in Figure 3.23.

(4) Films annealed at 523K

Films annealed at 523K showed properties similar to that of films annealed at 383K. The contact is ohmic

Fig. 3.18
 $\ln I$ vs $\ln V$ curves of a-Si film
 annealed at 423 K

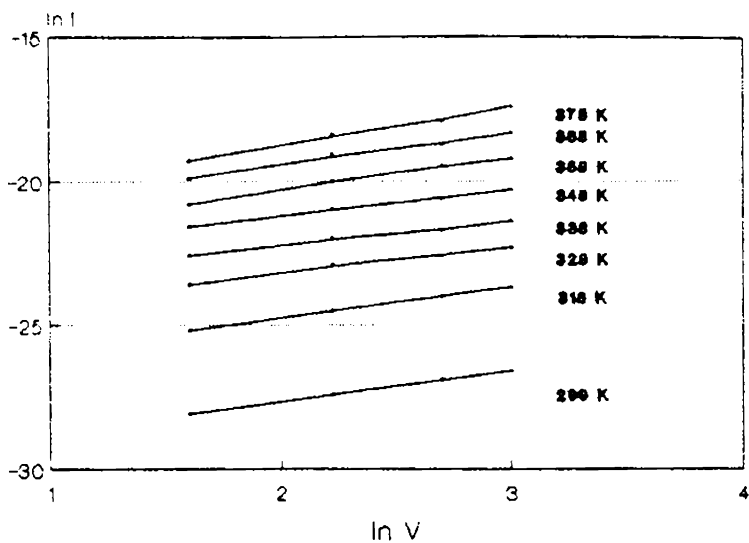


Fig. 3.19
 $\ln \sigma$ vs $10^3/T$ curve of a-Si
 film annealed at 423 K

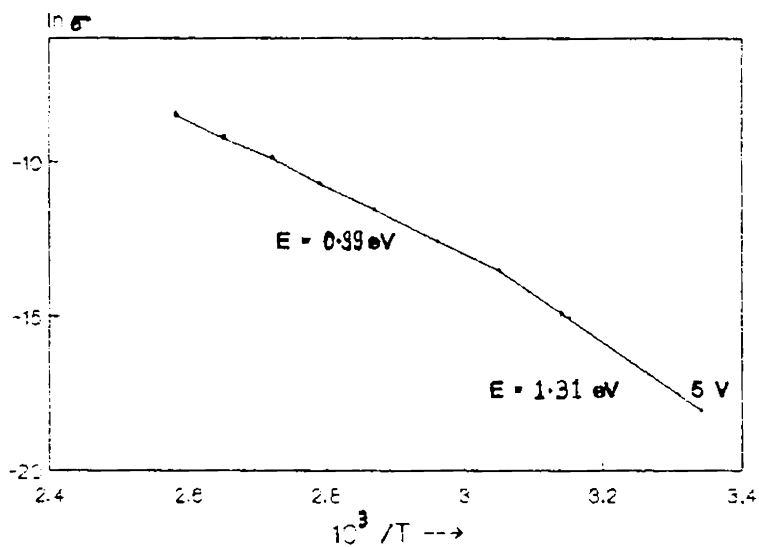


Fig. 3.20
 Resistance & TCR vs Temperature curves
 of a-Si film annealed at 423 K

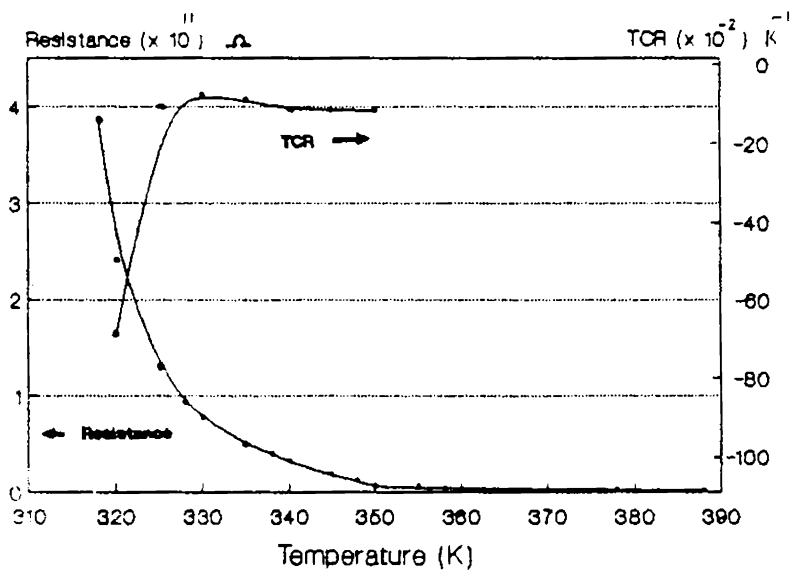


Fig. 3.21
 $\ln i$ vs $\ln V$ curves of a-Si film
 annealed at 473 K

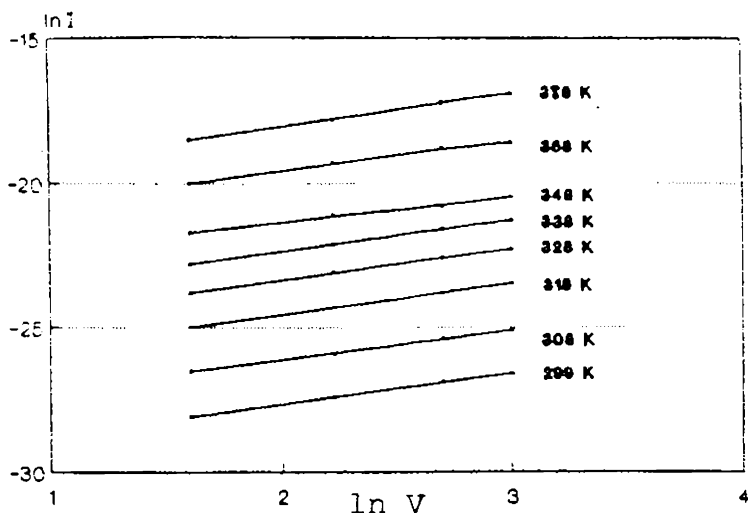
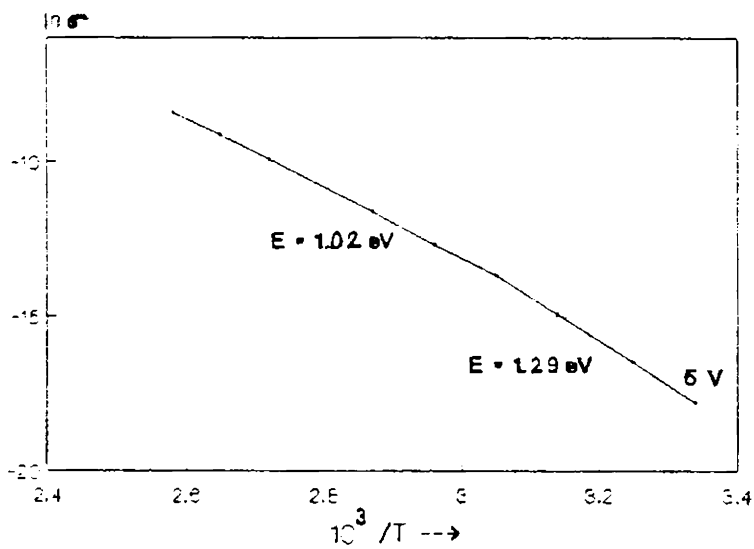


Fig. 3.22
 $\ln \sigma$ vs $10^3/T$ curve of a-Si
 film annealed at 473 K



Resistance & TCR vs Temperature curves
 of a-Si film annealed at 473 K

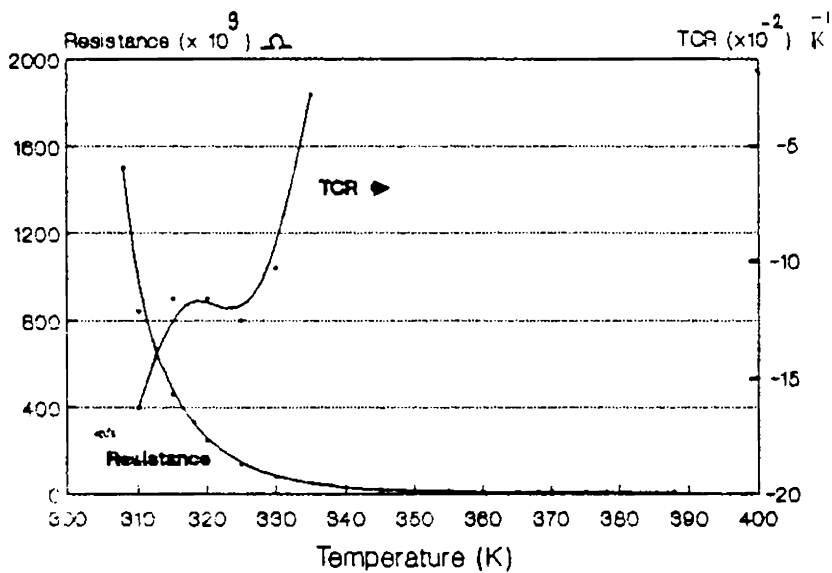


Fig. 3.24
 ln I vs ln V curves of a-Si film
 annealed at 523 K

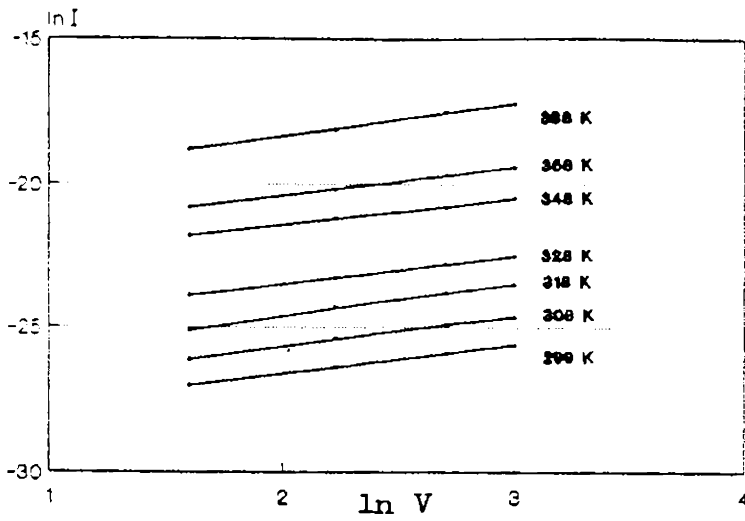


Fig. 3.25
 ln I vs $10^3/T$ curve of a-Si
 film annealed at 523 K

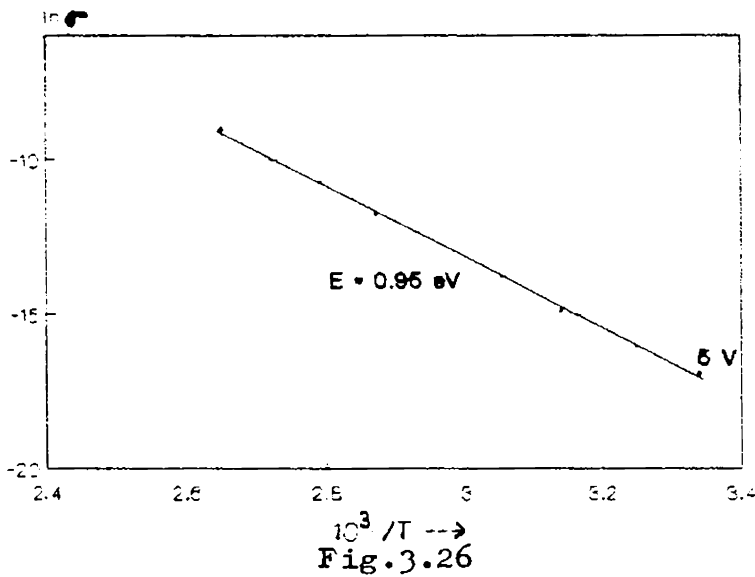
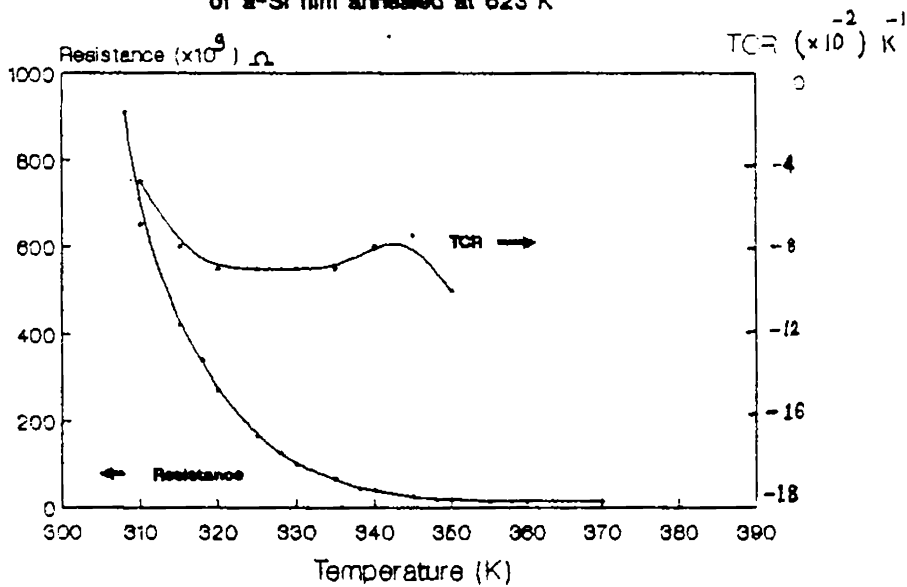


Fig. 3.26
 Resistance & TCR vs Temperature curves
 of a-Si film annealed at 523 K



at all measurement temperatures and $\ln \sigma$ vs $10^3/T$ curve exhibited only one slope showing a singly activated extended state conduction mechanism. The respective curves are given in Figures 3.24, 3.25 and 3.26.

The important observations are summarized in Table 3.10. From this table we see that as the annealing temperature was increased, the conductivity decreased. It is well known that evaporated thin films contain a lot of structural defects. Some of these defects can be annealed out by heat treatment. In general this will lead to a decrease in film resistivity. However, in certain cases heat treatment may lead to an increase in resistivity due to oxidation or agglomeration. Since in the present case, the films were annealed at $\sim 10^{-5}$ torr agglomeration seems to be the more probable reason for the increase in the resistivity than oxidation.

Another important observation is the appearance of two activation energies for films annealed at 423 and 473K. Here we observe a higher activation energy at lower measurement temperature. The existence of two activation energies was dealt with at length by Beyer et al. in the analysis of the transport properties of the glow discharge

Table 3.10

σ , σ_0 , E_a , β and TCR for films annealed at temperatures
383K, 423K, 473K and 523K

Annealing tempera- ture (K)	σ ($\Omega^{-1}\text{cm}^{-1}$)	σ_0 ($\Omega^{-1}\text{cm}^{-1}$)	E_a (eV)	β	TCR ($\times 10^{-2}\text{K}^{-1}$)
383	1.5×10^{-7}	6.8×10^8	1.08	1	-6.5(323K) -8.0(328) -11.0(333K)
423	1.6×10^{-8}	1.69×10^7	1.31 (High T)	0.37	-17.5(323K) -7.5(328K)
			0.99 (Low T)	0.37 0.37	-7.5(333K)
473	1.6×10^{-8}	4.13×10^7	1.29 (High T)	0.45	-2.2(323K) -11.0(328K)
			1.02 (Low T)		-8.6(333K)
523	4.4×10^{-8}	2.59×10^6	0.95	1	-9.5(323K) -9.0(328K) -9.0(333K)

produced a-Si:H alloys [19]. They have discussed about $\ln \sigma$ vs $10^3/T$ curves in which two activation energies are observed. Higher activation energies at lower temperatures are observed by them also with moderately Li doped a-Si:H films. But for highly doped films they got more conventional $\ln \sigma$ vs $10^3/T$ curves in which a higher activation energy occurred at higher temperatures. According to these researchers both the cases discussed above are due to the same mechanism namely the change in the statistical shift of the Fermi level and/or the band gap. This was first suggested by Rehm et al. in 1977 [20]. Beyer et al. have substantiated their argument by suggesting a transport model which assumes that the temperature dependence of the states responsible for electrical transport can be described by a rigid shift of the density of these states. Such a situation can arise for example, for polarons of different spatial sizes and thus with different coupling constants to lattice vibrations.

However in the analysis of the transport data of r.f. sputtered n-type a-Si:H films, Anderson et al. have discussed the same problem by assuming a two-transport level model [21]. This model was used by Jan et al. in 1979 to describe the behaviour of As doped a-Si:H and by

Jang et al. in 1980 for Li doped a-Si. In this model the explanation for the occurrence of two activation energies is that it marks a transition from one mechanism to another. According to them the total conductivity σ_{tot} can be written as

$$\sigma_{\text{tot}} = \sigma_1 + \sigma_2$$

The adjustable parameters in fitting the experimental data are σ_{01} , σ_{02} , E_1 and E_2 . By assuming suitable values for these parameters they claim that this model is adequate to explain the greater part of the experimental data although the fit in the region of the transition from one path to the other is not exact.

In the present case the two-transport model seems to be suitable to explain the observations. From Table 3.10 we observe that $\beta = 1$ for films annealed at 383K and 523K. This can occur in two cases: either when the contribution to the conduction from localized states and extended states is equal or when one mechanism (most probably the extended state conduction) completely takes over the conduction in the entire temperature range studied. Hence we can say that annealing at 383K results in an equally strong localized state conduction and extended state conduction.

But due to annealing at still higher temperatures the extended state conduction began to dominate as is evident from the β value (< 1) at these temperatures. Finally due to annealing at 523K the extended state conduction becomes completely dominant and a single activation energy is observed. Under such a circumstance it is not possible to define β . The decrease in the localized state conduction is a direct manifestation of the decrease in the density of localized states due to annealing out of defects.

3.14 Effect of annealing time on the electrical conduction in a-Si films

Annealing time is an important parameter in deciding the properties of a thin film. In this section the effect of annealing time on the electrical conduction in amorphous silicon films of thickness 930 Å is reported.

(a) Experimental

Eight films of same thickness (930 Å) were prepared in a single pump down, as discussed earlier. The area of the films was 1 cm². After deposition, the films were divided into four pairs and annealed separately at 383K for different durations of time, under a vacuum of $\sim 10^{-5}$ torr. First pair was annealed for 30 minutes second for 60 minutes third for 90 minutes and the fourth 120 minutes.

Each of these films was then subjected to current-voltage measurements at different temperatures.

(b) Results and discussion

The current-voltage characteristics of the films annealed for various intervals are presented in Figure 3.27. As before the contacts remain ohmic in all the cases. The $\ln \sigma$ vs $10^3/T$ curves are presented in Figures 3.28 and 3.29. Each curve has two portions with well defined slopes and a third irregular part above 376K. As the annealing time is increased from 30 to 120 minutes, the temperature at which the slope suddenly increases shifts to lower values (350 to 333K). In Figure 3.30 the conductivities are plotted against annealing time. The conductivity after an initial rise has fallen steadily with increase of annealing time. The dependence of the activation energies on annealing time is presented in Figure 3.31. The activation energies for temperatures below 328K exhibited only small differences among themselves while those above 328K varied widely with the annealing time.

The shift, of the point at which the slope of the $\ln \sigma$ vs $10^3/T$ curve suddenly changes to lower values, (Figures 3.28 and 3.29) means that as the annealing time increases from 30 minutes to 120 minutes, the transition from the localized state conduction to the extended state

Fig.3.27
ln I - ln V curves of a-Si films
annealed for different durations of time

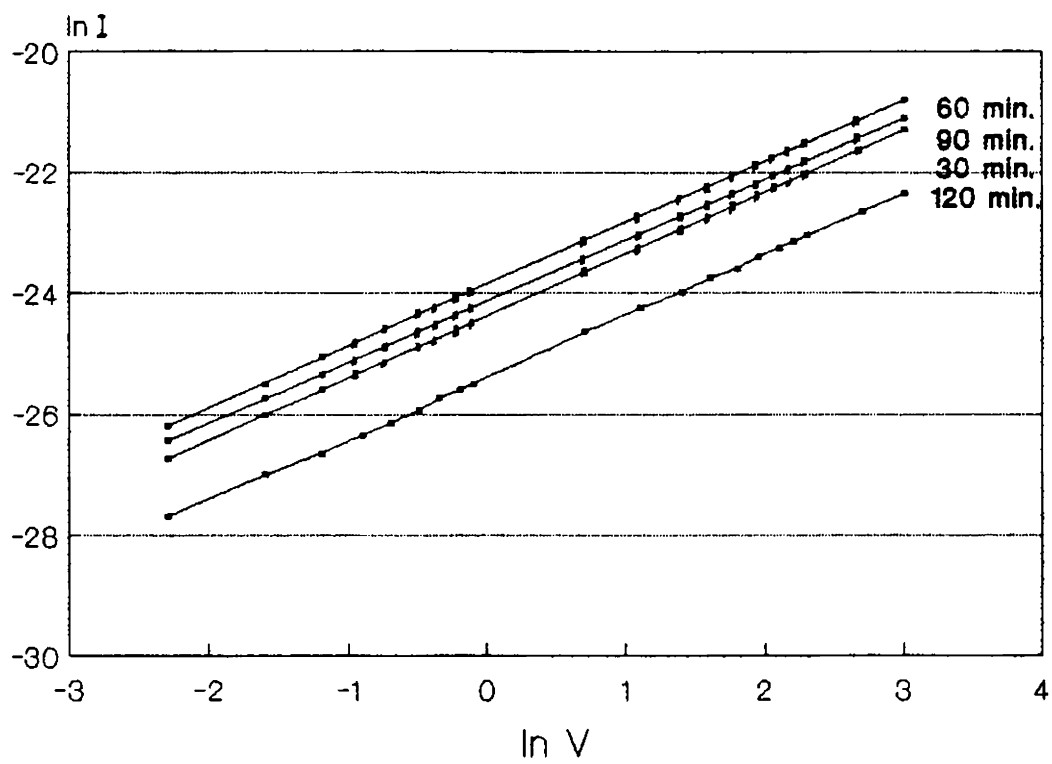


Fig.3.28
Effect of annealing time on the $\ln \sigma$ vs $10^3 / T$ curve of a-Si

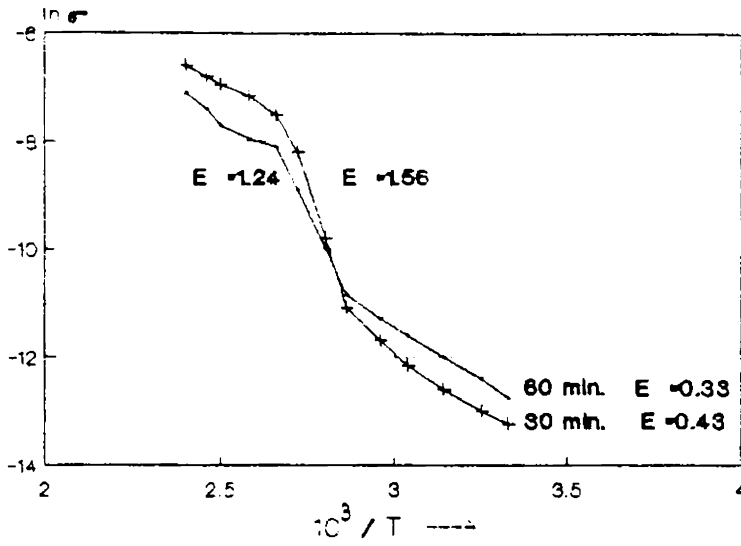


Fig.3.29
Effect of annealing time on the $\ln \sigma$ vs $10^3 / T$ curve of a-Si

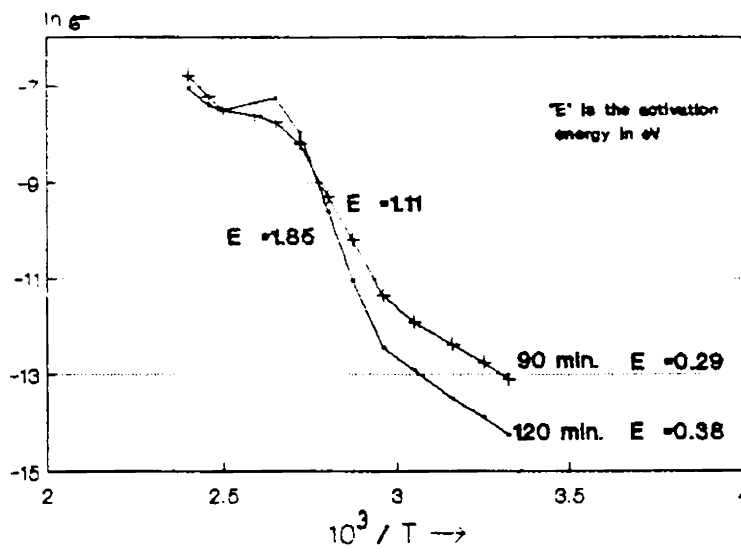


Fig.3.30

Conductivity vs annealing time plot
of a-Si thin films

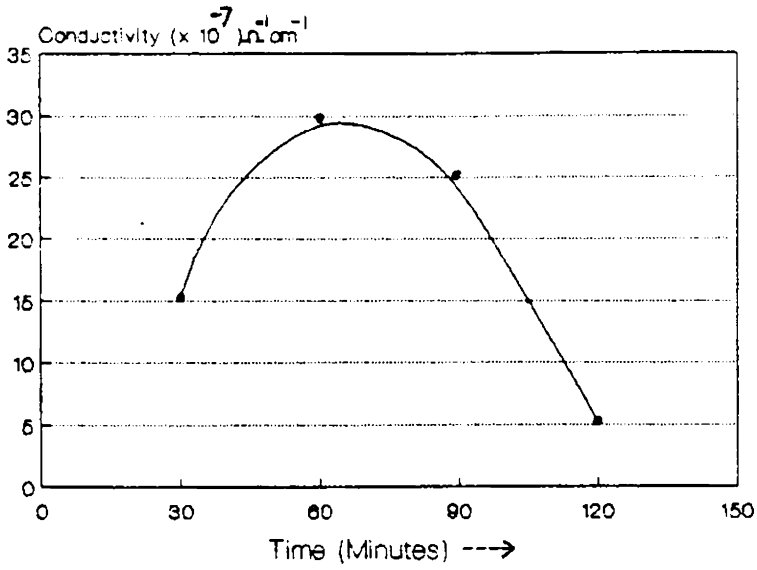
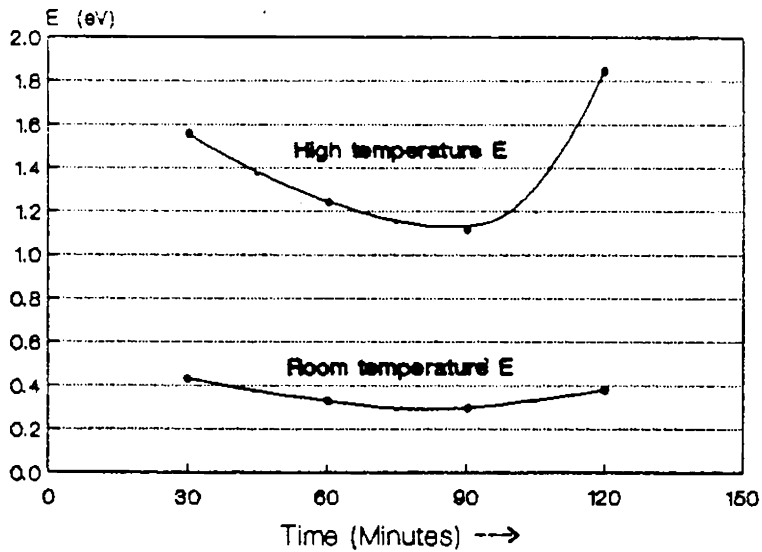


Fig.3.31

Dependence of the activation energies
of a-Si films on annealing time



conduction occurs at lower and lower temperatures. A somewhat similar phenomenon can be traced out from the $\ln\sigma$ vs $10^3/T$ curve of a-Si:H films annealed at different temperatures, reported by Dellafera et al. [9]. Here as the annealing temperature was increased from 378K to 613K the turning point in the curve shifted from 400K to 345K. The conductivity also decreases considerably due to increased annealing temperature in this case. Hence there is a general resemblance between the results of the gradually increasing annealing temperature and increasing annealing time. So this similarity in the results can be due to the same changes occurring in the films namely the annealing out of defects and the corresponding decrease in the localized state density. The behaviour of the low temperature activation energy shows that there is a strong band of trap levels between the conduction band and Fermi level whose position does not change much with time of annealing. The variation in the high temperature activation energy can be due to different annealing times.

3.15 Effect of substrate temperature on the electrical conduction in a-Si films

The substrate temperature is the most important variable in the thin film nucleation, since small changes

in it result in large changes of the supersaturation. The effect of an increasing substrate temperature is to lower the supersaturation, decrease the mean residence time of an adsorbed monomer and increase the surface diffusion coefficient of adsorbed monomers. It is reported that there is a critical condensation temperature above which the appearance of a condensed deposit cannot be observed. At certain substrate temperatures transition from one critical nucleus size to the next has been reported by many workers. Similarly onset of epitaxy might correspond to certain particular substrate temperatures [18]. The elevated substrate temperature in general supplies thermal energy for surface diffusion and ordering process at various stages of the growth of a thin film. Amorphous silicon films are deposited at different substrate temperatures and their electrical properties are studied in detail.

(a) Experimental

Films were deposited onto glass substrates keeping the substrates at temperatures of 323K, 423K, 523K and 623K. Two films were prepared at each temperature. The average value of the film thickness was 410 \AA . Thickness was controlled by evaporating a known amount of pure silicon. The films were not subjected to any annealing steps as it

would mask the effect of substrate temperature on the film properties. The films were transferred to the measurement cell immediately after the preparation and were subjected to current-voltage measurements at various temperatures.

(b) Results and discussion

The I-V characteristics given in Figure 3.32 show that the contact is ohmic for all the substrate temperatures. The variation of the conductivity with temperature for the four specimens is given in Figures 3.33 and 3.34. The dependence of the conductivity on the substrate temperature is presented in Figure 3.35. It is quite evident from the figure that as the substrate temperature (T_s) is increased from 323K to 423K the increase in the conductivity is negligible. But when T_s is increased further the conductivity increased rapidly and reached a value of $\sigma = 2.3 \times 10^{-6} \Omega^{-1} \text{cm}^{-1}$ which is higher by two orders of magnitude than the value of σ at $T_s = 323\text{K}$. The dependence of the activation energies measured at room temperature and at 385K are presented in Figures 3.36. If we take the conductivity at 385K we can see that it is nearly a constant for all substrate temperatures ($\sigma = 1.8 \times 10^{-4} \Omega^{-1} \text{cm}^{-1}$). But we can show that a decrease in E_a from 1.2 eV to 0.72 eV can cause a nearly

Fig.3.32
Effect of substrate temperature on
the I-V characteristics of a-Si films

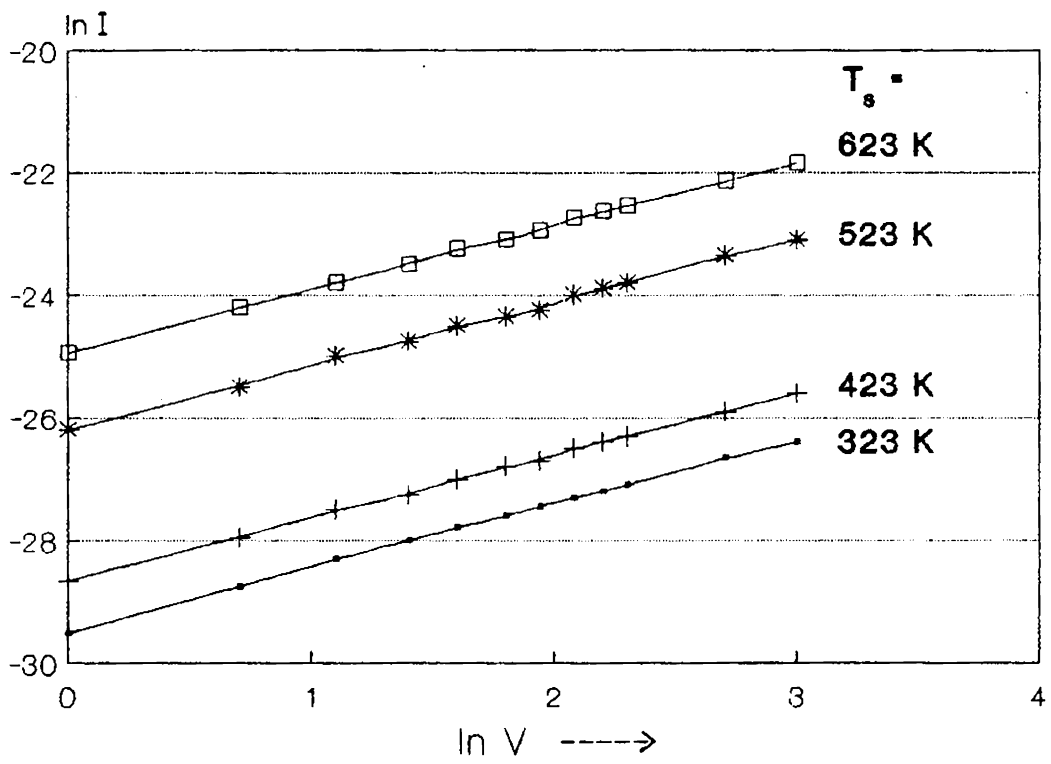


Fig.3.33

Effect of substrate temperature on the
 $\ln \sigma$ vs $10^3/T$ curve of a-Si films.

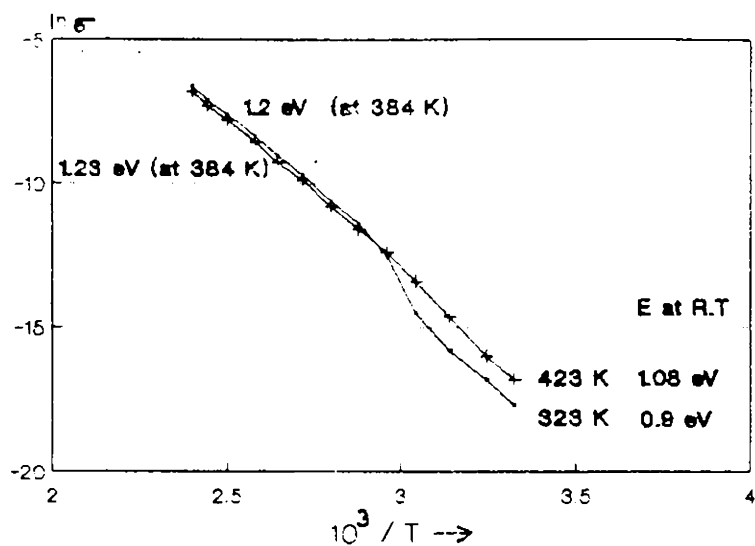


Fig.3.34

Effect of substrate temperature on the
 $\ln \sigma$ vs $10^3/T$ curve of a-Si films

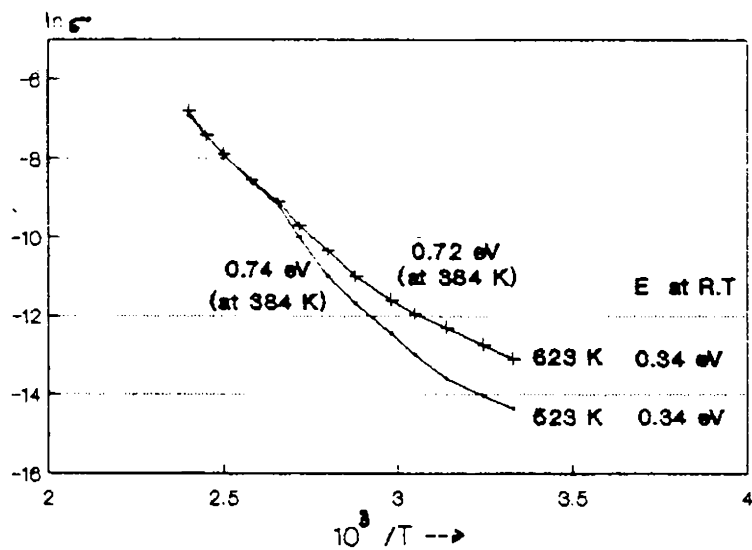
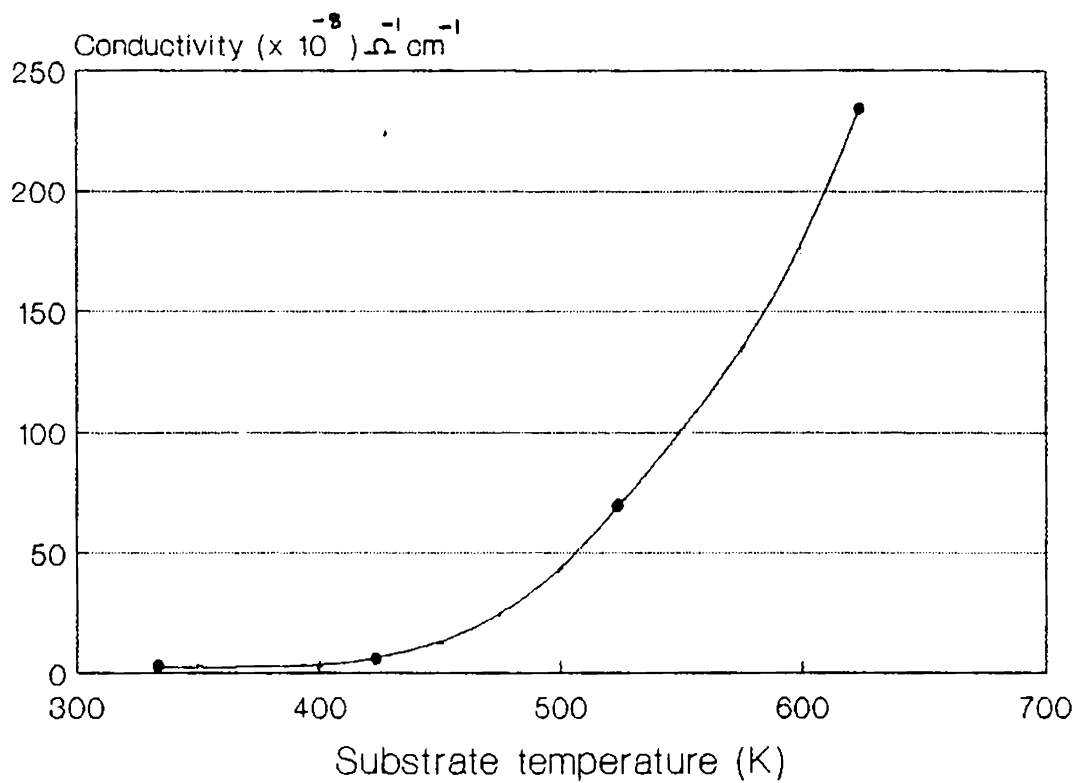


Fig.3.35

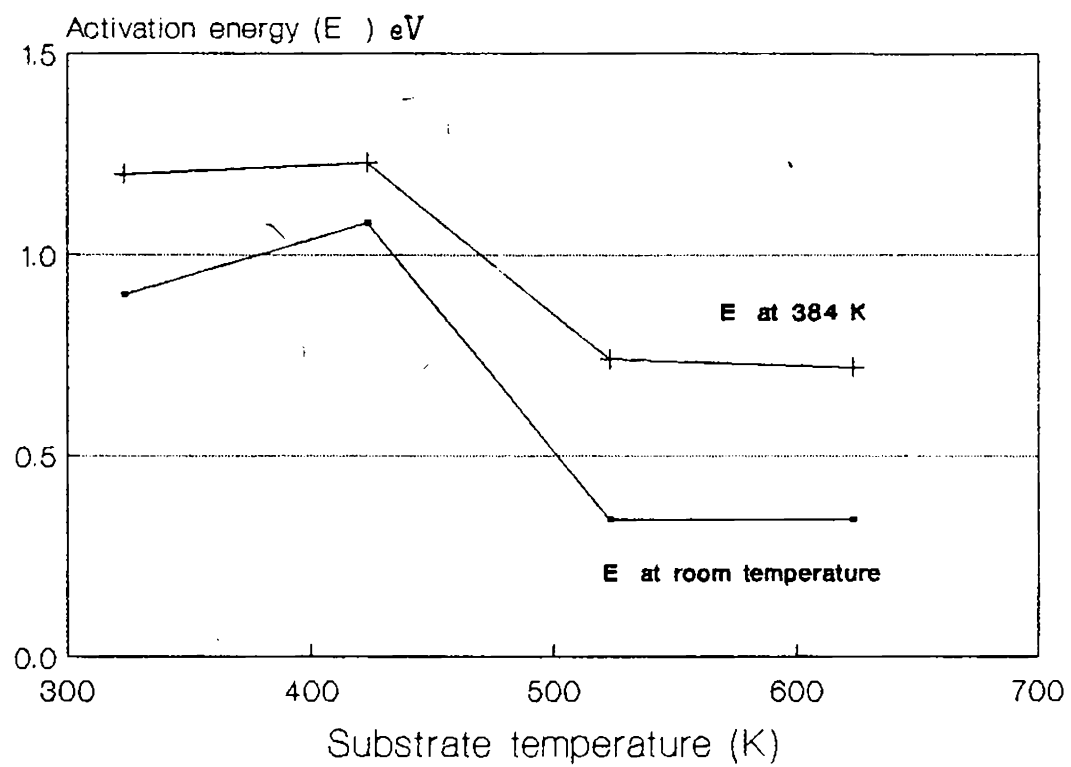
Effect of substrate temperature
on the conductivity of a-Si films



7
19.216:577.311 6.4 2.22
1.1

Fig.3.36

Effect of substrate temperature on the
activation energy of a-Si films



thirteen order increase in the value of the conductivity, if the pre-exponential factor remains a constant. Here the conductivity at 385K assumes a constant value irrespective of the decrease in the activation energy. This is due to the corresponding decrease in σ_0 . The same explanation holds good for the change in the conductivity at room temperature. Here also the activation energy decreases as the substrate temperature increases, but the pre-exponential factor σ_0 adjusts in such a way that the conductivity increases as observed in Figure 3.35. Such an explanation is given by Mott and Davis for the dependence of resistivity of a glow discharge produced amorphous silicon film on deposition temperature [Ref.18 page 295].

3.16 Thickness dependence of conductivity

As the thickness of a thin film is decreased, the transport of the charge carriers becomes more and more difficult due to size effects. This will show up in the electrical resistance of the films. This effect may not be a gradual one but can be a sharp step around certain critical thickness. Such a variation in the conductivity was reported earlier around 5000 Å by Ast et al. [5]. In the present study it is found that the conductivity decreases by two orders as the film thickness goes below ~ 590 Å and is presented in Figure 3.37. The room temperature activation

Fig.3.37
Effect of film thickness on the
conductivity of a-Si thin films

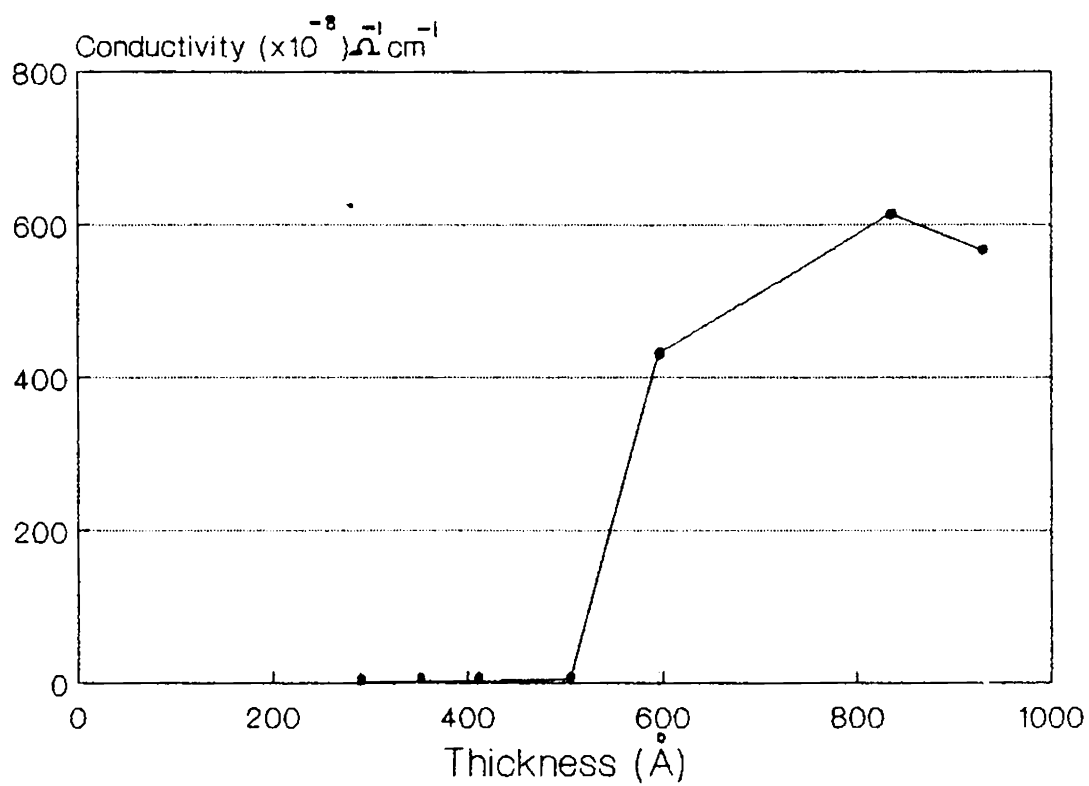


Fig.3.38

Effect of film thickness on the
 $\ln \sigma$ vs $10^3 / T$ curve of a-Si

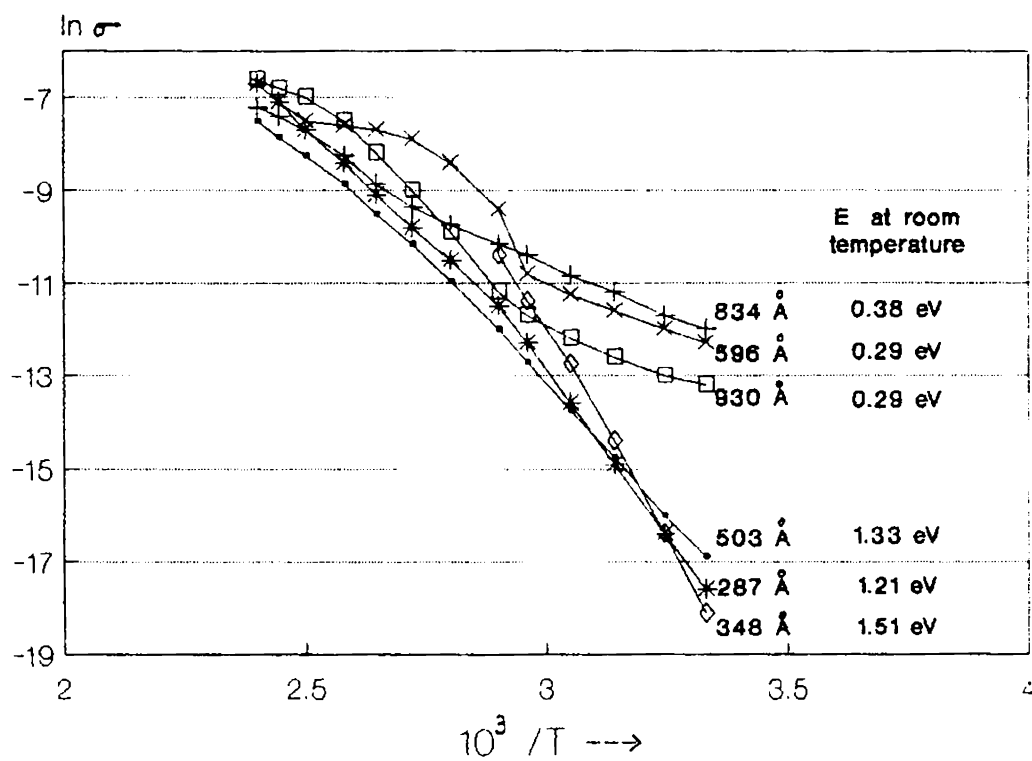
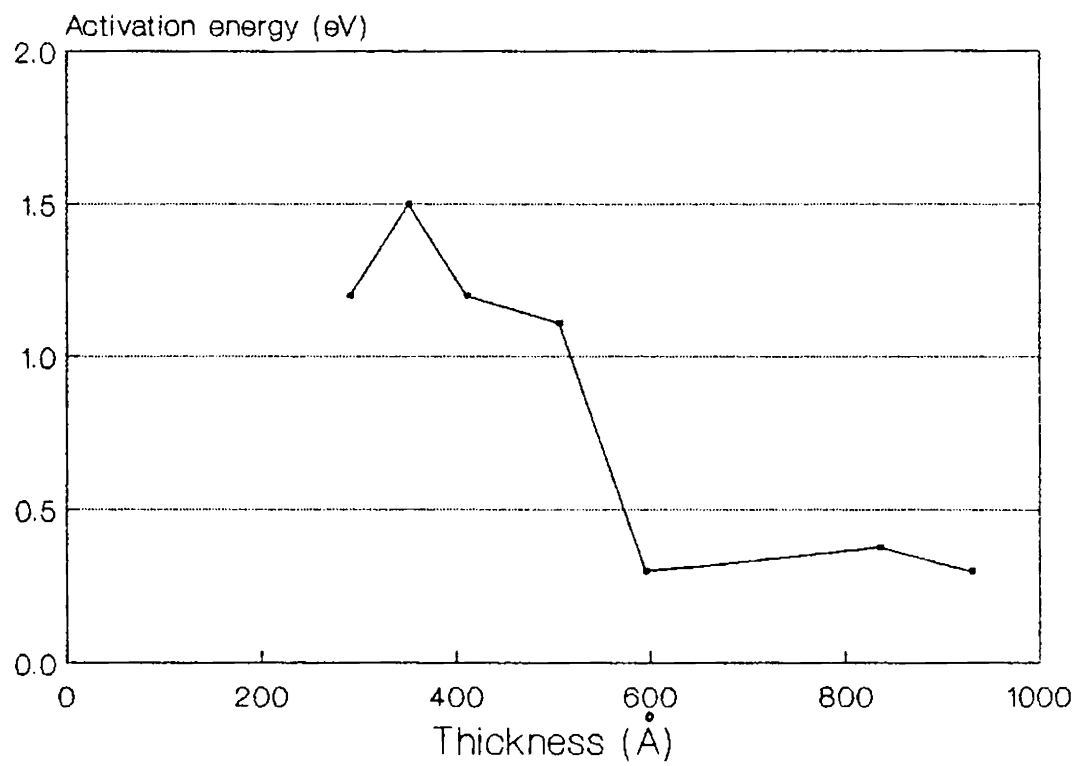


Fig.3.39

Effect of film thickness on the activation energy of a-Si thin films



energies were calculated from $\ln \sigma$ vs $10^3/T$ curves given in Figure 3.38 and is plotted against thickness in Figure 3.39.

Just as in the case of Figure 3.37 where it was found that the value of σ changes abruptly between 500 Å and 595 Å, a sudden change in the room temperature activation energy between 500 Å and 595 Å is observed. In a similar study conducted by Ast et al. [5] in glow discharge produced, phosphorus doped a-Si:H films with thicknesses ranging from 0.099 μm to ~ 4 μm, it was found that the room temperature activation energy decreases above a film thickness of 0.5 μm and assumes a value of 0.22 eV. For thicknesses less than 0.5 μm the activation energy increases suddenly and reaches a value of 0.41 eV for a thickness of 0.099 μm. But in the present case the study was concerned more with thinner and undoped unhydrogenated samples. It can be seen that in this case, the variation of the activation energy is much higher than the reported values of Ast et al. [i.e., 1.5 eV for 348 Å and 0.25 eV for 930 Å].

3.17 Effect of hydrogenation temperature on the electrical properties of hydrogenated amorphous silicon films

As discussed in Chapter 1, the post hydrogenation of amorphous silicon has several advantages over the glow

discharge method. In the present method of annealing a-Si in a hydrogen plasma, the temperature of annealing is a very critical parameter, as it can control the diffusion, adsorption and residence time of the ionized gas molecules on the film surface. So it was felt necessary to carry out a detailed investigation on the effect of the temperature of hydrogen plasma annealing on the electrical properties of the amorphous silicon films.

(a) Experimental

Eight films of amorphous silicon of the same thickness (437 \AA) were prepared in the same run. These films were then hydrogenated by annealing them in hydrogen plasma at different temperatures as discussed in Chapter 2. The temperatures used were 300K, 395K, 523K and 573K. Two films were annealed at each temperature. The hydrogen partial pressure was 0.05 torr. The hydrogenated films were immediately transferred to another coating unit for the deposition of aluminium electrodes and were subjected to various measurements.

(b) Results and discussion

The d.c. electrical conductivity was studied by measuring the current-voltage characteristics from 16 V/cm to 80 V/cm and is presented in Figure 3.40. From the

Fig.3.40

Effect of hydrogenation temperature on the I-V characteristics of α -SiH films

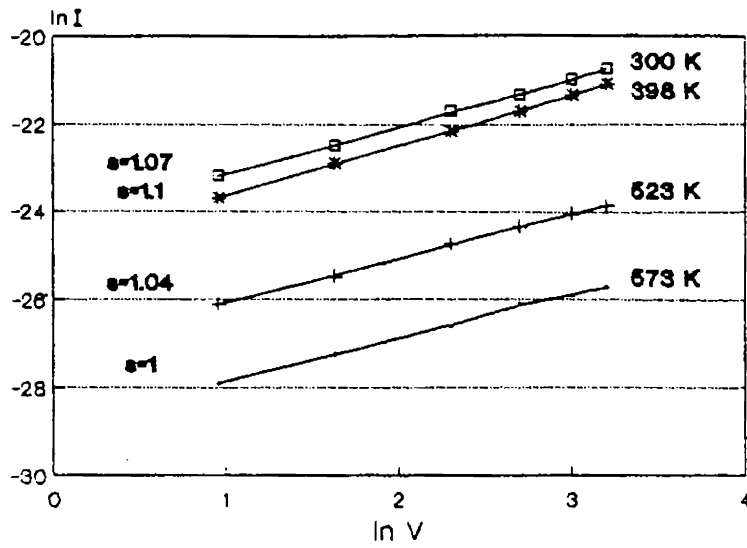
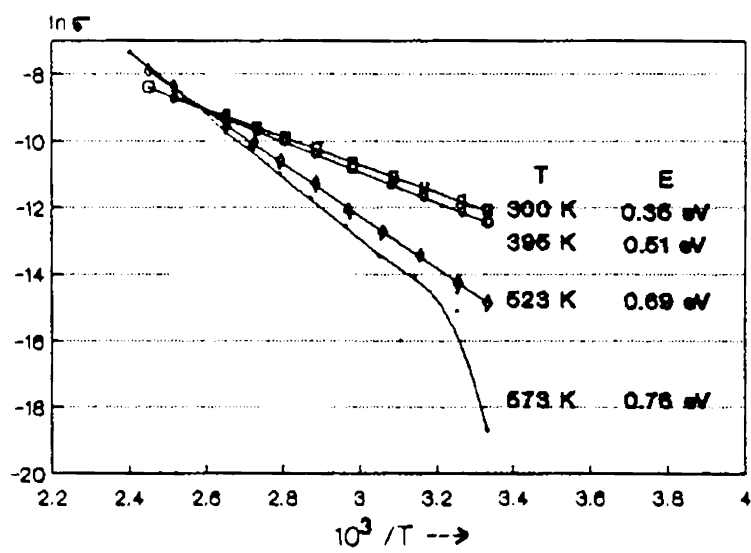


Fig.3.41

Dependence of the $\ln I_0$ vs $10^3/T$ curve on hydrogenation temperature



$\ln \sigma$ vs $10^3/T$ curve given in Figure 3.41, the following observations can be made.

1. $\sigma_{d.c}$ decreases with increasing hydrogenation temperature.
(Figure 3.42)
2. The activation energy (E_a) and the pre-exponential factor (σ_0) increases with increasing hydrogenation temperature.
3. At a temperature T_c [= 392K] all films irrespective of their hydrogenation temperature exhibited a constant conductivity $\sigma_c = 1.01 \times 10^{-4} \Omega^{-1} \text{cm}^{-1}$.

Since E_a can be considered as ($E_c - E_F$), the distance of the Fermi level from the conduction band mobility edge, for extended state conduction [19], it can be seen from Figure 3.42 that as the annealing temperature is increased the Fermi level goes down in the mobility gap. It should be noted that similar studies carried out on unhydrogenated samples yielded activation energies ranging from 0.94 eV to 1.3 eV in the high temperature region. So it has become evident that due to annealing in hydrogen plasma, E_a decreased and reached a minimum value of 0.35 eV for films subjected to hydrogen plasma at room temperature (300K) for 60 minutes. This indicates a successful incorporation of hydrogen [11]. Intrinsic conditions were obtained for these films at an annealing temperature of 573K, with $E_a = 0.76$ eV

Fig.3.42

Effect of hydrogenation temperature on the conductivity & activation energy

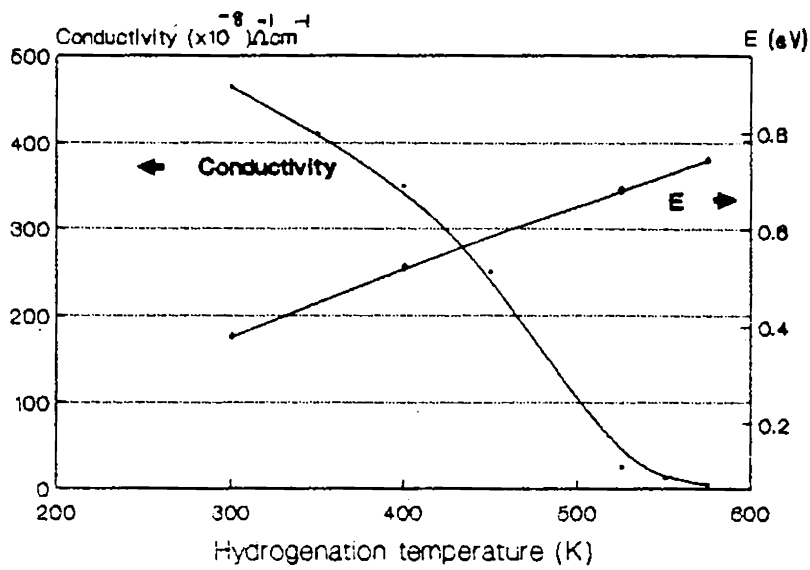
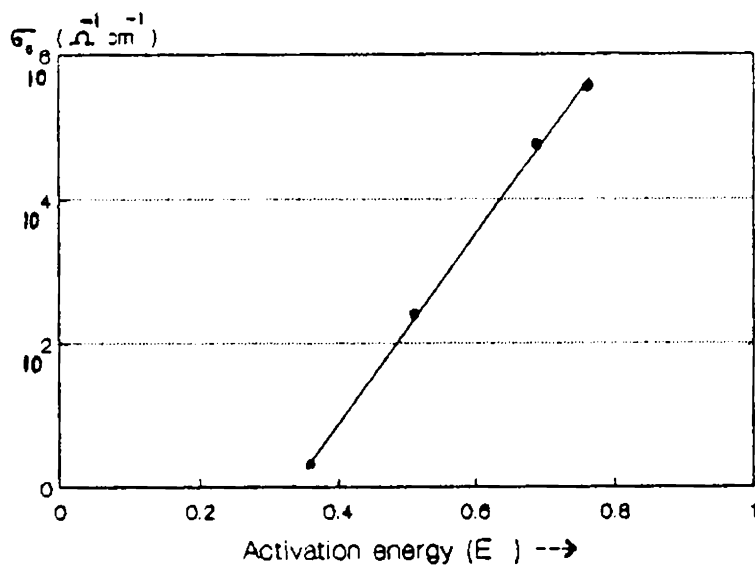


Fig.3.43

Relation between the pre-exponential factor and activation energy of a-Si:H



$\sigma = 4 \times 10^{-9} \Omega^{-1} \text{cm}^{-1}$. These values are comparable to the values reported for glow discharge produced films. At lower temperatures there is a possibility of some hydrogen going into the interstitial positions which itself can create gap states. But at higher temperatures since the sticking time of hydrogen ions impinging upon the film surface will be less, only those ions which get firmly bonded to the unpaired silicon atoms can stay in the film. This will cause a considerable reduction in the gap states and lowering of the conductivity.

The pre-exponential factor σ_0 was found by extrapolating the $\ln \sigma$ vs $10^3/T$ curve towards the y-axis. σ_0 was also calculated using equation (3.10), by putting $\sigma = \sigma_c$ and $T = T_c$. The calculated and extrapolated values were found to agree supporting the earlier observation of constant σ_c at T_c . This enabled us to verify the dependence of σ_0 on E_a (Figure 3.43). Similar behaviour (i.e., dependence of σ_0 on E_a) was reported earlier for glow discharge produced a-Si:H films which was attributed to the statistical temperature shift in the Fermi level [24,25].

3.18 Effect of hydrogen partial pressure

(a) Experimental

Thin films of a-Si of thickness 450 \AA were prepared as discussed earlier. These films were then hydrogenated

Fig.3.44

Effect of hydrogen partial pressure on
the I-V curve of a-Si:H thin films

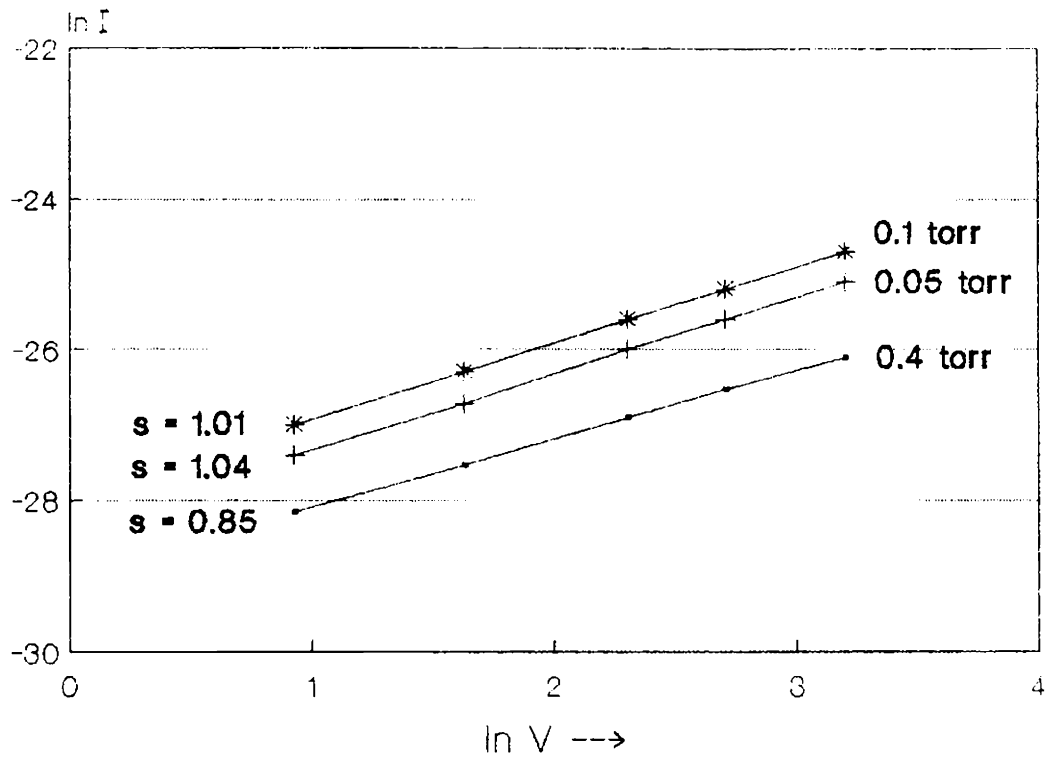
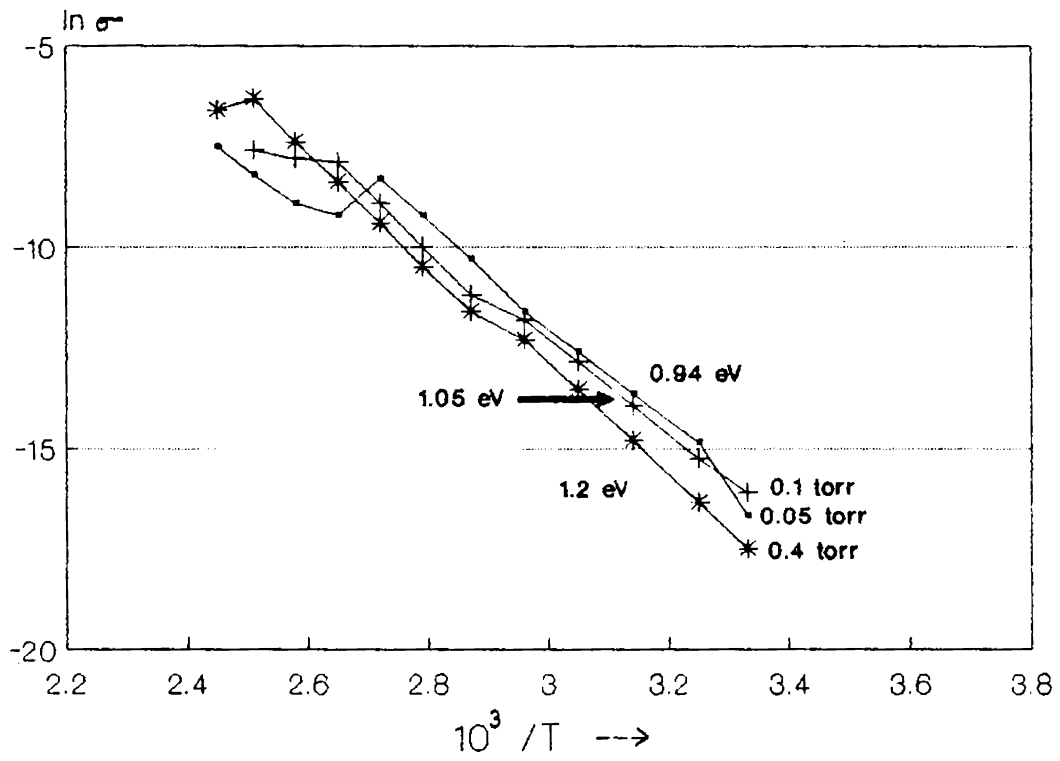


Fig.3.45

Effect of hydrogen partial pressures on
the $\ln \sigma$ vs $10^3 / T$ curve of a-Si:H



by keeping the partial pressure of the hydrogen at 0.4 torr, 0.1 torr and 0.05 torr. When the pressure was below 0.05 torr, the plasma became unstable. The annealing temperature was 573K and time duration 60 minutes. After hydrogenation the films were given aluminium electrodes in the planar structure and were subjected to measurements.

(b) Results and discussion

The current-voltage characteristics of the films are presented in Figure 3.44. In Figure 3.45 variation of $\ln \sigma$ with inverse temperature is given.

The minimum conductivity of $2.8 \times 10^{-8} \Omega^{-1} \text{cm}^{-1}$ was obtained for films annealed at 0.4 torr. But in this case it was found that the slope of the I-V curve is only 0.85. In the case of films annealed at 0.1 torr pressure the conductivity was $1.02 \times 10^{-7} \Omega^{-1} \text{cm}^{-1}$ and the slope of the curve (1.01) indicated a good ohmic contact. For films annealed at 0.05 torr the conductivity was $6.8 \times 10^{-8} \Omega^{-1} \text{cm}^{-1}$ and the contact was ohmic (slope = 1.04). Activation energies were calculated from Figure 3.45. The highest value was obtained for the films annealed at a pressure of 0.4 torr ($E_a = 1.2 \text{ eV}$) and the lowest value ($E_a = 0.94 \text{ eV}$) for those annealed at a pressure of 0.05 torr. It is already well established by different researchers that due to successful

hydrogenation the dark conductivity and the density of gap states decrease [6] and the Fermi level moves towards the conduction band and the activation energy lies near 0.7 to 0.8 eV [11]. Considering all these we can say that a hydrogen partial pressure of 0.05 torr in the chamber is sufficient to successfully hydrogenate a-Si films.

3.20 A.C.conduction in a-Si and a-Si:H thin films

3.21 Introduction and theory

Frequency dependence of conductivity in disordered solids has attracted so many researchers and a great amount of work has been reported in this direction. A variation of σ with frequency (ω) is expected if the conductivity of the material is inhomogeneous on a macroscopic scale. For example it has been reported that a material of bulk conductivity σ_0 contains barriers with bulk conductivity σ_B occupying a fraction 'f' of the volume, an elementary analysis shows that, for $\omega < 16\pi^2 \sigma_0 \sigma_B$ conductivity is proportional to σ_B for $\omega > \sigma_0$ the conductivity is σ_0 and between these limits it increases as ω^2 .

Pollak [3] has observed that the a.c. conductivity studies carried out on materials such as As_2Se_3 [26-30],

As_2S_3 [27], As_2Te_3 [31], Al_2O_3 [32], CS_2 [33], GeTe [34], Ge [34] and V_2O_5 [35] reveal that,

1. The conductivity is a nondecreasing function of frequency which indicates hopping conduction by electrons or ions.
2. In all the materials there exist a range of frequency in which $\sigma(\omega)$ varies as the first power of frequency or slightly less rapidly.
3. In certain materials there is a region in which $\sigma(\omega)$ varies as the second power of ω and this appears at the higher frequencies.
4. In certain materials at high frequencies $\sigma(\omega)$ varies very slowly with ω . Such a slowly varying region can occur also near $\omega = 0$.
5. The temperature dependence of $\sigma(\omega)$ is more pronounced where σ varies as ω than it is where σ varies as ω^2 and
6. The changeover from linear to quadratic regions of $\sigma(\omega)$ occur approximately at 10^6 Hz.

Pollak has proposed a theory suitable for hopping conduction in the pseudogap of amorphous semiconductors and derived expressions applicable under various conditions. It has been pointed out by Mott and Davis [6] that all the three mechanisms that contribute to direct current in amorphous semiconductors can contribute also to the a.c. conductivity. Three mechanisms of a.c. conductivity as given by Mott and Davis are given below.

(a) Transport by carriers in the extended states near E_c or E_v . For this $\sigma(\omega)$ is given by the formula

$$\sigma(\omega) = \sigma(0) / (1 + \omega^2 \tau^2) \quad (3.14)$$

Since the relaxation time τ is of the order of 10^{-15} s, equation (3.14) is not really applicable for such small values of τ . Even when τ is large, deviation from this formula are expected if the density of states varies with energy over a range of h/τ . So it can be said that upto 10^7 Hz no frequency dependence of the conductivity due to carriers in the extended states is expected.

(b) Transport by carriers excited into the localized states at the band edges can be a possibility when the conductivity varies approximately as $\omega^{0.8}$. The temperature

dependence of this component of the a.c. conductivity should be the same as that for the part of d.c. conductivity involving excitation to the band edges. For the valence band it must vary as

$$\exp -(E_F - E_B)/kT$$

where E_B is the energy at the band edge.

(c) The third mechanism is the hopping by carriers near the Fermi level. The frequency dependence will be the same as that for process (b) but the temperature dependence will be proportional to T , if kT is small compared to the width of the occupied part of the defect band and independent of T otherwise. Accordingly $\sigma(\omega)$ is obtained by Austin and Mott [31] as

$$\sigma(\omega) = \frac{1}{3} \pi e^2 kT \{N(E_F)\}^2 \alpha^{-5} \omega \left\{ \ln(\nu_{ph}/\omega) \right\}^4 \quad (3.15)$$

Here $N(E_F)$ is the density of states at the Fermi level and α^{-1} is a measure of the spatial extension of the wave function $\exp(-\alpha r)$ associated with localized states. ν_{ph} is the phonon frequency.

In 1977 Elliott [18] pointed out certain defects in the Austin-Mott theory and proposed a new theory of a.c.

conductivity [1,2] for amorphous materials. His objections to the Austin-Mott (AM) theory were the following.

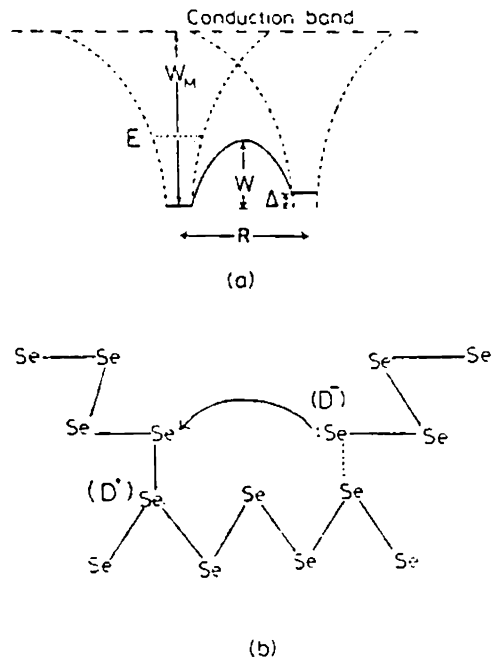
1. According to the AM theory $\sigma_{a.c.}$ is directly proportional to temperature T , which is rarely observed in experiments.
2. The slope (s) of the a.c. conductivity vs frequency plotted double logarithmically is not a constant but is dependent on the frequency of the applied field.
3. Taking a reasonable value of ν_{ph} ($\sim 10^{13}$ Hz) and choosing $\omega \sim 10^4 \text{ S}^{-1}$, slope (s) is observed as 0.81. Higher values of s is obtained only by taking unreasonably large values for ν_{ph} .
4. There is no explicit dependence of the slope on T . But a temperature dependence can arise if the carrier forms a polaron of binding energy W_p . But then the theory predicts a decrease in the slope as T is decreased, contrary to the experimental observation where the slope decreases as T increases.
5. Finally the density of states obtained by AM theory yields values which are larger by several orders of magnitude compared to that deduced by other means.

According to Elliott's theory an electrical conductivity having a frequency dependence ω^s where $s < 1$ can occur due to the hopping of two electrons over a potential barrier between defect sites, the height of the barrier being correlated with the intersite separation. The hopping process is explained as follows. Carriers are ejected from a D^- site (Figure 3.46a) into one of the excited levels designated as E in Figure 3.46(b). Assuming that a two electron wave function can exist within the potential spanning both centres, the carriers may transfer to the neighbouring site without recourse to tunnelling. The carriers ejected from the initial D^- centre drop into the D^+ centre, converting it to a D^- . The energy W_M , assumed to be constant here, is the energy that would be required to take two electrons from the D^- state to the conduction band in the absence of a nearby D^+ centre. The energy Δ is the difference in energies between two D^- sites owing to randomness. The potential barrier W over which carriers must hop is the random variable in the problem. Variations in W arise from variations in the distance R separating the two centres.

The final expression for the a.c. conductivity is given by

$$\sigma_{a.c}(\omega) = \frac{\pi^2 N K}{24} \left[\frac{8e^2}{K W_M} \right]^6 \frac{\omega^s}{\tau_0^\beta} \quad (3.16)$$

Fig. 3.46



- (a) Schematic diagram of the potentials experienced by carriers a distance R apart. W_M is the energy required to remove two electrons from a D^- centre to form a D^+ , W is the height of the barrier over which the carriers must hop. Bound states designated by the intermediate stage of the hopping process are designated by E .
- (b) Schematic diagram of the hopping process considered here. Two electrons transfer from a D^- to a D^+ centre which thereby exchange places (represented by the dotted line).

where N is the density of states at the Fermi level, K is the dielectric constant, e is the electronic charge, ω is the frequency of measurement and $\beta = (1-s)$. W_M , the thermal energy required to remove two electrons from a D^- state, is given by

$$W_M = B - W_1 + W_2 \quad (3.17)$$

where B is the band gap energy of the material and W_1 and W_2 are approximately the distortion energies associated with the D^0 and D^+ states respectively. It is assumed that no distortion energy is associated with the D^- state since it does not bond with a lone pair orbital.

The slope s of the $\ln \sigma_{a.c}$ vs $\ln \omega$ plot is related to β , the power of the relaxation time τ_0 , in equation (3.16), by the relation

$$s = (1 - \beta)$$

β is given by

$$\beta = \frac{6kT}{W_M} \quad (3.18)$$

where k is the Boltzmann constant and T is the absolute temperature.

Substituting this value of β in the equation for s we get

$$s = 1 - \frac{6kT}{W_M} \quad (3.19)$$

Equation (3.19) predicts that as T increases s decreases as is often found in experiments. The density of states calculated using this model for so many chalcogenides agree well with those derived by other methods. Eventhough the theory is well suited for chalcogenide glasses there arise certain serious problems when it is employed for other amorphous semiconductors. These are given below.

1. As pointed out by Elliot himself the approximation of the binding energy (W_M) as the band gap energy is not possible in the case of non-chalcogenide amorphous materials. This is due to the reason that the top of the valence band in chalcogenides is derived from the lone-pair orbitals of the chalcogen [37]. Hence significant rearrangements in chemical bonding may take place within the glass and utilizing the lone-pair orbitals, the chalcogen atoms can become overcoordinated. It is these arrangements that can be responsible for doubly occupied defect states. Such a bipolaron formation could be expected to be much less prevalent in tetrahedrally bonded materials, since no lone-pair orbitals

exist in them. However, David Emin has suggested that formation of bipolarons is possible in the case of certain amorphous semiconductors [40].

2. The slope s of the $\ln \sigma$ vs $\ln \omega$ is given by equation (3.19). From this equation we can see that the maximum value s can assume is only 1 corresponding to $T = 0$ or $W_M = \infty$. Hence in the practical cases s can assume a maximum value just below 1.

3.22 Experimental

Amorphous silicon films of thickness 460, 500, 840 and 1312 Å were prepared on glass substrates pre-coated with aluminium electrodes. These films were then subjected to hydrogenation as described in Chapter 2. The hydrogen partial pressure, hydrogenation time and temperature were 0.05 torr, 60 minutes and 573K respectively. The hydrogenated films were taken out and counter aluminium electrodes were deposited with an electrode overlapping area of 0.88 cm². The a.c. conductivity of the films were studied using the HP 4277 A LCZ bridge as a function of frequency in the range 10 kHz to 1 MHz and temperature in the range 300K to 398K.

3.23 Results and discussion

The frequency dependence of $\sigma_{a.c}$ is given in Figures

3.47A and 3.47B for different temperatures for two films ($t = 500 \text{ \AA}$ and 1312 \AA). It can be seen from Figure 3.47A that there are five well defined regions in the graph. The lowest slope occurs from 10 kHz to 30 kHz. The slope in this region varies from 1 to 1.14. From 30 kHz to 90 kHz the slope varies from 1.42 to 1.67. Generally the slope decreased as the measurement temperature was increased. The slope of the curve is slightly higher above 90 kHz. This is the third region. At 157 kHz--well within the third region--all the curves crossed each other. The maximum conductivity was observed in the fourth region; i.e., from 300 kHz to 400 kHz. In this region, the conductivity remained almost a constant as the frequency was increased and any further increase caused the conductivity to decrease. In this region at 636 kHz the curves again crossed each other. The slope in this region varied from 1.25 to 1.74. It is interesting to note from Figure 3.48 in which $\ln \sigma_{a.c}$ vs $10^3/T$ is plotted that while in regions one and two the film has negative temperature coefficient of a.c. resistance, in region three it has positive temperature coefficient. At a measurement frequency of 30 kHz a 66.7% increase in $\sigma_{a.c}$ was observed as the measurement temperature varied from 300K to 423K. The temperature dependence of the slope decreased as the measurement frequency was increased. Film 2 ($t = 1312 \text{ \AA}$) exhibited

Fig. 3.47(A)
 Dependence of the a.c. conductivity of
 a-Si:H on the frequency of measurement

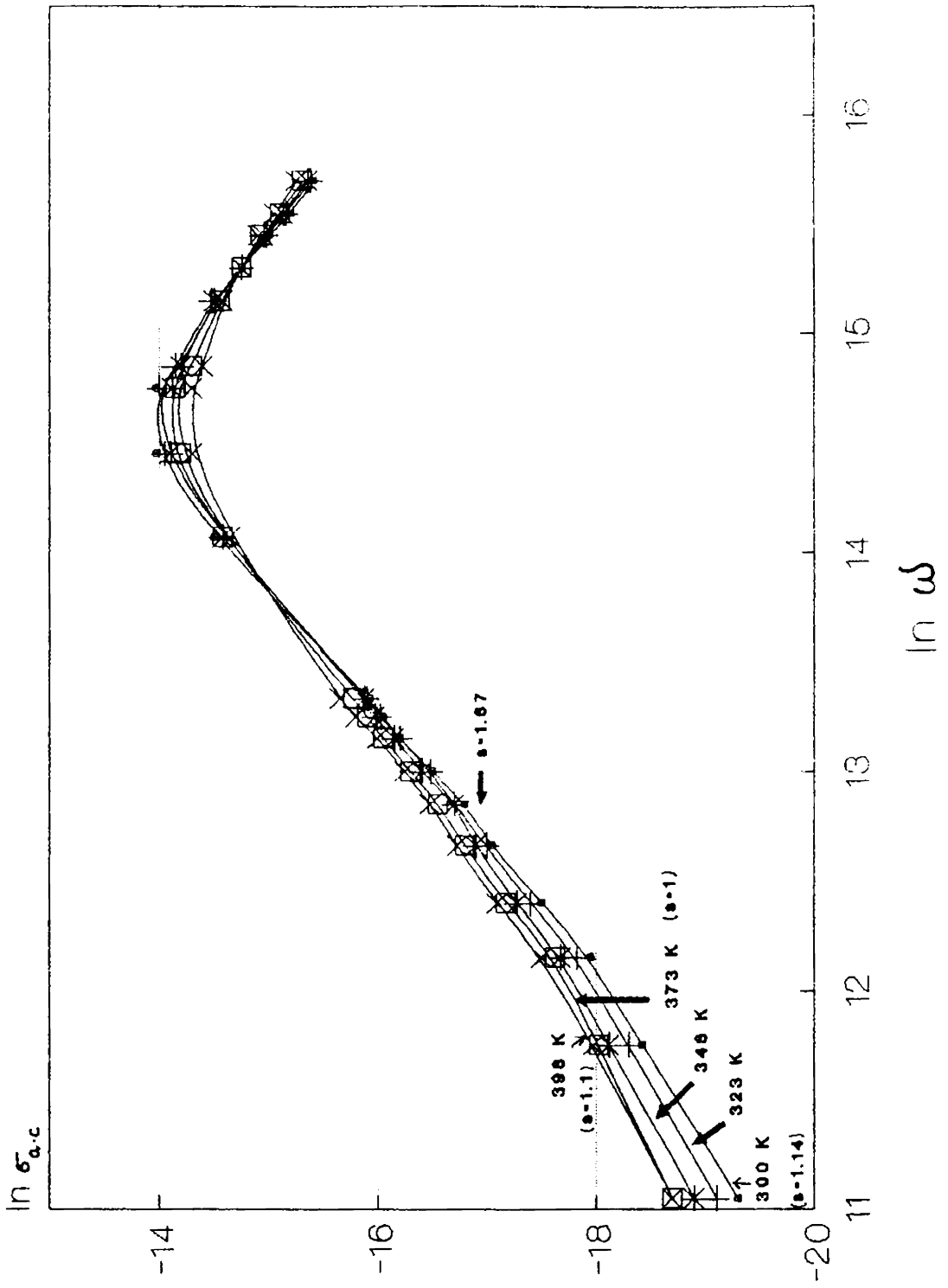


Fig.3.47(B)

Dependence of the a.c conductivity of
a-Si:H on the frequency of measurement

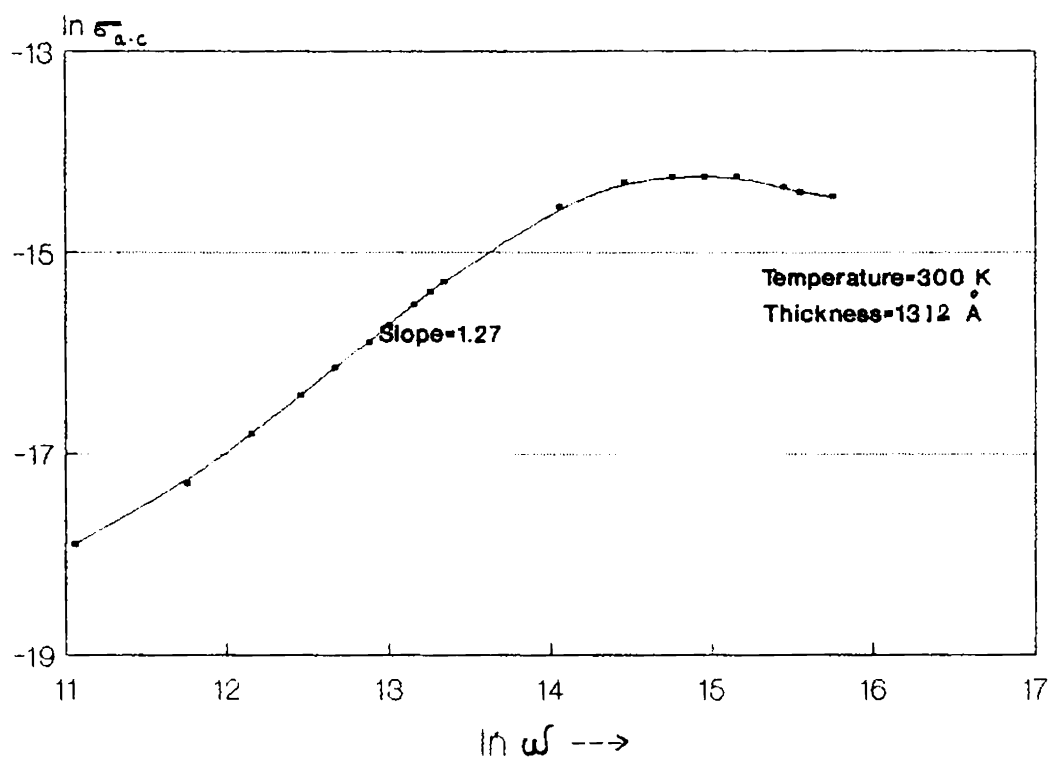


Fig.3.48

$\ln \sigma_{ac} 10^3 / T$ curves for a-Si:H films at different frequencies

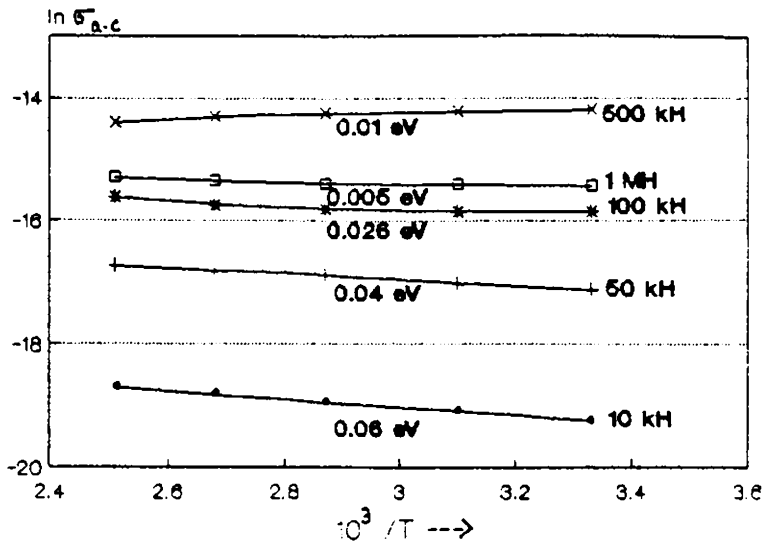
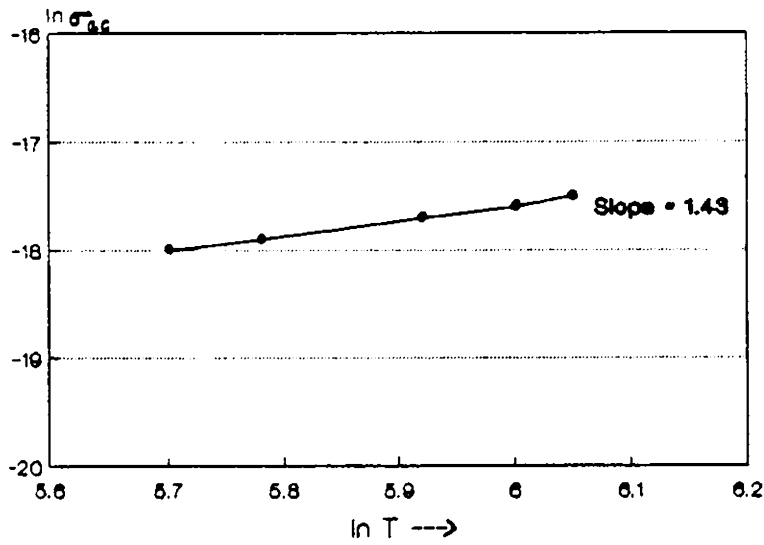


Fig.3.49

Dependence of the a.c conductivity of a-Si:H thin films on temperature



only one well defined part with a slope $s = 1.27$ at 300K, in the frequency range 20 kHz to ~ 115 kHz. Below and beyond this range there was a levelling off of the curve as shown in Figure 3.47B.

The important observations for film 1 can be summarized as follows.

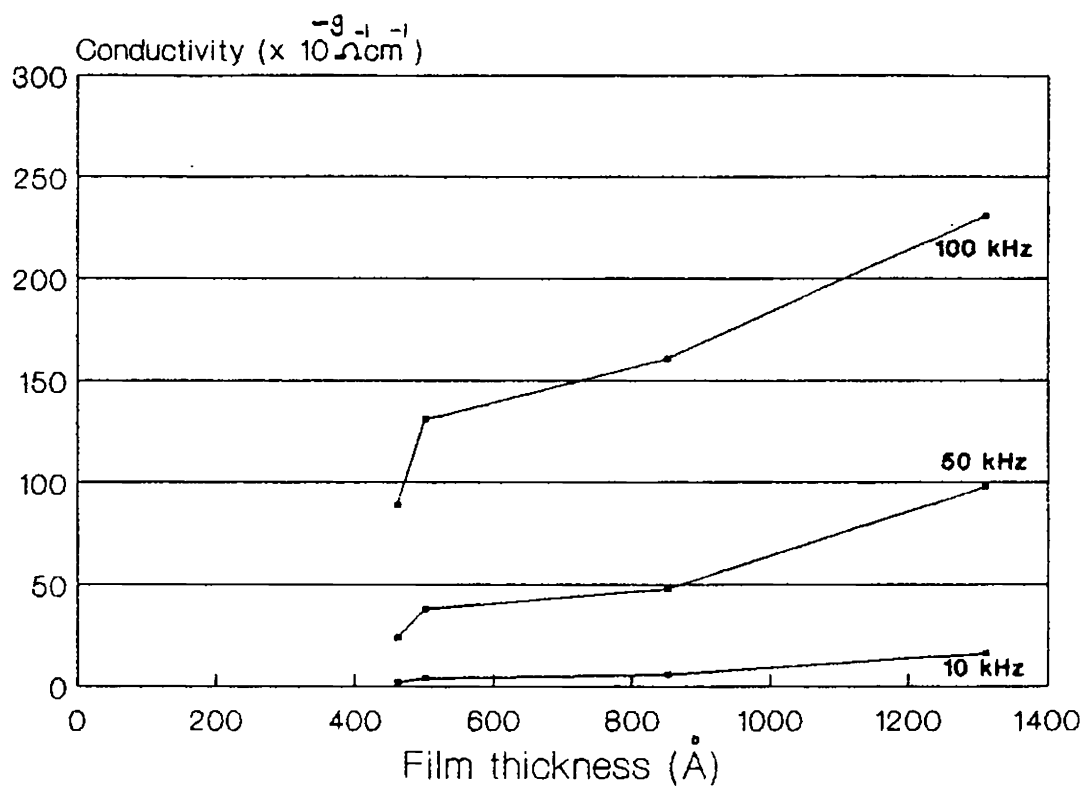
1. At 300K $\sigma_{a.c}$ increases as $\omega^{1.4}$ in the frequency range 10 kHz to 30 kHz and as $\omega^{1.67}$ in the range 30 kHz to 90 kHz.
2. At 300 kHz $\sigma_{a.c}$ was maximum and in the region 300-400 kHz $\sigma_{a.c}$ remained a constant with increase in the frequency and then decreased as frequency was further increased.
3. From 400 kHz to 1 MHz $\sigma_{a.c}$ decreased with increase in the frequency.
4. As the measurement temperature was increased the slope of the $\ln \sigma_{a.c}$ vs $\ln \omega$ curve decreased and in the region 10-30 kHz the slope reached a value 1 at 373K.
5. As the measurement frequency was increased the temperature dependence of the slope decreased.

6. The temperature dependence of $\sigma_{a.c}$ was observed to be $\sigma_{a.c} \propto T^{1.4}$ (Figure 3.49).

From the foregoing observations and discussions it becomes clear that neither Elliott's theory nor AM theory can be used to explain the a.c. conduction behaviour of the present films. Indeed such high values for the slope was reported earlier, like $s = 1.08$ for a-Se by Lakatos and Abkowitz [38] and $s = 1.2$ for $CdAs_2 + Si_x$ and $CdAs_2 + Sb_x$ by Kocka et al. [39] but such values were ruled out by Elliott as unreasonable. In the present case also except the high value of s all other observations, especially observations (4), (5) and (6) strongly support the Elliott's model. However, the density of states at the Fermi level cannot be calculated for the present case using Elliott's equation since $s > 1$ here.

In Figure 3.50 room temperature $\sigma_{a.c}$ is plotted against thickness of the films for three measurement frequencies (10 kHz, 50 kHz and 100 kHz). A sharp decrease in $\sigma_{a.c}$ is noticeable below a film thickness of 500 Å at 50 kHz and 100 kHz, but at 10 kHz such a change is not discernable.

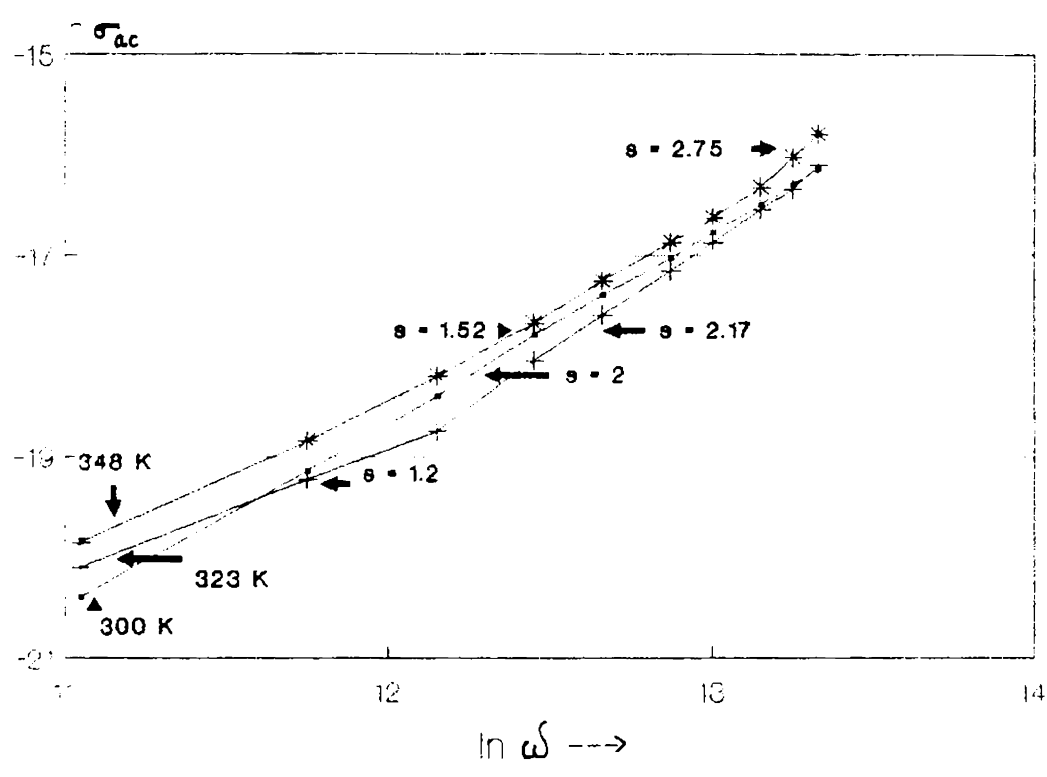
Fig.3.50

**Thickness dependence of a.c conductivity
of a-Si:H thin films**

In Figure 3.51 the $\ln \sigma_{a.c}$ vs $\ln \omega$ curve for an unhydrogenated amorphous silicon film of thickness 603 \AA is presented in the frequency range 10 kHz to 100 kHz. In this case the $\sigma_{a.c}$ varies as ω^2 at 300K. However, at 323K and 348K there are more than one slope. The lower slope occurs at lower frequencies and the higher slope at higher frequencies. In all the cases s was found to be greater than 1. The ω^2 dependence associated with direct optical absorption was derived by Tanaka et al. [41] and more generally by Mott [42]. But this mechanism was ruled out by Pollak [3]. Instead he has suggested that the phenomenon of $\sigma_{a.c} \propto \omega^2$ can occur due to a lower cut-off in the relaxation time τ of hopping. When this is true $\sigma_{a.c}$ at 10^6 Hz will be around $2 \times 10^{-7} \Omega^{-1} \text{cm}^{-1}$ by assuming a density of states at the Fermi level $N(E_F) = 2 \times 10^{19}$. In the present experiment $\sigma_{a.c}$ at 10^6 Hz is obtained as $9.7 \times 10^{-8} \Omega^{-1} \text{cm}^{-1}$ which is in a good order of magnitude agreement with the prediction.

Hence from our a.c. conductivity measurements we can conclude that certain fundamental changes occur to the amorphous silicon films due to hydrogenation. This is evident from the fact that in unhydrogenated samples the $\ln \sigma$ vs $\ln \omega$ curves at different temperatures had a slope around 2 in the 30 kHz to 100 kHz frequency range whereas in the hydrogenated samples this slope is between 1 and 1.67. In the

Fig.3.51
Dependence of the a.c conductivity of
a-Si films on measurement frequency



low frequency range (10 kHz to 30 kHz) for unhydrogenated films slope varied between 2 and 1 and for hydrogenated films the range was between 0.75 and 1.4 depending upon the film thickness and measurement temperature.

3.30 Adsorbate induced conductivity changes

3.31 Introduction

The pioneering work on the effect of gaseous ambients on real surfaces was carried out by Brattain and Bardeen by exposing germanium surfaces to wet and dry oxygen, nitrogen and ozone [43]. As a result of these investigations, it has been concluded that the contact-potential (CP) between platinum and germanium could be cycled between two extremes about 0.5 V apart by changing the gaseous ambient. Ozone or pentoxide vapours gave the CP extreme corresponding to the largest dipole at the Ge surface. Vapours with OH radicals produced the other extreme. A theory is given, that explains the observed results, in terms of donor-type and acceptor-type surface traps. The results are the direct evidence for the existence of a space charge layer at the free surface of a semiconductor. According to the same authors this space charge is nothing but the part of the surface dipole layer which in a semiconductor extends upto 10^{-6} - 10^{-4} cm into the material. Thus by what has come to

be known later as Brattain-Bardeen cycle, they have found that wet gases give rise to n-type surfaces while ozone and dry gases yield p-type surfaces, as the surface potential varied over the range 0.4-0.5 eV during the cycling.

Fritzsche et al. [44] have made attempts to apply the methods of Bardeen and Brattain to amorphous germanium and have found that only minute conductivity changes were produced by exposure to various gases. However, the adsorption was not confined to the surface but that the adsorbates penetrated the bulk of the amorphous germanium film through a network of microvoids. The smallness of the conductivity change was attributed to the relatively large density of localized gap states which effectively screen the changes in the surface potential [44].

Since the a-Si:H contains much fewer gap states its surface conductance should be strongly affected by adsorbates. A reversible change of the conductance of a-Si:H films, which results from the adsorption and desorption of various gases, in particular water and ammonia was reported by Tanielian et al. [45]. These films were of thickness 3600 Å and were prepared from SiH₄ by glow discharge. Their observations can be summarized as follows:

1. The reversible conductance changes caused by light and those caused by gases are two quite different processes.
2. Adsorbates are limited to the surface of the films prepared by glow discharge method while in the case of films prepared by evaporation water vapour penetrated the bulk of the films.
3. Moisture and NH_3 decreases the conductance of p-type films and increases that of n-type films. These adsorbates therefore act as n-type layers.
4. The conductance change is monotonous and it saturated at a particular value after a certain period of time.

Further studies are reported by Tanielian on the effect of adsorbates on the electrical conductance of a-Si:H in 1981 [4]. The dependence of the effect of adsorbates on the sign of the majority carriers, adsorbate partial pressure, temperature, sample thickness, activation energy of the samples and sample history are reported in detail. In most of the experiments in which moisture was the ambient gas he observed a sudden increase in the conductance followed by a slow increase. An explanation for such a behaviour was put forward by Tanielian [4]. There are two different

reactions between the adsorbed water and the a-Si:H films: one is a fast process in which donor-like states are formed close to the conduction or valence bands representing the weakly bound water on the surface of the film and the other is a slow process associated with the slower formation of acceptor-like states close to the middle of the gap arising from the more strongly bound compound formed by the reaction of water with SiO surface.

Such investigations on the effect of ambient gases on the electrical conductance of a-Si:H films are very important, since the large irreproducibilities encountered in the investigations of the properties of these films at different times in different laboratories is partly due to the effect of different ambient conditions. The effects are more pronounced for thinner films. For the above reasons a similar investigation was carried out in the present vacuum evaporated a-Si and a-Si:H films. The main direction of the work was to study the effect of different gases on the electrical conduction of these films, keeping all other parameters constant. Very thin films were used for the investigations because of the reason mentioned earlier.

3.32 Experimental

Thin films of unhydrogenated amorphous silicon of thickness 544 \AA (eight numbers) were prepared in a single

run. They were annealed for 30 minutes at 573K under $\sim 10^{-5}$ torr. They were then transferred to the metallization chamber for electrode deposition. Electrodes were deposited in the planar structure with a separation of 0.3 cm. The films were then held in a special glass cell for taking measurements. The cell was covered with metal sheets to minimise stray electrical signals. It was provided with an inlet tube for the introduction of the desired gas, a second opening for connecting a mercury manometer and a third one for the pumping port. The film was held inside the chamber using two copper clamps which acted as the electrical feed-throughs. All the gases except the water vapour were introduced into the chamber through a CaCl_2 drying column. The gases used were H_2 , O_2 , H_2S , NH_3 , CO_2 and H_2O vapour in the case of unhydrogenated films. H_2O vapour, NH_3 and CO_2 were the gases used in the case of hydrogenated films. The gases except H_2O vapour and NH_3 were produced by suitable chemical reactions and were collected inside a 3 litre glass jar by the downward displacement of water. NH_3 was produced using fresh ammonia solution and was collected inside an evacuated 3 litre glass jar. Water vapour was sent into the chamber by bubbling air through a vessel containing distilled water. The measurement steps were as follows:

1. The film was connected inside the chamber and the chamber was pumped down to 10^{-2} torr using a 200 l/minute rotary pump.
2. When minimum pressure was reached, the current-voltage measurement was carried out on the film by applying 2.5 V to 24.5 V in six steps.
3. After this the chamber was isolated from the pump and the required gas was introduced into the chamber (50 torr) after noting the time.
4. Measurements were again carried out after 15 minutes, 30 minutes and 1 hour. Thereafter the readings were taken every one hour nearly 15 hours.

The same procedure were followed for a-Si:H films also. Here the thickness of the films was 484 Å and were prepared in the same run. The time and temperature of hydrogenation were 60 minutes and 573K. Hydrogen partial pressure during annealing was 0.05 torr.

3.33 Results and discussion

The changes in the current through the unhydrogenated films due to exposure to various gas ambients are

presented in Figures 3.52, 3.53 and 3.54. After an exposure of 15 hours to H_2 , O_2 , H_2S and CO_2 conductivity σ decreased by 50% for H_2 , 26% for H_2S and 60% for CO_2 . Due to an exposure of 15 hours to NH_3 gas there was remarkable increase of 1900% in the value of σ . There was a sudden increase in the current during the first 30 minutes. Even at the end of 17 hours there was no sign of saturation. But the most dramatic change was observed due to the exposure of films to water vapour. At the end of 15 hours a tremendous increase in σ of 7.4×10^5 percent of the initial value was registered in this case. The sharp increase in the current was observed upto 5 hours after which the current began to show saturation. After 8 hours it was almost saturated.

The increase in the conductivities due to exposures in NH_3 and water vapour was particularly interesting. It was found that between 30 minutes and 14 hours of exposure to NH_3 gas the conductivity increased exponentially with time according to the relation

$$\sigma = C \exp(0.12t) \quad (3.20)$$

Here C , the pre-exponential factor was found to be $5.57 \times 10^{-7} \Omega^{-1} \text{cm}^{-1}$, t is the time of exposure in hours. Figure 3.55 shows the plot of $\ln \sigma$ vs time.

Fig.3.52

Conductivity of the a-Si films exposed
to different gas ambients vs time

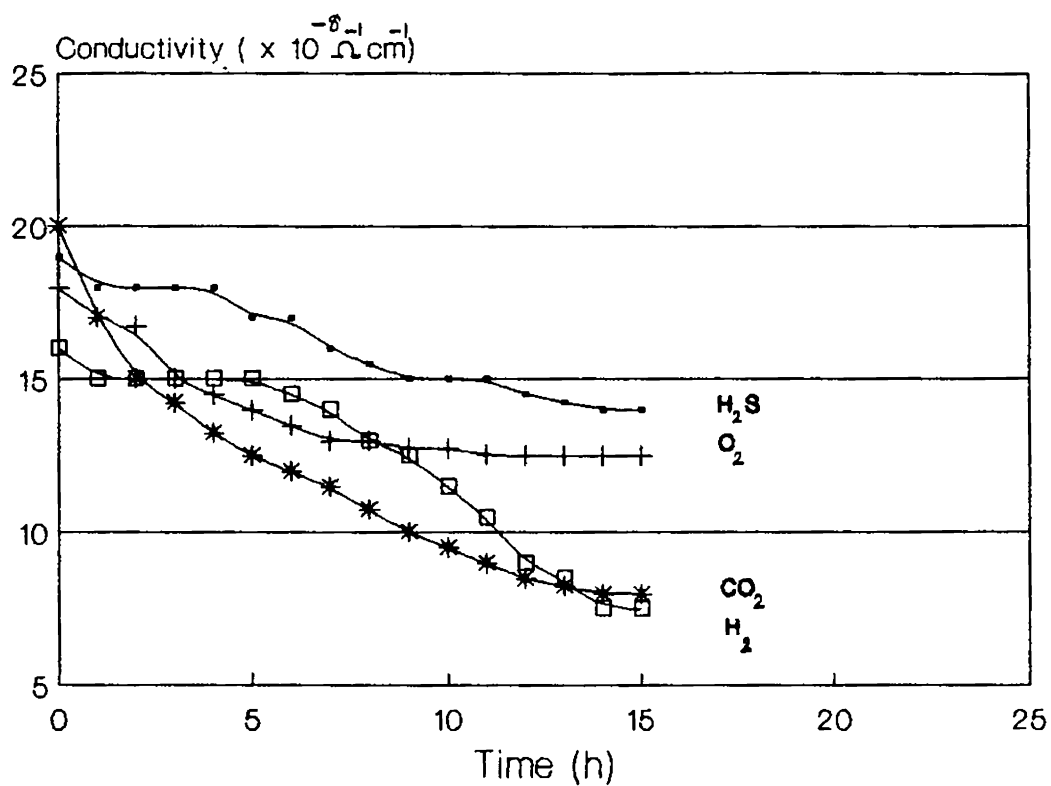


Fig.3.53

Conductivity of a-Si film exposed to ammonia gas vs time

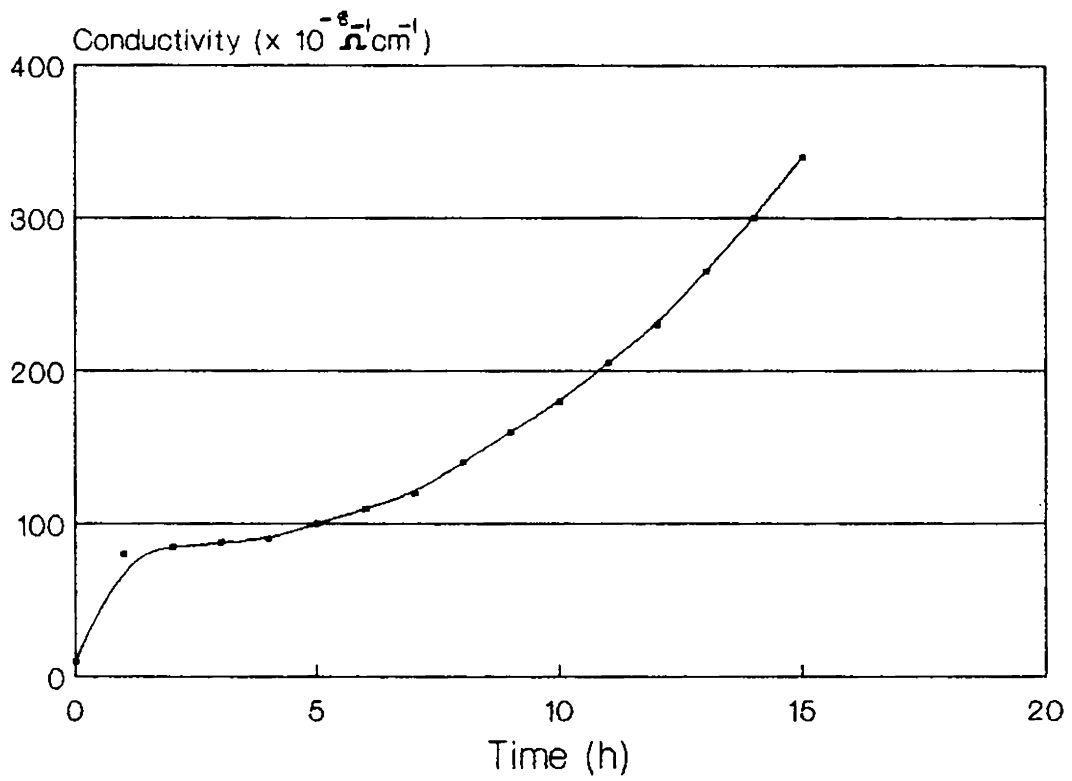


Fig.3.54

Conductivity of a-Si film exposed to
water vapour vs time

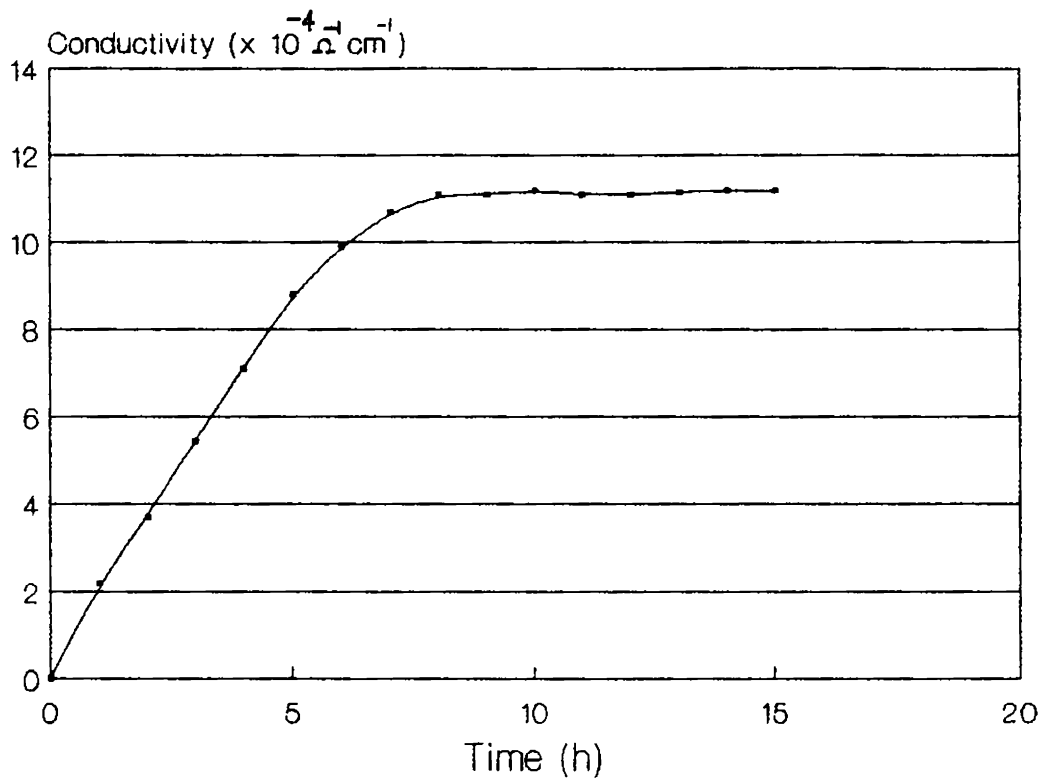
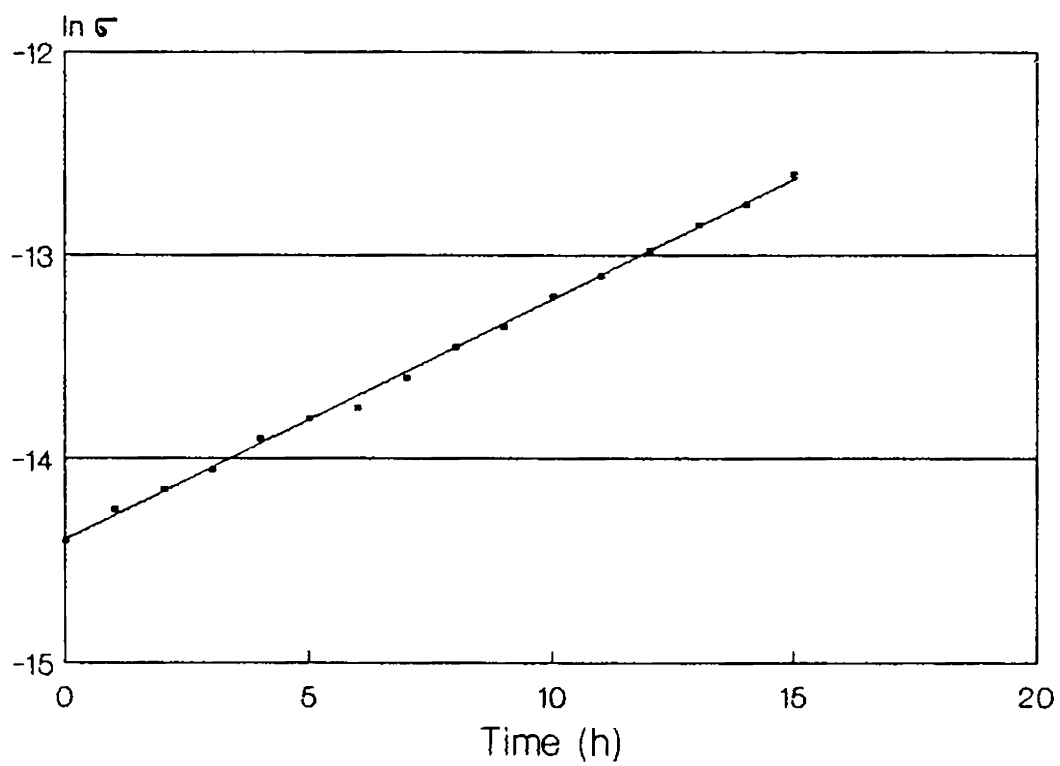


Fig.3.55
 $\ln \sigma$ vs time for a-Si film exposed to
ammonia gas



Similarly it was found from Figure 3.54 that when the amorphous silicon films were exposed to water vapour the conductivity increased linearly with time in range 30 minutes to 5 hours.

a-Si:H films were subjected only to three ambients CO_2 , NH_3 and H_2O which were the three typical examples of electron acceptors (CO_2) and donors (NH_3 and H_2O), found in the previous study. It was also evident from the previous experiments that H_2 , O_2 and H_2S were very weak electron acceptors. They were therefore not studied in the case of a-Si:H. However as a typical case of electron acceptor CO_2 was also used as an ambient along with the donors NH_3 and H_2O .

In Figures 3.56, 3.57 and 3.58 the effects of CO_2 , NH_3 and H_2O vapour on the electrical conductivity of a-Si:H films are given. It is very interesting to note that the general shape of the curves are very much different from that for a-Si films. In the present case, CO_2 atmosphere produced a 15.6% decrease in the conductivity σ at the end of the first two hours and thereafter σ increased monotonously and assumed a value 19% higher than the initial value, at the end of 15 hours. The net effect is σ increased

Fig.3.56

Conductivity of a-Si:H film exposed to
 CO_2 vs time

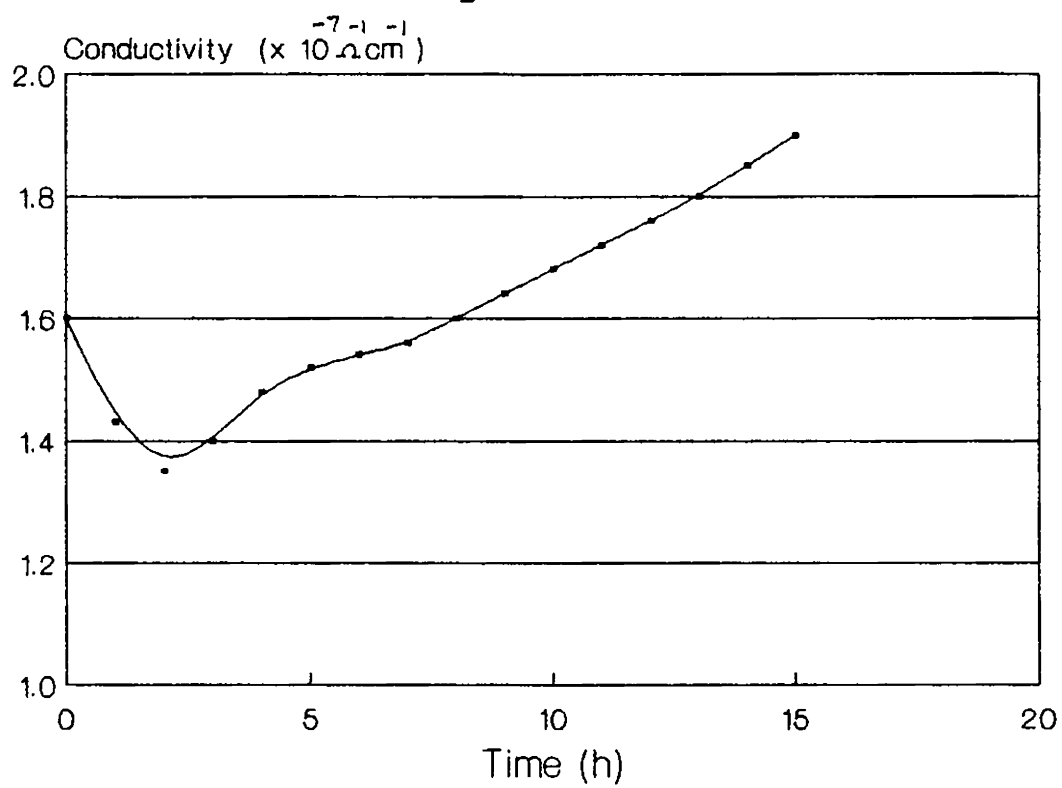


Fig.3.57

Conductivity of a-Si:H film exposed to ammonia gas vs time

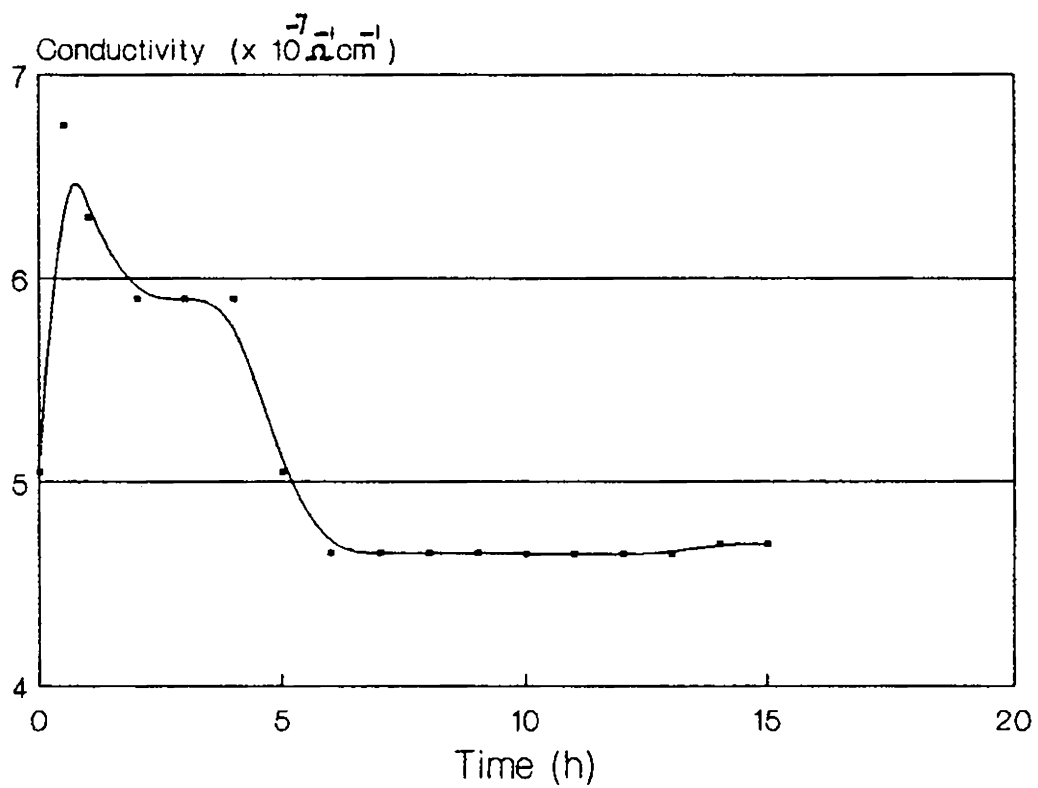
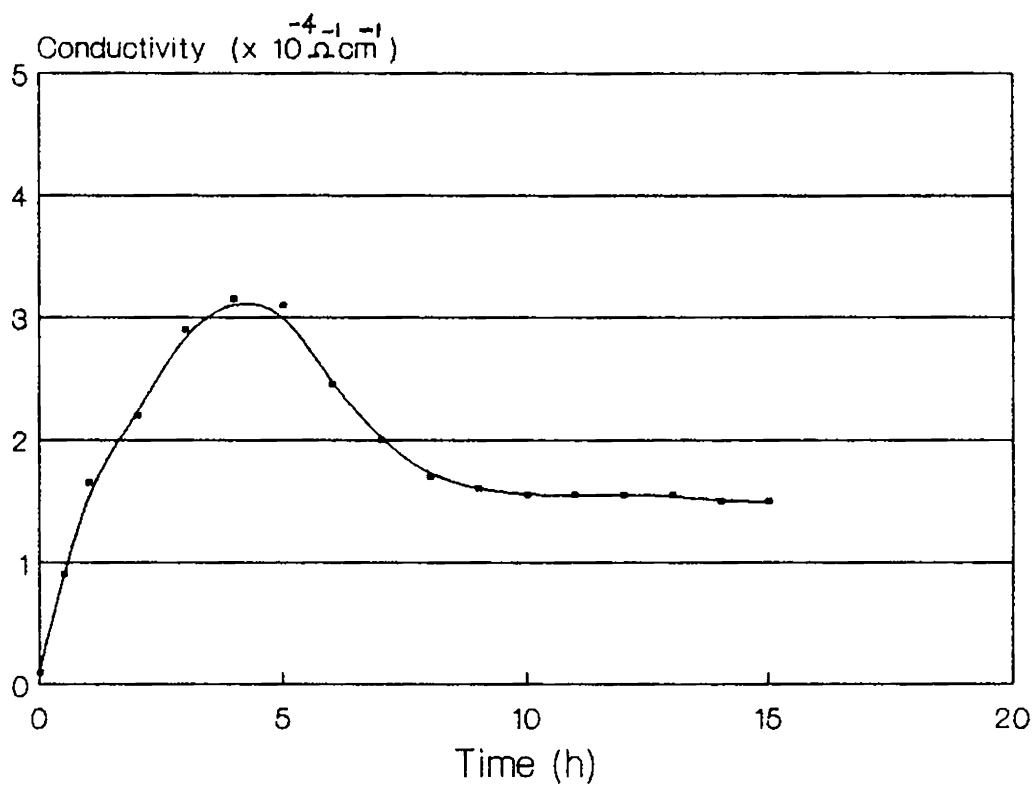


Fig.3.58

Conductivity of a-Si:H film exposed to
water vapour vs time



due to the exposure to CO_2 . Similarly in the case of NH_3 there was a sharp decrease in σ in the first 30 minutes and assumed a value 33.4% higher than the initial value. Thereafter σ decreased rapidly and became 8.3% of the original value after 8 hours and saturated there. Just like in the case of unhydrogenated samples the highest change in σ was observed due to an exposure to water vapour. In the present case after 4 hours of exposure σ increased to 6.8×10^4 percent of the starting value and then decreased and saturated at a value 3.7×10^4 percent higher than the initial value at the end of 10 hours.

The results of the experiment on the adsorbate induced conductivity changes are summarized as follows.

1. In the case of a-Si films the exposure to H_2 , O_2 and H_2S atmosphere for about 15 hours produced a maximum of 50% change in the conductivity.
2. NH_3 atmosphere caused $\sim 1900\%$ increase in σ for a-Si films. But for a-Si:H films exposure to NH_3 caused an initial increase followed by a decrease of 8.3% at the end of 15 hours.

3. Exposure to H_2O vapour caused an increase of 7.4×10^5 percent for a-Si films and an initial increase of 6.8×10^4 percent followed by a decrease, in the case of a-Si:H films.

4. Exposure to CO_2 decreased the value of σ by 60% in the case of a-Si films. But for a-Si:H films CO_2 produced an initial decrease of 15.6% and a monotonous increase thereafter and reached a value of $\sim 19\%$ higher than the initial value at the end of 15 hours.

5. The increase in σ of a-Si films due to the exposure to NH_3 followed an exponential relation with time almost in the whole range of measurement. Similarly for the same films exposure to water vapour caused σ to increase linearly with time from the first 30 minutes to 5 hours. Such relationships were not found in a-Si:H films.

6. There was generally a monotonous increase or decrease in σ for a-Si films whereas for a-Si:H films the change was faster in the initial stages of exposure followed by a gradual change in the opposite direction.

The simple monotonous variations of σ can be explained by assuming that the gas ambients react with the

film and donor-like or acceptor-like centres are formed on the surface depending upon the type of the gas. Since electron donors like NH_3 and H_2O cause σ of the present a-Si films to increase it is safe to consider these films as weakly n-type eventhough not intentionally doped. In the case of a-Si:H the two reactions--one faster and another slower postulated by Tanielian [4] possibly explains the present experimental results. But unlike the results of Tanielian, in the present experiment in which a-Si:H films are exposed to NH_3 and CO_2 we see that the slower reaction in which opposite type of carriers are generated dominates in the final stages of exposure. This ultimately leads to a conductivity change which is opposite to the changes in the initial stages of exposure.

REFERENCES

1. S.R.Elliott, *Phil.Mag.*, **36** (1977) 1291.
2. S.R.Elliott, *Phil.Mag.B*, **37** (1978) 553.
3. M.Pollak, *Phil.Mag.*, **23** (1971) 519.
4. M.Tanielian, *Phil.Mag.B*, **45** (1982) 435.
5. E.A.Davis and N.F.Mott, *Phil.Mag.*, **22** (1970) 903.
6. N.F.Mott and E.A.Davis, "Electronic Processes in Non-crystalline Materials", Clarendon Press, Oxford (1971) 200.
7. N.F.Mott, *J.Non-Cryst.Solids*, **1** (1969) 1.
8. D.G.Ast and M.H.Brodsky, *Phil.Mag.B*, **41** (1980) 273.
9. P.Dellafera, R.Labusch and H.H.Roscher, *Phil.Mag.B*, **45** (1982) 607.
10. G.Muller and P.G.LeComber, *Phil.Mag.B*, **43** (1981) 419.
11. G.W.Neudeck and A.K.Malhotra, *J.Appl.Phys.*, **46** (1975) 239.
12. G.W.Neudeck and A.K.Malhotra, *J.Appl.Phys.*, **46** (1975) 2662.
13. Nancy, B.Goodman, *Phil.Mag.B*, **45** (1982) 407.
14. Toshio Nakashita, Kenji Kohno, Takeshi Imura and Yukio Osaka, *Jpn.J.Appl.Phys.*, **22** (1983) 1766.

15. S.Hasegawa and Y.Imai, *Phil.Mag.B*, **46** (1982) 239.
16. I.Solomon, "Fundamental Physics of Amorphous Semiconductors", F.Yonezawa (Ed.), Springer-Verlag (1981) 33.
17. P.K.Abraham, K.Rajeev Kumar and K.Sathianandan, "Proceedings of the Solid State Physics Symposium", BARC, Bombay, **30C** (1987) 403.
18. L.I.Maïssel and R.Glang, "Handbook of Thin Film Technology", McGraw-Hill Book Company, New York (1983) 13-26.
19. W.Beyer and R.Fischer, *Phil.Mag.B*, **39** (1979) 205.
20. W.Rehm, R.Fischer, J.Stuke and H.Wagner, *Phys.Stat.Solidi (b)*, **79** (1977) 539.
21. D.A.Anderson and William Paul, *Phil.Mag.B*, **45** (1982) 1.
22. Z.S.Jan, R.H.Bube and J.C.Knights, *J.Electron Mater.*, **8** (1979) 47.
23. J.Jang, J.H.Kang and C.Lee, *J.Non-Cryst.Solids*, **35,36** (1980) 313.
24. D.E.Carlson, "Polycrystalline and Amorphous Thin Films and Devices", Academic Press, New York (1980).
25. H.Overhof and Beyer, *Phil.Mag.B*, **43** (1981) 433.
26. R.F.Shaw, Ph.D.Thesis, University of Cambridge (1969).

27. A.E.Owen, *Glass Industry*, (1967) 695.
28. E.B.Ivkin and B.T.Kolomiets, *J.Non-Cryst.Solids*, 3 (1970) 41.
29. A.E.Owen and J.M.Robertson, *J.Non-Cryst.Solids*, 2 (1970) 40.
30. E.A.Davis and R.F.Shaw, *J.Non-Cryst.Solids*, 2 (1970) 106.
31. H.K.Rockstad, *J.Non-Cryst.Solids*, 2 (1970) 192.
32. F.Argall and A.W.Jonscher, *Thin Solid Films*, 2 (1968) 185.
33. W.S.Chan and A.K.Jonscher, *Phys.Stat.Solids*, 32 (1969) 749.
34. S.K.Bahl and K.L.Chopra, *J.Appl.Phys.* 41 (1970) 2196.
35. G.S.Linsley, A.E.Owen and F.M.Hayatee, *J.Non-Cryst.Solids*, 4 (1970) 208.
36. I.G.Austin and N.F.Mott, *Adv.Phys.*, 18 (1969) 41.
37. M.Kastner, *Phy.Rev.Lett.*, 28 (1972) 355.
38. A.I.Lakatos and M.Abkowitz, *Phy.Rev.B*, 3 (1971) 1791.
39. J.Kocka, J.Kristofik, *Phys.Status Solidi A*, 45 (1978) 559.
40. David Emin, "Polycrystalline and Amorphous Thin Films and Devices, Lawrence L.Kazmerski (Ed.), Academic Press, New York (1980) 30.

41. S.Tanaka, M.Kobayashi, E.Hanamura and K.Uchinokura, Phys.Rev.,
134 (1964) A.256.
42. N.F.Mott, Phil.Mag., 19 (1969) 835.
43. W.H.Brattain and J.Bardeen, Bell Syst.Tech.J., 32 (1953) 1.
44. H.Fritzsche and M.Kastner, Mater.Res.Bull., 5 (1970) 631.
45. M.Tanielian, H.Fritzsche, C.C.Tsai and E.Symbalisky, Appl.
Phys.Lett., 33 (1978) 353.

Chapter 4

DIELECTRIC PROPERTIES OF a-Si AND a-Si:H

Abstract

Studies are reported on the dependence of the dielectric constant, loss factor, impedance and equivalent series resistance of a-Si and a-Si:H capacitors on the film thickness, frequency of measurement (from 10 kHz to 1 MHz) and ambient temperature. It is found that a-Si:H film has a higher dielectric constant than a-Si film of the same thickness, which is interpreted as due to the decrease in the density of states in the energy gap of the material as a result of hydrogenation. It is also found that the interfacial polarization is negligible in thinner films while in thicker films it is evident to some extent. The influence of the electrodes and the lead resistance on the dielectric properties is clear from the increase in the loss factor with frequency.

4.00 Introduction

In recent years a great deal of interest has developed in the use of high quality dielectric films. The preparation of thin dielectric films has been motivated by their use in small volume capacitors. This improved the flexibility of thin film circuits and substantially increased their ability to meet the needs of circuit designers. The fabrication of capacitors using techniques compatible with those employed to form resistors and conductors has been one factor responsible for the rapid development of all thin film circuits [1]. It has also been stimulated by the increasing quality and complexity of electronic circuits and paved the way for the birth of thin film microelectronics. From an analysis of the properties of several thin film insulators, it becomes evident that a large number of dielectric materials are available for the fabrication of thin film capacitors. But only those films which are thermally and chemically stable are actually used in the fabrication of capacitors. The materials which are usually employed in the fabrication of thin film capacitors are oxides of metals and semiconductors such as Ta_2O_5 , Al_2O_3 , SiO and SiO_2 , of which the last two are the most common and thoroughly investigated [2].

But there is another important aspect for the study of the dielectric properties of materials. These studies help

to understand certain fundamental physical properties of the system, like the presence of structural defects, microvoids and impurities present in the film. The various polarization and relaxation mechanisms and the behaviour of electrode insulator interfaces are also studied in detail by many schools of research.

A thin insulator film departs considerably from the idealized theoretical model. Kohn in 1958 has shown theoretically, that the dielectric constant of the insulator should be independent of film thickness to a few atomic layers [3]. But it is a commonly observed fact that in films obtained by vapour deposition, the dielectric constant falls rapidly with decreasing thickness. This is because the films obtained by this method are porous and as the film thickness decreases, porosity increases and in turn causes a decrease in the dielectric constant. The theoretical predictions of Kohn is true only in the case of structurally perfect organic films [4]. This convincingly proves the need for extensive experimental studies on the dielectric properties of a material prepared by different methods.

The bulk of the dielectric studies carried out are on insulating materials like the ones sighted earlier. Rare earth oxides are also subjected to thorough dielectric investigations. But a close survey of the literature reveals that

eventhough the electrical properties of a Si:H are investigated thoroughly their dielectric properties are seldom subjected to a systematic study. Even the few investigations carried out are on the optical frequency dielectric constant and that too with a view to explain certain optical properties of the material [5-7]. More exactly these studies are centred around the fact that the imaginary part of the dielectric function and density of states of a-Si obtained from experiments exhibit properties which could not be obtained from a simple averaging of the crystalline spectra.

It becomes obvious that the few experimental and theoretical studies carried out on the optical frequency dielectric properties of amorphous silicon are in fact to supplement and explain the optical data of these materials. Again the fact that even the intrinsic a-Si:H films are well inferior to the conventional insulators as a dielectric material further discouraged any attempt at a systematic study of their dielectric properties. Hence we felt it necessary to carry out an investigation on the dielectric properties of the a-Si and a-Si:H thin films prepared by the vacuum evaporation method.

The investigation is in no way an exhaustive one but only intended to understand the basic dielectric behaviour of the material. A brief but relevant theory is given in the

first part followed by experimental details and concludes with a discussion on the results.

4.10 Theory

A theory for the dielectric behaviour of a metal-insulator-metal system, in which the insulator is highly doped and in which Schottky barriers exist at the metal-insulator-metal interfaces, was formulated by Simmons et al. in 1970 [8]. This theory could explain the observed minimum in the quality factor vs temperature curve and dependence of capacitance on frequency and temperature of evaporated molybdenum oxide films [9]. Later, in 1973, Goswami et al. [10] developed another theory for the dielectric properties of insulators. It was found that the second theory was more suitable for the present case and hence it is given below.

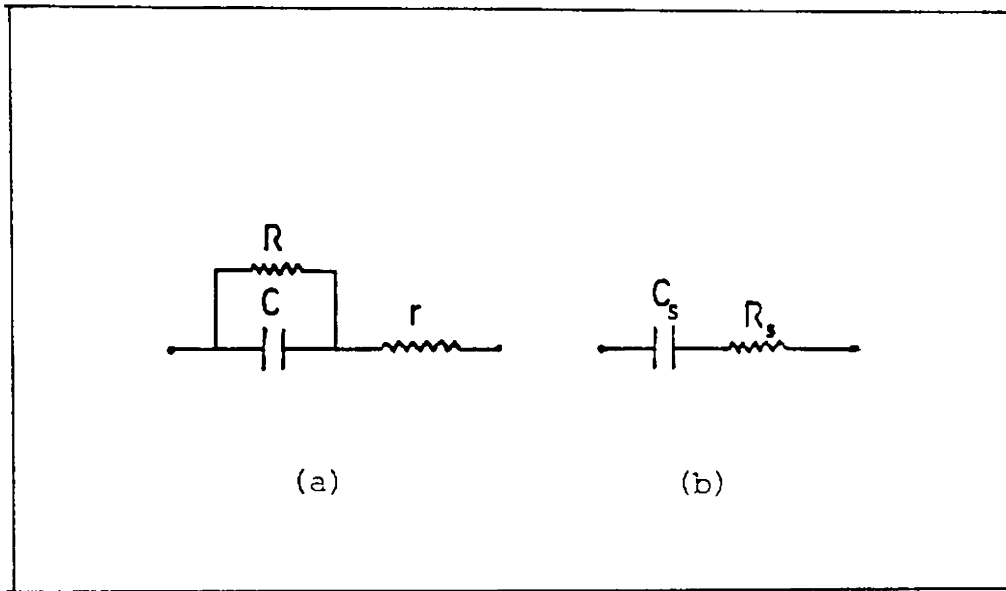
In Goswami's theory each capacitor system was assumed to comprise of the following:-

- (i) An inherent capacity element (C) unaffected by frequency (f) and temperature,
- (ii) a discrete resistance element (R) due to the dielectric film in parallel with C, and
- (iii) a series resistance (r) due to the leads.

Fig.4.10

(a) Capacitor elements (C,R,r)

(b) Equivalent circuit



It is assumed that R is temperature dependent since $R = R_0 \exp(\Delta E/kT)$ where R_0 is the pre-exponential factor, ΔE activation energy and T the absolute temperature. But the lead resistance $r (\ll R)$ is temperature independent. Figures 4.10(a) and (b) show the different elements and the equivalent series circuit.

Impedance (z) of the circuit in Figure 4.10(a) in terms of C , R , r and ω ($=2\pi f$) is given by the equation

$$\begin{aligned} Z &= \frac{R}{1+j\omega CR} + r \\ &= \frac{R+r(1+\omega^2 R^2 C^2)}{1+\omega^2 R^2 C^2} - \frac{j\omega CR^2}{1+\omega^2 R^2 C^2} \end{aligned} \quad (4.10)$$

In the equivalent series circuit this can be represented by

$$R_s + \frac{1}{j\omega C_s} \quad \text{or} \quad R_s - j \frac{1}{\omega C_s} \quad (4.11)$$

where R_s and C_s are equivalent series resistance and equivalent series capacitance. From the real and imaginary parts of the above equations, we have,

$$C_s = \frac{1+\omega^2 R^2 C^2}{\omega^2 R^2 C^2} = (1+D^2)C \quad (4.12)$$

and
$$R_s = \frac{R+r(1+\omega^2 R^2 C^2)}{(1+\omega^2 R^2 C^2)} = r + \frac{D^2}{\omega^2} R \quad (4.13)$$

where $D = \frac{1}{\omega RC}$. Since $\tan \delta = \omega C_s R_s$ we have

$$\begin{aligned} \tan \delta &= \frac{\omega (1+\omega^2 R^2 C^2) [R+r(1+\omega^2 R^2 C^2)]}{(\omega^2 R^2 C) (1+\omega^2 R^2 C^2)} \\ &= \frac{1}{\omega RC} + \frac{r}{\omega R^2 C} + \omega RC \\ &= D(1 + \frac{r}{R}) + \omega RC \end{aligned} \quad (4.14)$$

When $\omega^2 R^2 C \gg r$ or $\frac{r}{R} \ll 1$ which is true for all cases, equation (4.14) reduces to

$$\tan \delta = \frac{1}{\omega RC} + \omega RC \quad (4.15)$$

When ω is small, $\frac{1}{\omega RC} \gg \omega RC$. Then

$$\tan \delta = \frac{1}{\omega RC} \quad (4.16)$$

When ω is large $\frac{1}{\omega RC} \ll \omega RC$ and then

$$\tan \delta = \omega RC \quad (4.17)$$

Equations (4.16) and (4.17) predict conditions when the loss factor will be inversely or directly proportional to .

The effect of temperature on capacitance is obtained from equation (4.12) which can be written as

$$C_s = \frac{1}{\omega^2 R^2 C} + C \quad (4.18)$$

Since R depends on temperature C_s will also vary with temperature.

4.20 Experimental

Amorphous silicon films of thicknesses ranging from 460 Å to 1300 Å were prepared on glass substrates pre-coated with aluminium electrodes of breadth 1 cm. The area of the a-Si films was 2 cm x 2 cm. Over this, aluminium counter electrodes were deposited so that the two metal electrodes had an overlapping area of 0.8 cm², with the a-Si film sandwiched between them. In the fabrication of a-Si:H capacitors the Si films were subjected to hydrogenation as described in Chapter 2,

before depositing the counter electrode. The hydrogenation temperature, partial pressure and time of annealing were 573K, 0.05 torr and 60 minutes respectively. In the case of unhydrogenated samples the films were subjected to annealing in a vacuum ($\sim 10^{-5}$ torr) at 573K for 60 minutes prior to the deposition of the counter electrode. The completed devices were subjected to dielectric measurements using the HP 4277 A LCZ bridge, in the frequency range 10 kHz to 1 MHz and temperature range 300K to 373K.

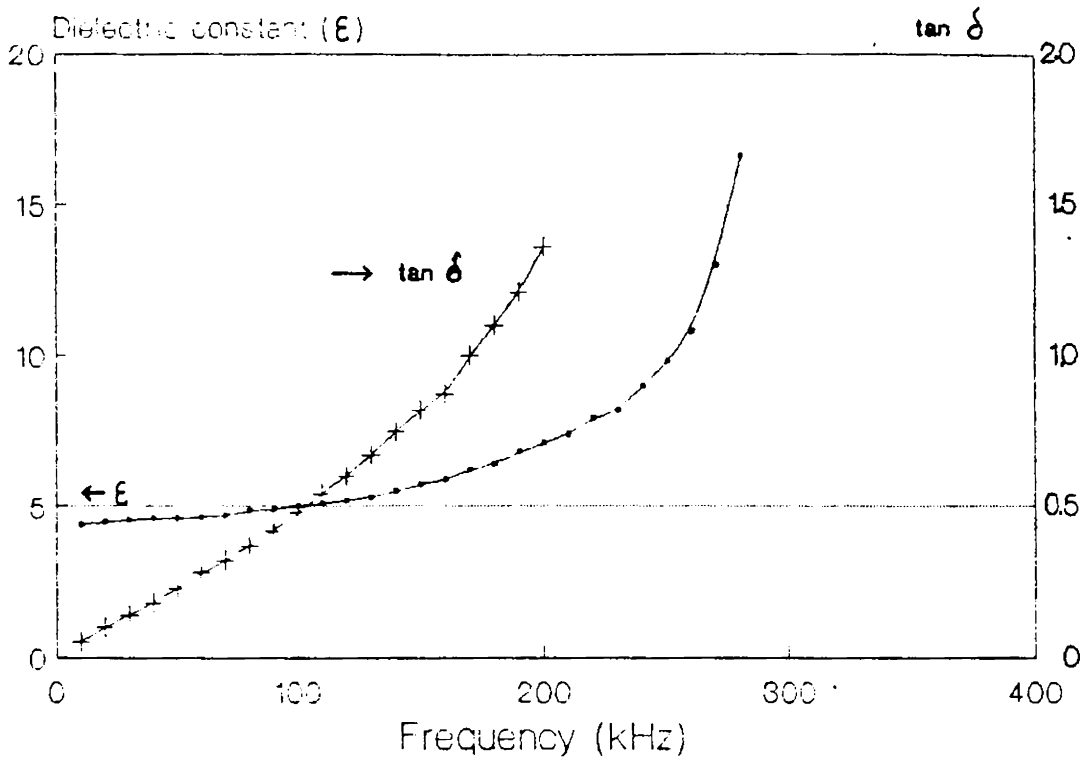
The parameters measured were capacitance (C) loss factor ($\tan\delta$) and equivalent series resistance (ESR).

4.30 Results and discussion

4.31 Unhydrogenated amorphous silicon (a-Si)

In this case the thickness of the a-Si film was 603 Å. In Figure 4.30 the frequency dependence of the dielectric constant (ϵ) and loss factor ($\tan\delta$) are given. The value of ϵ at 10 kHz is 4.4 and it increased to 16.4 as the frequency was increased to 275 kHz. Above 275 kHz it was not possible to find the value of ϵ as the capacitance value was above the range of the instrument. In the same figure the loss factor ($\tan\delta$) is plotted against frequency.

Fig.4.30

Dielectric constant & $\tan \delta$ vs Frequency

Loss factor also increased with increase of frequency. The temperature dependence of ϵ is presented in Figure 4.31. It is clear from this figure that ϵ is independent of temperature in the range 300 to 373K. In Figure 4.32 the logarithm of the impedance (Z) of the capacitor is plotted against the logarithm of frequency. Z decreased upto 300 kHz above which it increased. In the same figure the equivalent series resistance (ESR) of the capacitor is plotted against frequency. A sharp decrease in ESR is observed between 10 kHz and 60 kHz. From 100 kHz to 1 MHz the curve exhibits a negligible frequency dependence. It is interesting to note that at 274 kHz the capacitance increased sharply and went out of the range of the LCZ bridge. Again the capacitance appeared at 500 kHz with a negative sign (not plotted in Figure 4.30) and this negative capacitance began to decrease and approach zero as the frequency was increased. It was around this frequency (at 300 kHz) the impedance showed the minimum value and began to increase with the further increase of frequency. But the ESR did not exhibit any change at 300 kHz.

4.32 Hydrogenated amorphous silicon (a-Si:H)

Four films of a-Si:H with thicknesses 461 Å, 500 Å, 837 Å and 1312 Å were subjected to measurements. The frequency dependence of their dielectric constants (ϵ) is given in

Fig. 4.31

Temperature dependence of the
Dielectric constant (ϵ) of a-Si

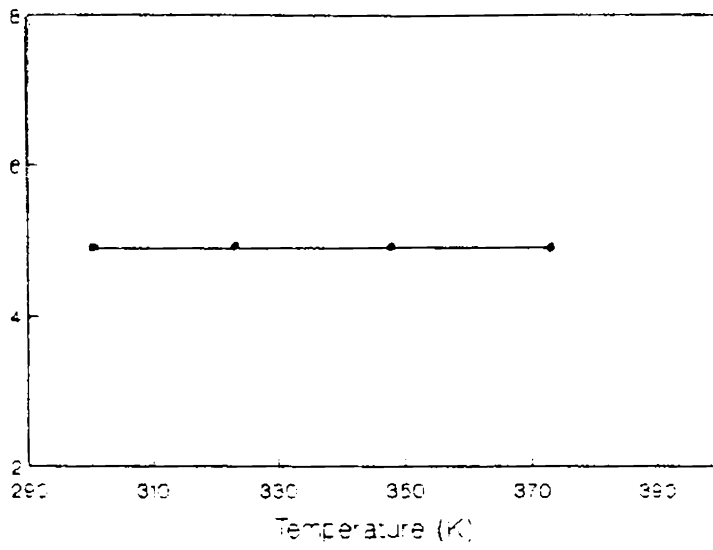


Fig. 4.32

Frequency dependence of the
Impedance (Z) of a-Si

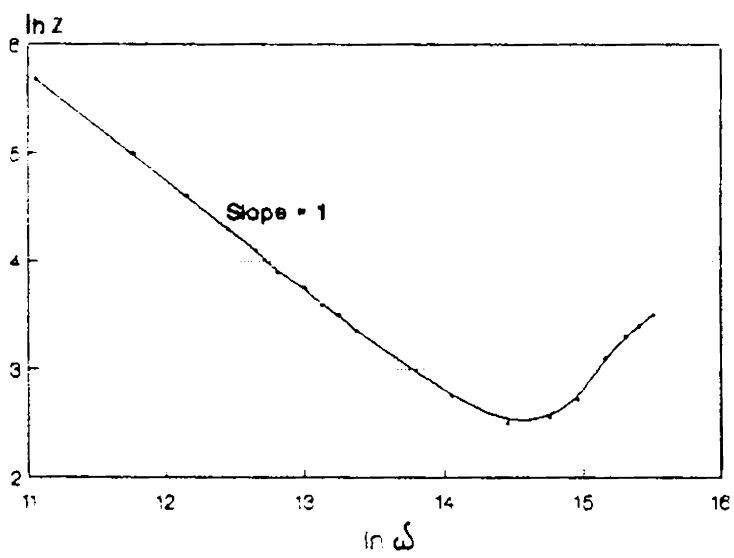


Figure 4.33. It can be seen from this figure that for films 1 and 2 (i.e. 461 Å and 500 Å), there is negligible increase of ϵ as the frequency is varied from 10 kHz to 100 kHz. But ϵ becomes 12.4 and 12.5 for films 1 and 2 at 240 kHz and 260 kHz respectively. In the case of films 3 and 4 (837 Å and 1312 Å), ϵ decreases at first reaches a minimum value and then increases. For film 3 this minimum occurs at 50 kHz and for film 4 at 90 kHz. For all the films the loss factor ($\tan \delta$) increased as the frequency was increased and at lower frequencies $\tan \delta$ increased as the thickness of the film was increased (Figure 4.34). Temperature dependence of ϵ and $\tan \delta$ are given in Figures 4.60 and 4.70. While for films 1 and 2 ϵ was independent of temperature, for film 3 ϵ slightly increased upto 350K and became steady at that value in the temperature range studied. Loss factors of these films also were weakly dependent upon the temperature. But in the case of film 4, there was a strong dependence of both ϵ and $\tan \delta$ on temperature. ϵ increased by 123.5% and $\tan \delta$ by 114% as the temperature was varied in the range 300K to 373K. The thickness dependence of the dielectric constant is given in Figure 4.35. Between 461 Å and 500 Å there was a sharp increase in ϵ and as the thickness was increased further there was a more gradual increase of ϵ . In Figure 4.36 a typical

Fig.4.33

Dielectric constant vs Frequency

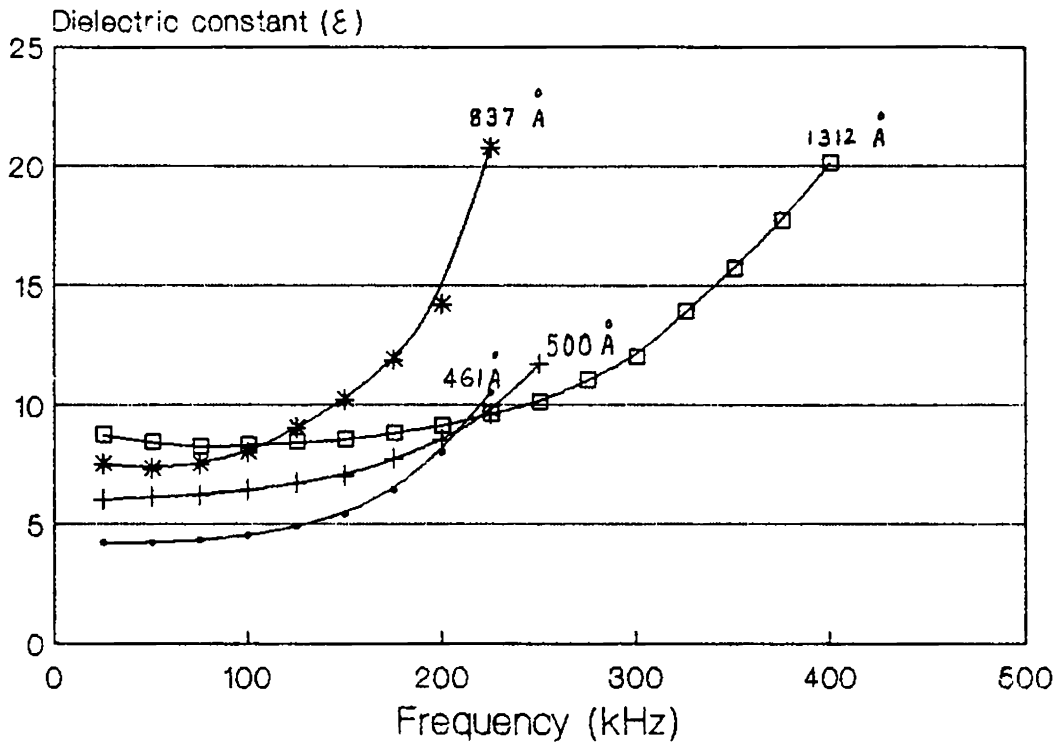


Fig.4.34

Loss factor vs Frequency

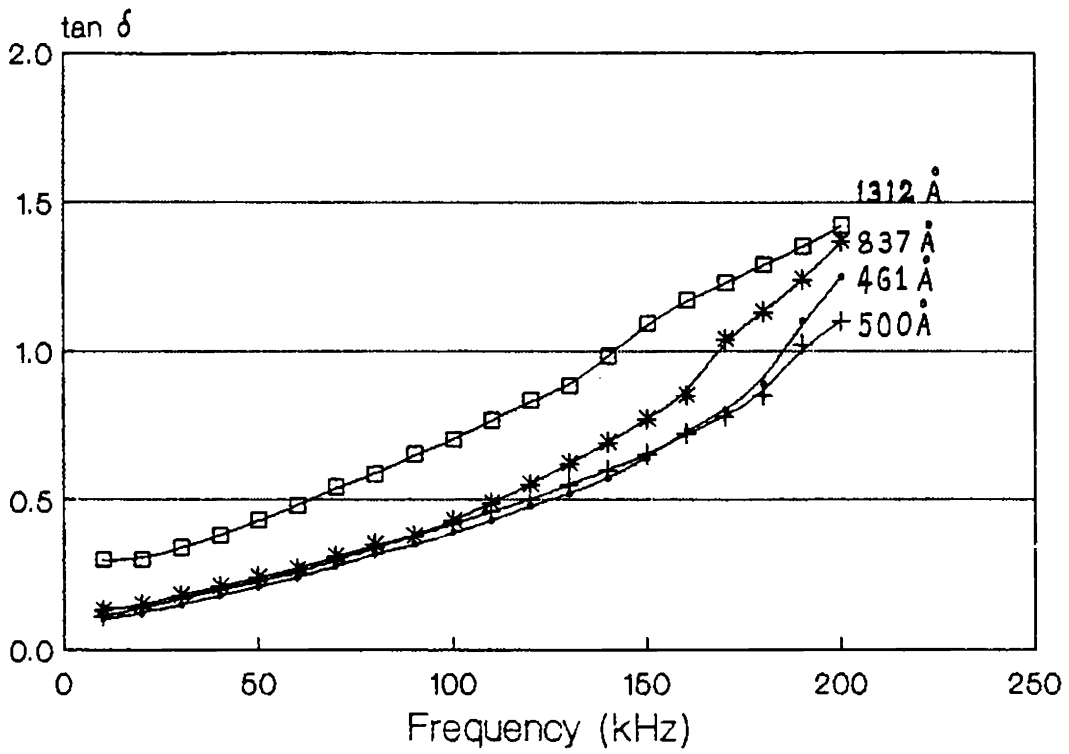


Fig.4.35

Thickness vs Dielectric constant
(measured at frequency 10 kHz)

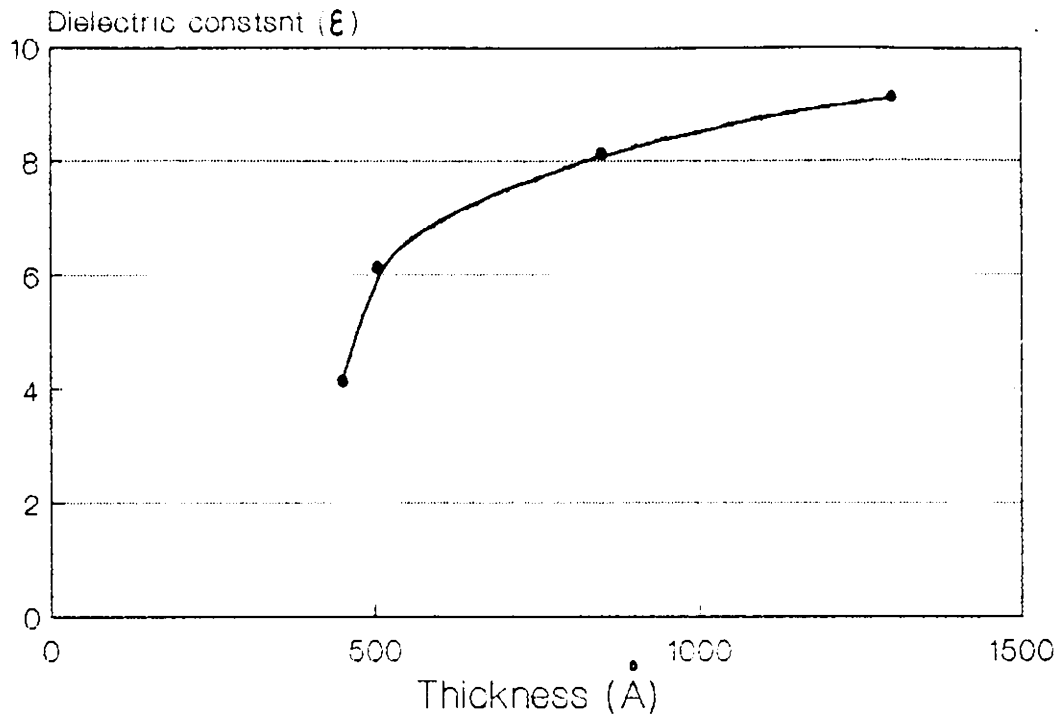


Fig.4.36
 Frequency dependence of the Impedance(Z)
 and ESR of a-Si:H thin films

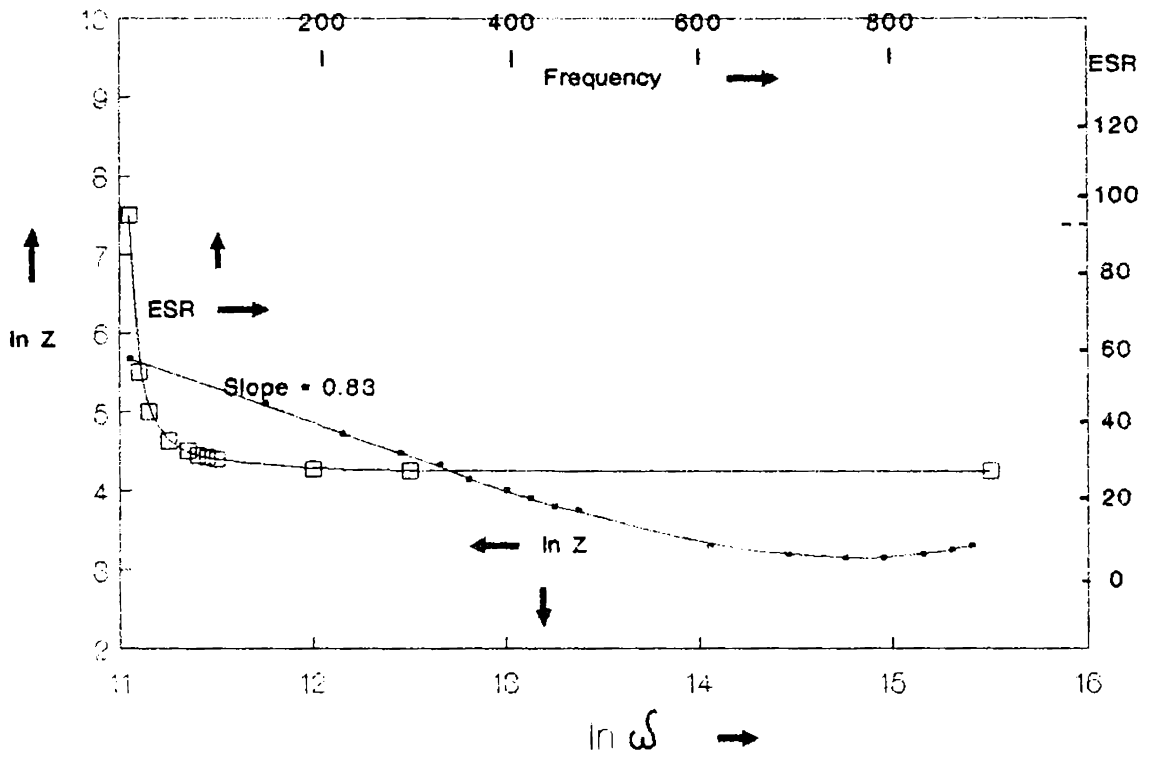


Fig.4.60
Temperature dependence of the Dielectric constant (ϵ) of a-Si:H thin films

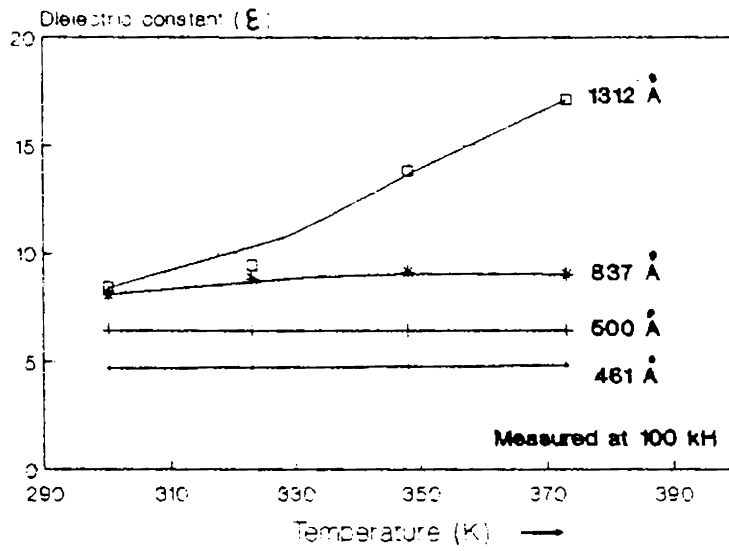
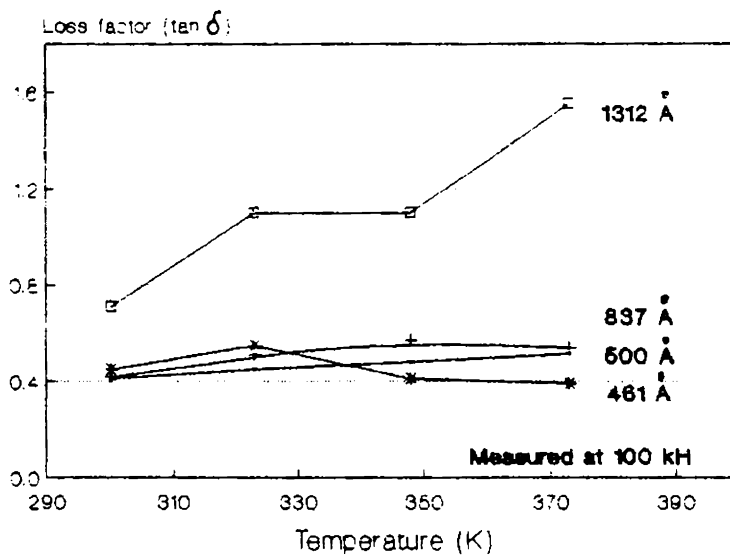


Fig.4.70

Temperature dependence of the Loss factor ($\tan \delta$) of a-Si:H thin films



plot of $\ln Z$ vs $\ln \omega$ and ESR vs frequency for a-Si:H films are given. In this particular case the film thickness is 1312 Å. The slope of the straight line part of $\ln Z$ vs $\ln \omega$ plot is 0.83 unlike in the case of a-Si, where it was 1. Z shows a minimum value at 500 kHz, beyond which it increases. ESR exhibits a sharp decrease when the frequency changes from 10 kHz to 25 kHz. From 200 kHz to 1 MHz ESR remains almost independent of frequency.

An analysis of the above results is presented below. It is well known that all the main polarizations are possible in the case of an amorphous thin film. In an MIS structure interfacial polarization can arise due to the accumulation of space charge at the metal-dielectric interfaces. Both bulk material properties and interfacial effects can contribute to the polarization mechanisms in these films. Interfacial polarization is not a characteristic of the material while polarizations resulting from imperfections, defects and ion-vacancies in the film structure are characteristic of the material [11].

It is generally observed that ϵ increases towards the low frequency side in the case of interfacial polarization. In this case ϵ increases with increase in temperature.

In the present case we have observed that in unhydrogenated samples ϵ increases with increasing frequency. In this case ϵ is independent of temperature in the range measured (Figure 4.20). So here interfacial polarization can be ruled out. Since electronic polarization becomes dominant at very high frequencies, the most probable mechanism will be polarization resulting from imperfections, defects and microvoids in the film.

In hydrogenated films, for certain film thicknesses (837 Å and 1312 Å) ϵ decreases with increasing frequency upto a certain value of frequency and then increases with further increase in frequency. It is also observed that for these films ϵ increases with increase in the measurement temperature (Figure 4.60). Hence it can be concluded that interfacial polarization is present in addition to polarization due to defects **and microvoids in these films and also that the contribution** due to the latter is comparatively less than in the case of unhydrogenated samples. This is more due to the passivation of Si dangling bonds by hydrogen than due to the annealing out of microvoids since both hydrogenated and unhydrogenated films were subjected to the annealing step upto 573K. But thinner a-Si:H films (461 Å and 500 Å) behaved like unhydrogenated samples.

It is usually observed that as the frequency increases $\tan \delta$ initially decreases, passes through a minimum and then increases. Here in hydrogenated and unhydrogenated cases and for different film thicknesses we have observed a steady increase in $\tan \delta$ with frequency, in the frequency range studied. This is due to the effect of electrodes and lead resistances [24].

The dielectric constant of a solid is a property which depends on the atoms and molecules present and their arrangements. Hence it is a bulk property. However, practically in the case of thin films it depends on the thickness of the films [12,13]. The thickness dependence of the dielectric constant is thought to arise owing to the presence of voids in the thinner films. As the films become thicker the density of voids decreases resulting in a higher value of dielectric constant and when the films become sufficiently thick for the voids to disappear, the dielectric constant becomes thickness independent.

From the value of the dielectric constant, loss factor, impedance, equivalent series resistance and parallel conductance of the a-Si:H films with different thicknesses at 10 kHz frequency the values of these parameters at 603 Å

are deduced. The following values are obtained. Dielectric constant (ϵ) = 7, loss factor ($\tan\delta$) = 0.11, impedance (Z) = 170 $k\Omega$, equivalent series resistance (ESR) = 0.021 $k\Omega$ and parallel conductance (G) = 0.6 ms. The corresponding values of a-Si film of the same thickness are $\epsilon = 4.4$, $\tan\delta = 0.05$, $Z = 292 k\Omega$, ESR = 0.02 $k\Omega$ and $G = 0.19$ ms. So it becomes clear that after hydrogenation the dielectric constant increased considerably. This was accompanied by an increase of the loss factor. The increase in ϵ is due to the decrease of the localized states in the energy gap. The increase in the loss factor is due to the increase in the parallel conductance which indicates that the main loss mechanism is conductive.

4.40 Conclusion

From the dielectric studies of hydrogenated and unhydrogenated amorphous Si thin films it was found that the **unpaired silicon bonds known as dangling bonds** contribute to the polarization mechanisms. In thinner films the interfacial polarization is negligible in the frequency range studied. But in thicker hydrogenated films interfacial polarization is evident to some extent. The increase of the loss factor with frequency indicated the role of electrodes and lead resistance in the measurements. From these studies it can be concluded that eventhough the resistivity of the a-Si and

a-Si:H films is very high their dielectric parameters are very much dependent upon the frequency and temperature of measurement.

From the study of the dielectric parameters of a-Si:H thin films with different thicknesses the values of those parameters at a thickness of 603 \AA were found out and were compared with those of a-Si thin film of the same thickness. The appreciable increase in ϵ noticed in the case of a-Si:H film is interpreted as due to the decrease in the localized gap states.

REFERENCES

1. Robert W. Berry, Peter M. Hall and Murray T. Harris, "Thin Film Technology", Van Nostrand Reinhold Co. (1968) 371.
2. L.I. Maissel and R. Glang, "Handbook of Thin Film Technology", McGraw Hill Book Company, New York (1970) 19-1
3. W. Kohn, Phys. Rev., 110 (1958) 857.
4. K.L. Chopra, "Thin Film Phenomena", McGraw Hill Book Company, New York (1969) 465.
5. J.D. Joannopoulos and M.L. Cohen, Solid State Commun., 13 (1973) 1115.
6. J.H. Weaver, R.W. Alexander, L. Teng, R.A. Mann and R.J. Bell, Phys. Status Solidi A, 20 (1973) 321.
7. A.V. Gelatos and J.D. Cohen, Appl. Phys. Lett., 47 (1985) 412.
8. J. Simmons, G.S. Nadkarni and M.C. Lancaster, J. Appl. Phys., 41 (1970) 538.
9. G.S. Nadkarni and J.G. Simmons, J. Appl. Phys., 41 (1970) 545.
10. A. Goswami and A.P. Goswami, Thin Solid Films, 16 (1973) 175.

11. T.Mahalingam, M.Radhakrishnan and C.Balasubramanian, Thin Solid Films, 59 (1979) 221.
12. U.Saxena and O.N.Srivastava, Thin Solid Films, 33 (1976) 185.
13. A.Goswami and A.P.Goswami, Thin Solid Films, 20 (1974) 53.

Chapter 5

FABRICATION AND CHARACTERIZATION OF METAL-OXIDE- SEMICONDUCTOR FIELD EFFECT TRANSISTORS

Abstract

In this chapter the fabrication and characterization of thin film field effect transistors using a-Si and a-Si:H are presented. Europium oxide is used as the gate insulator. The transistor characteristics are good and reproducible. It is found that hydrogenated samples generally exhibit more ordered and well shaped characteristics. Maximum amplification factor is obtained for a europium oxide thickness of 715 Å. The main drawback of the present device is its low value of the gain-bandwidth product.

5.00 Introduction

The invention of the transistor by Bardeen and Brattain in 1948 was a great leap forward in the field of electronics [1,2]. It replaced the vacuum tubes which dominated the scene until then. The introduction of transistors made the electronic instruments compact, robust and power efficient. Moreover, the ease with which it could be mass produced also contributed significantly to its extremely rapid expansion.

The first transistors made were of point contact type. Later p-n junction transistors were invented by Shockly [3]. Along with this, different transistor circuits were developed by Ryder et al. [4]. Of the several types of transistors, the field effect transistor (FET) is of particular interest because it is easy to fabricate it in thin film form. An FET operates on the principle that the thickness and hence the resistance of a conducting channel of semiconductor material may be regulated by the magnitude

of the potential applied to the gate electrode. Thin film FETs show sufficiently good electrical characteristics to permit useful circuits to be built. The deposition of thin film transistors (TFTs) upon the same substrate with passive components permits the fabrication of complex integrated circuits entirely by evaporation. A complete circuit can be deposited in one pump-down of the vacuum system, using movable masks for pattern delineation. Several semiconducting materials can be used to fabricate TFTs, the best results have been obtained with cadmium sulphide, cadmium selenide and tellurium [5]. Since the successful development of CdS TFTs by Weimer [5] much debate has occurred as to their quality, stability, reproducibility and usefulness. To their detriment, TFT integrated circuits were compared with the rapidly emerging crystalline Si technology. Hence systematic research necessary to understand the problems of the TFT were continued only by a few groups. However from 1970 onwards it became clear that the TFT offered an ideal solution for the problem of addressing large area display panels. This application has revived widespread interest in the TFT [6]. Following Weimer's pioneering work in CdS TFTs, several new materials have been added to the list, like lead sulphide [7] indium antimonide [8], lead telluride [9] and finally silicon. Due to these initial investigations, it was increasingly becoming clearer that to achieve significantly high

gain-band width products, the technology should be improved to produce near single crystal mobilities and control of the fast trapping states at the semiconductor-insulator interface. Due to the investigations on a wide range of semiconductor-insulator combinations, it was found that the performance of the devices was often dominated by 'slow' trapping states which caused decay of the source-drain current over periods from seconds to hours. An analysis of the TFT characteristics by Graeffe showed that the modulation in CdSe TFTs was mainly due to the variation of the barrier potential at the grain boundaries by gate field. This was further developed by Anderson [10,11,12] and has suggested that TFTs operated by barrier modulation and are not analogous to the single crystal metal-oxide-semiconductor transistors.

During the initial stages of the development of TFTs, chalcogenides dominated the list of the materials used for fabrication. This may be, as mentioned earlier, due to the successful fabrication of CdS TFTs by Weimer. Amorphous silicon is a comparatively newcomer in the scene. The possibility of the application of a-Si:H in the fabrication was originally suggested by the field effect studies in the 1970s, which showed that large current changes could be obtained for moderate fields produced by the gate electrode [13,14].

In 1976 itself many researchers have proposed the use of amorphous silicon field effect devices in the addressing of liquid crystal matrix displays as an alternative to the thin film CdSe transistors. They reasoned that an elemental covalently bonded material such as amorphous silicon should have distinct advantages over the more complex II-VI compounds as far as ease of preparation, reproducibility and stability were concerned. The design and characteristics of an amorphous silicon insulated gate field effect transistor (FET) suitable for driving liquid crystal displays were reported by LeComber et al. [15].

Despite such progress and availability of advanced techniques for the fabrication of thin film active components, the TFTs have not yet been used for widespread applications, except the few mentioned earlier, because of the variations in their characteristics. Therefore, many investigators are working on ways to stabilise the characteristics through the use of various semiconductor-insulator combinations.

Since the field effect studies were used from 1975 to evaluate the density of states of glow-discharge produced a-Si:H [16], it was relatively easy to fabricate a-Si:H FETs. But a quick survey of the literature shows that most of these devices are fabricated by amorphous silicon

produced by glow discharge. It was Malhotra and Neudeck [17] who first fabricated vacuum evaporated a-Si FETs successfully. In a subsequent paper [18] they have presented in detail the sample preparation and experimental procedures. They have used $\langle 100 \rangle$ oriented n-type silicon of 5-25 Ω cm resistivity as the substrate and thermally grown silicon dioxide as the gate insulator. But it will be really more advantageous if we can use glass substrates and insulators which have good dielectric properties and which are easy to deposit in thin film form by vacuum evaporation. An attempt was made in this direction and fabrication and characterization of thin film a-Si and a-Si:H FETs with europium oxide as the gate insulator are presented here. Since rare earth oxides are good insulators and are used in the fabrication of FETs by several researchers [19-23], the properties of the present FETs depend largely on the behaviour of the amorphous silicon films.

5.10 Theory of the conductance modulation by field effect

The first attempt to develop a theory for the modulation of conductance of thin films of semiconductors by surface charges was made by Shockley and Pearson in 1948 [24]. The theory is summarised below.

When charge is induced on the free surface of a semiconductor, by making it one plate of a parallel plate

condenser, some of the charge density δq goes into the surface states and some into the space charge in the barrier layer beneath the surface. If the applied field produces a change in potential δV on the surface, then δq_s the increased charge per cm^2 in the surface states will be $q N_s \delta V$ where q is the electronic charge and N_s is the number of surface states per unit area per unit voltage. The charge in the interior can be estimated from the Schottky exhaustion layer theory and is given by

$$\delta V = \frac{4\pi\rho b \delta b}{\epsilon} \quad (4.10)$$

where ρ is the net charge density of the impurities, ϵ the dielectric constant and δb the thickness of the exhaustion layer. This gives a charge of

$$\delta q_b = \rho \delta b = \epsilon \delta V / 4\pi b \quad (4.20)$$

which is produced by removing conduction electrons. Hence a fraction

$$\begin{aligned} \beta &= \delta q_b / (\delta q_b + \delta q_s) \\ &= \frac{(\epsilon / 4\pi b)}{[q N_s + (\epsilon / 4\pi b)]} \end{aligned} \quad (4.30)$$

of the total charge induced per unit area on the semiconductor is accounted for by reduced conduction electrons in the interior.

Let L be the thickness of the semiconductor and b the thickness of the exhaustion layers on both sides, then the total charge per unit area is

$$- \rho (L - 2b) \quad (4.40)$$

and the conductance parallel to the layer is

$$\sigma = \rho (L - 2b) \mu \quad (4.50)$$

where μ is the mobility.

The applied field changes the charge by $\delta q_b = \beta \delta q$ and therefore changes the conductance of the layer by

$$\frac{\delta \sigma}{\sigma} = \pm \frac{\beta \delta q}{\rho (L - 2b)} \quad (4.60)$$

where the minus sign holds for n-type materials and plus sign for p-type.

This simple theory by Shockley and Pearson explains all the features of the field effect modulation of the conductance of semiconductors.

The important transistor parameters are the following:

1. The transconductance (g_m) defined as the ratio of the change in the drain current (ΔI_d) to a given change in the gate voltage (ΔV_G).

$$\text{ie., } g_m = \Delta I_d / \Delta V_G$$

2. The drain resistance (r_d) at a particular gate voltage V_G

$$r_d = \left[\frac{V_d}{I_d} \right]_{V_G}$$

3. Gain-bandwidth product (GB) given by

$$\text{GB} = \frac{g_m}{2\pi C_g}$$

where C_g is the capacitance of the gate insulator.

4. Amplification factor (μ) defined as

$$\mu = g_m r_d$$

These parameters describe the behaviour of a thin film FET and they can be calculated from the different transistor characteristics.

5.20 Structure of thin film FETs

Thin film FET structures consist of two coplanar electrodes called 'source' and 'drain' joined by a thin semiconductor film, whose conductivity can be modulated by a third electrode called the 'gate'. The source and drain make ohmic contact to the semiconductor, but the gate is separated from the semiconductor by a thin insulator. There are two forms of FETs which have been used in integrated circuits. They are coplanar electrode FET and staggered-electrode FET. In the coplanar FET the semiconductor is first deposited onto the substrate over which the source-drain electrodes, insulator and gate electrodes are deposited in that sequence. In the latter, the sequence of deposition is source-drain electrodes, semiconductor, insulator and gate electrode (Figure 5.20).

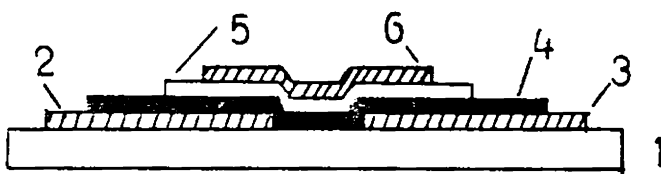
An advantage of the coplanar-electrode structure is that the semiconductor can be deposited and processed at elevated temperatures without requiring the electrodes to undergo such treatment. This structure was used success-

Fig.5.20

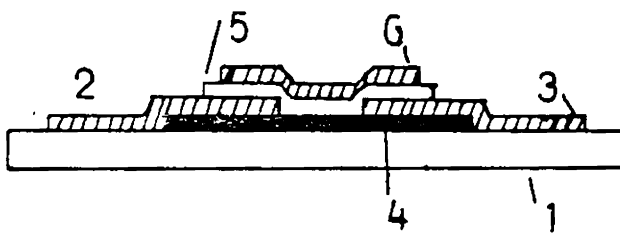
Cross section of two forms of thin film FETs

(a) Staggered - electrode FET

(b) Coplanar FET



(a)



(b)

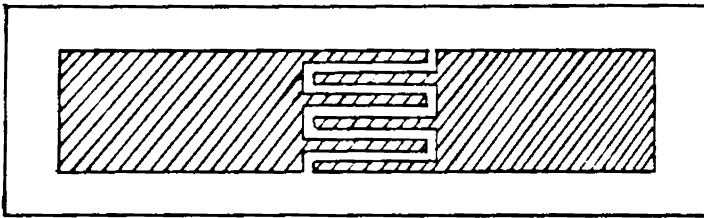
1. Substrate
2. Source electrode
3. Drain electrode
4. Semiconductor
5. Insulator
6. Gate electrode

fully for many of the early cadmium sulphide transistors, having aluminium as source and drain electrodes.

5.30 Experimental

In the present case the FETs were prepared in the coplanar structure. Optically flat glass slides were used as the substrates. They were chemically and ultrasonically cleaned and finally subjected to ion-bombardment cleaning. The amorphous silicon film was deposited onto this. The area of the silicon film was 1.5x1.5 cm. Over this, source and drain electrodes were deposited in an interdigitated structure using a suitable mask (Figure 5.30). Since the source-drain field must be kept small relative to the gate field to obtain a uniform space charge layer, and also must be large enough to make the current measurable, a very small source-drain electrode separation becomes necessary. This would usually require photo resist masking and etching. But this process leaves the exposed surface of the a-Si:H film in a condition which is often irreproducible and probably leads to a conducting surface space charge layer especially in the case of nearly intrinsic films [25]. Hence we chose an electrode separation of 0.15 cm. The total width was greatly increased by the finger structure and was 3 cm. In the fabrication procedure of a-Si:H FETs, the amorphous silicon films were subjected to hydrogenation as described in Chapter 2, before

Fig.5.30
Interdigitated finger structure for source
and drain electrodes



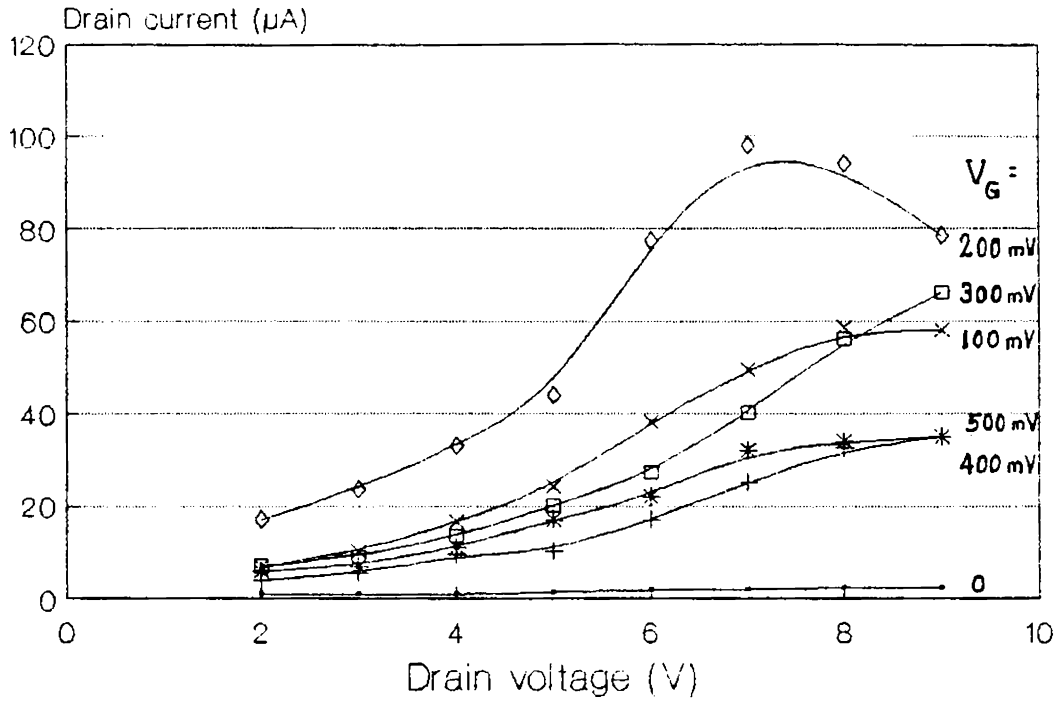
depositing the source and drain electrodes. The hydrogenation parameters were as follows: Hydrogenation temperature 573K, hydrogen partial pressure 0.05 torr and hydrogenation time 60 minutes. Over this europium oxide was deposited as the gate insulator by vacuum evaporation and finally aluminium gate electrode was deposited over the insulator such that it covered the channel between the source and drain. In the case of unhydrogenated silicon films, the completed devices were annealed at 573K at $\sim 10^{-5}$ torr. The devices were then subjected to electrical characterisation. A fixed voltage V_D was applied between the source and drain and drain current (I_D) was measured as a function of the gate voltage (V_G). This was repeated for different values of V_D . The measurements included the variation of impedance between source and drain with frequency. Gate-drain and gate-source capacitances were also measured as a function of frequency.

5.40 Results and discussion

In Figure 5.40 the source-drain current (I_D) versus source-drain voltage (V_D) for an FET fabricated with unhydrogenated amorphous silicon (thickness 683 Å) and europium oxide insulator (thickness 410 Å) is presented. From this figure it is seen that at gate voltage $V_G = 0$, I_D increases very slowly as V_D increases from 2 to 8V. But at higher V_G , the increase in I_D is more for a given increase in V_D . This

Fig.5.40

Drain current vs Drain voltage



is better illustrated in Figure 5.41 where I_D is plotted against V_G at different V_D . It can be seen from this figure that as V_G is increased, I_D increases at first, reaches a maximum at 200 mV and then decreases. In an n-channel FET (n-type semiconductor) the application of a positive gate bias causes I_D to increase. A detailed study of the effect of the positive and negative gate voltages on I_D is shown in Figure 5.42. The maximum value of transconductance was found to be $617 \mu \text{ mho}$ at $V_D = 7\text{V}$ and $V_G < 200 \text{ mV}$. The gain-band width product was 3.27 kHz. The capacitance of the gate insulator increased by $\sim 12\%$ as the measurement frequency was varied in the range 10 kHz to 100 kHz and above 100 kHz it suddenly increased and went out of range. The channel impedance (Z) is plotted against the measurement frequency logarithmically. Z exhibits a linear decrease with frequency in the range 10-500 kHz. This means that even though the number of charges developed on the semiconductor is almost independent of the signal frequency, that is applied on the gate (which is evident from Figure 5.43) the final output of the transistor may boost high frequency signals, since the channel conductance is a function of frequency (Figure 5.44).

The transistor characteristics, showing the variation of drain current I_D with drain voltage V_D at constant

Fig.5.41

Drain current vs Gate voltage

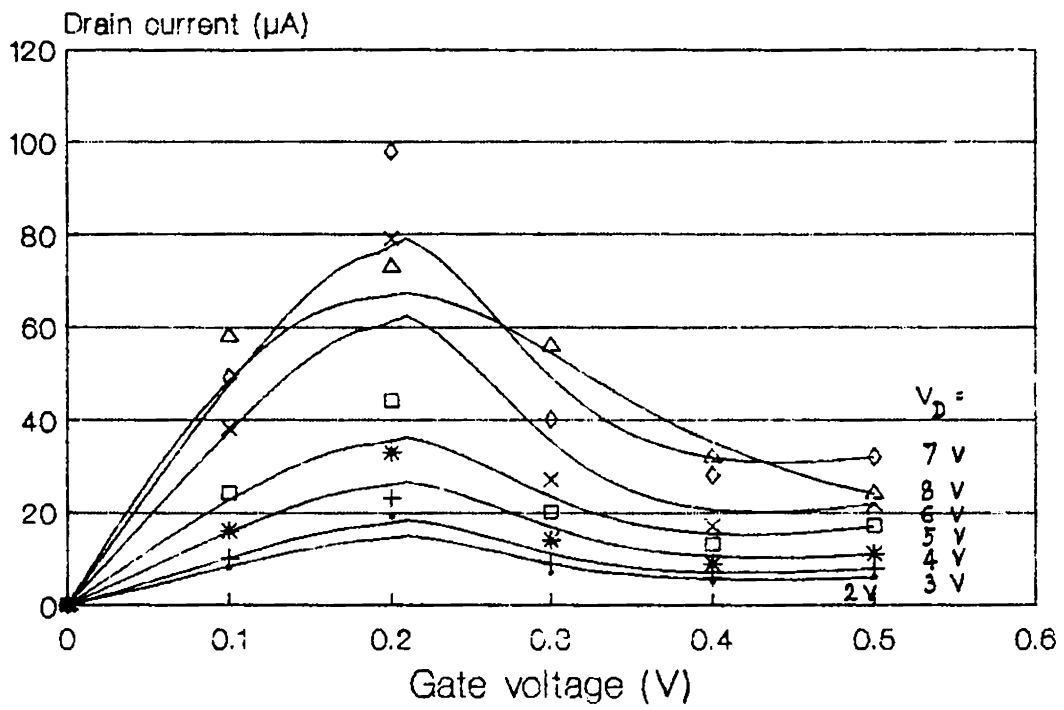


Fig.5.42

Drain current vs Gate voltage

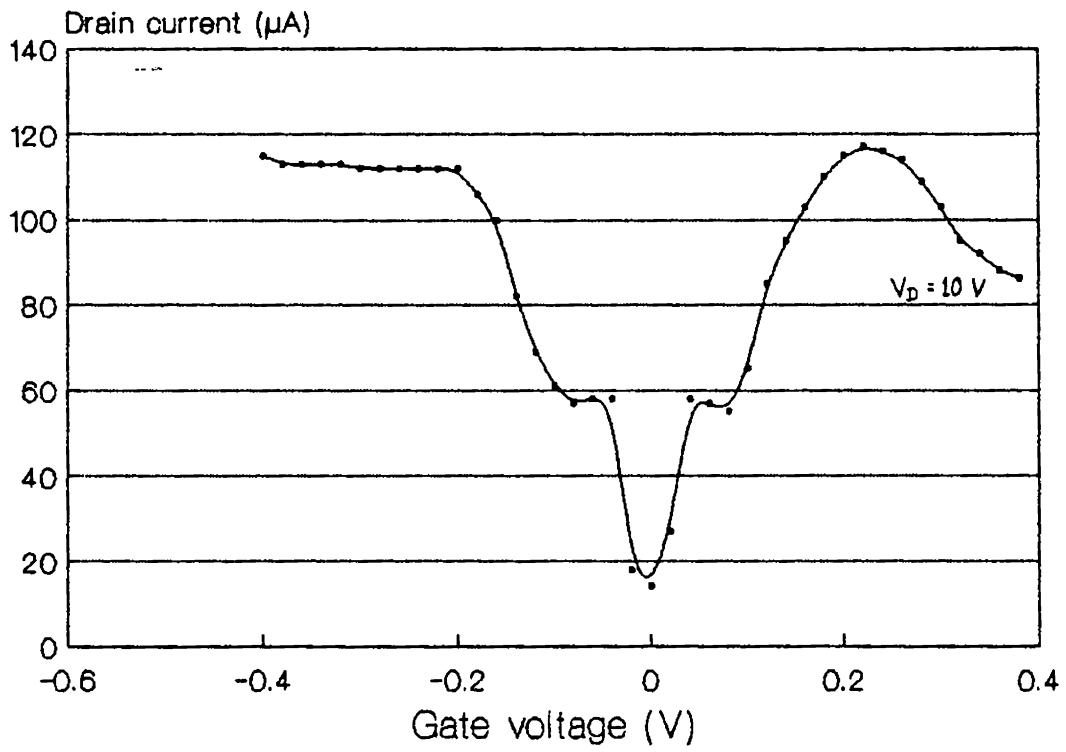


Fig.5.43

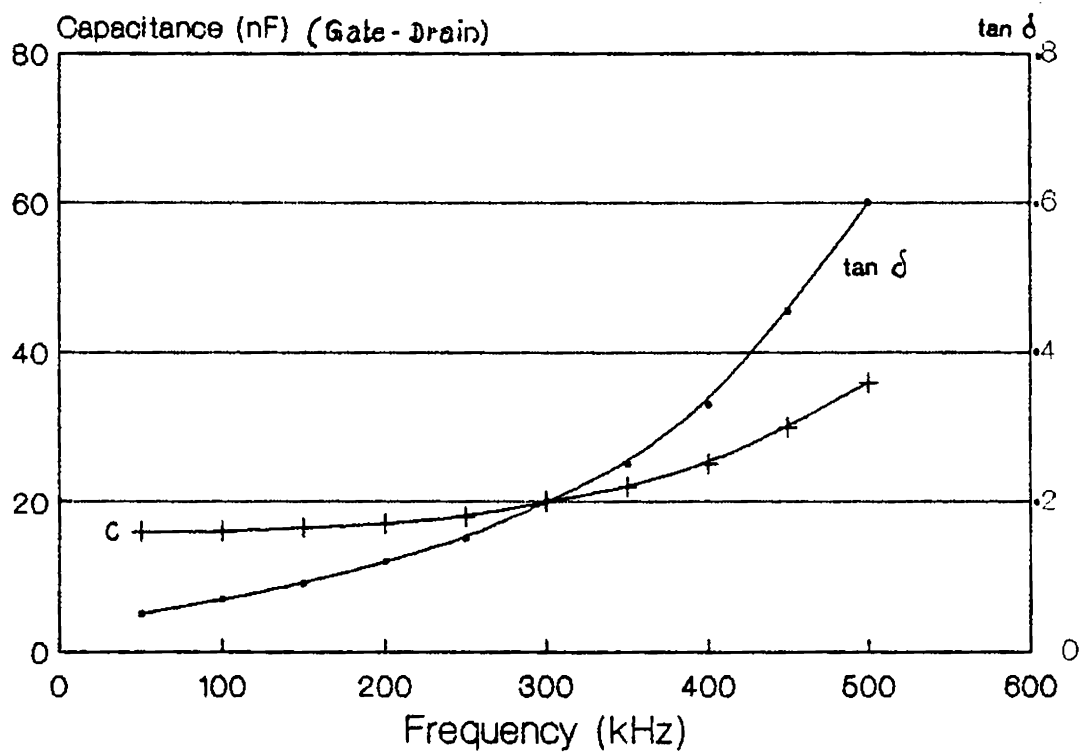
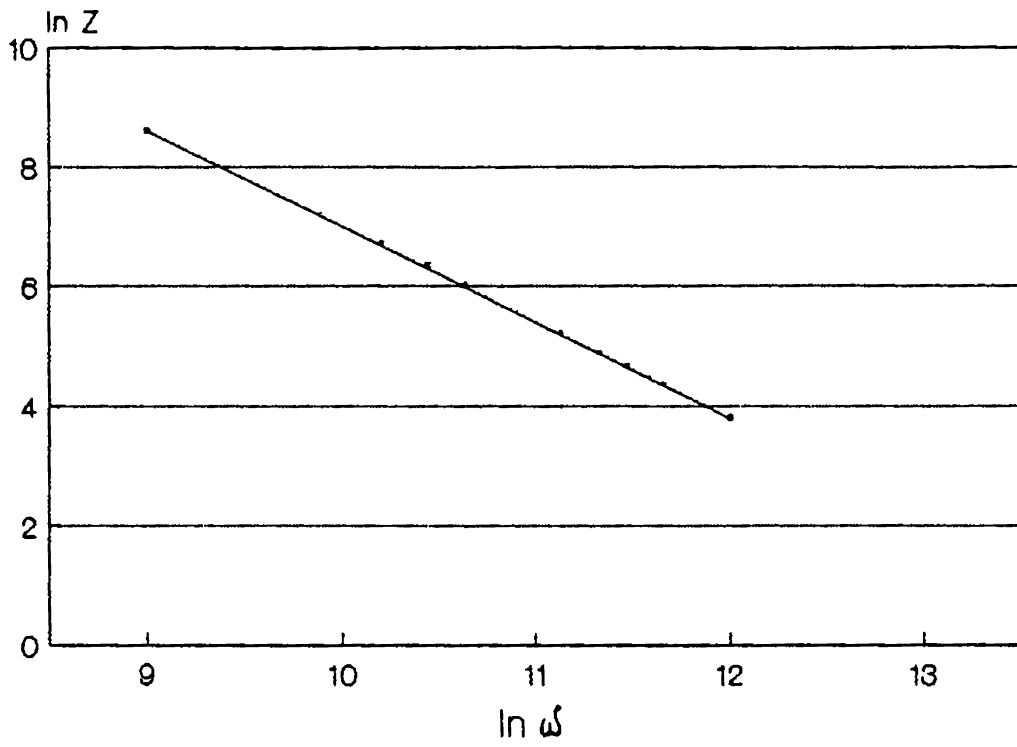
Capacitance and $\tan \delta$ vs Frequency

Fig.5.44
Impedance vs Frequency



gate voltage V_G are shown in Figure 5.45 for a a-Si:H FET. In Figure 5.46 the drain current I_D is plotted against gate voltage V_G at constant V_D . The thickness of the a-Si:H film was 683 \AA and that of europium oxide was 715 \AA . The transconductance (g_m) was calculated to be $486 \mu\text{mho}$ and the gain-bandwidth product (G.B.) was 4.8 kHz . The drain current (I_D) as a function of positive and negative gate voltages is given in Figure 5.47. The curve is found to be symmetrical. FETs were fabricated with the same a-Si:H film thickness, but different europium oxide thicknesses. In Figure 5.48 the I_D vs V_D curves at $V_G = 1\text{V}$ for three FETs with europium oxide thickness of 305 \AA , 715 \AA and 1317 \AA and Si thickness 683 \AA are presented. The maximum transconductance was observed for the FET with 715 \AA thick europium oxide. But the maximum gain-bandwidth product of 5 kHz was observed for europium oxide thickness of 1317 \AA . The calculated parameters of various transistors are listed in Table 5.40.

From the above table it is evident that the FET with europium oxide thickness of 715 \AA and a-Si:H thickness of 683 \AA exhibits superior performance compared to the other FETs. It has a reasonably good gain bandwidth product (GB) and a very high amplification factor compared to the other transistors.

Fig.5.45

Drain current vs Drain voltage

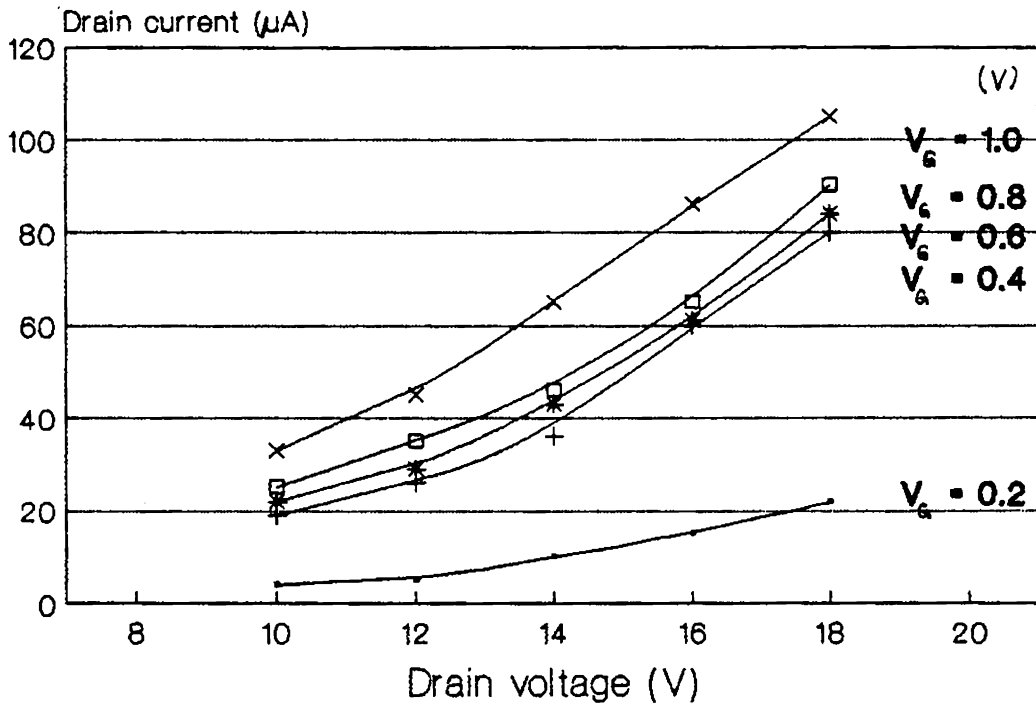


Fig.5.46

Drain current Vs Gate voltage

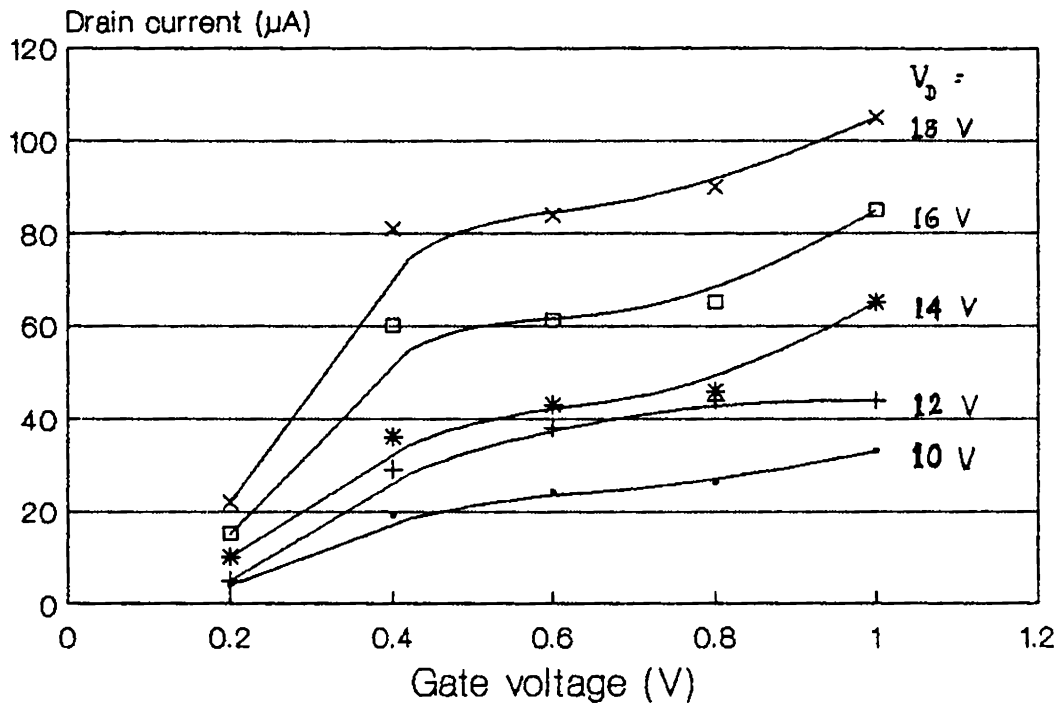


Fig.5.47

Drain current Vs Gate voltage

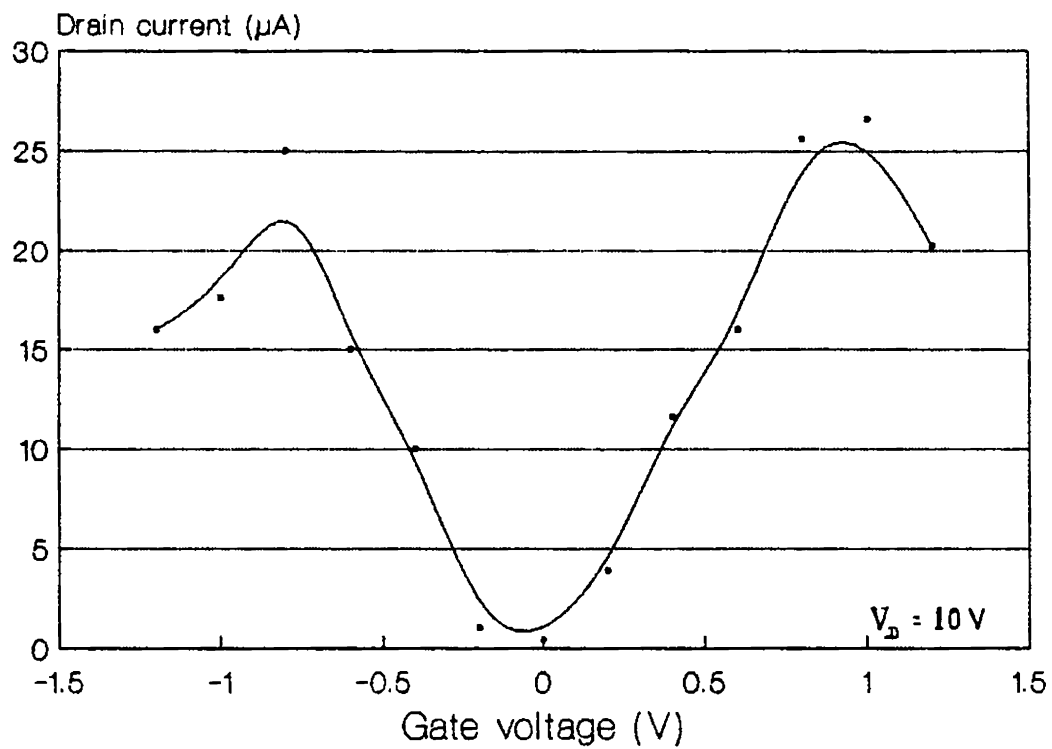


Fig.5.48

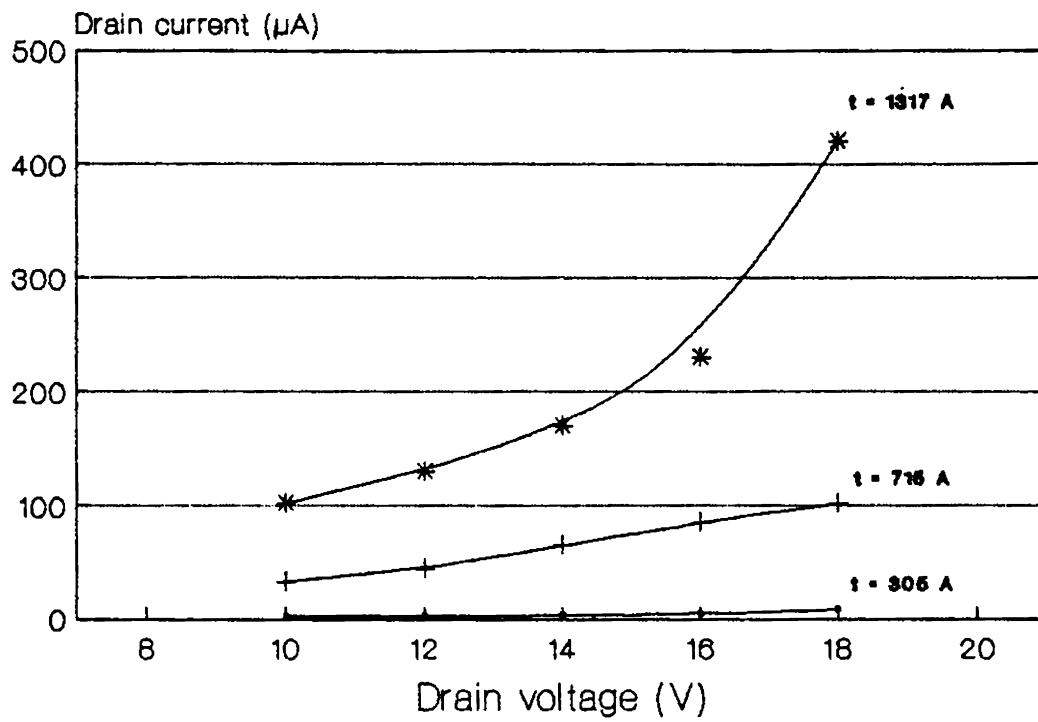
Drain current vs Drain voltage
(Gate voltage = 1 V)

Table 5.40

Parameter	a-Si	a-Si:H		
		Insulator thickness		
		305 Å	715 Å	1317 Å
Transconductance (g_m μ mho)	617	52.5	486	318
Gain/Bandwidth product (GB.kHz)	1.2	0.24	4.8	5.0
Output resistance (r_d) at $V_G=200$ mV (Ω)	1.5×10^5	1.7×10^6	4×10^5	5×10^4
Amplification factor ($\mu = g_m \times r_d$)	92.55	89.25	194.4	15.9

The main difference that was observed between a-Si and a-Si:H FETs was that in the former case the I_D vs V_G curves displayed a peak at a particular value of V_G . On one side of this peak the device resembles an n-channel FET and on the other side a p-channel FET. Such a behaviour was absent in the latter case. This can be due to the following reason. Consider the devices to be with a channel which is intrinsic or weakly n-type. When a positive field is applied to the gate electrode, I_D increases due to the increased number of electrons drawn to the surface from the bulk of the semiconductor. This explains the ascending portion of the $I_D - V_G$ curve (Figure 5.41). But when the field reaches a particular value leakage currents across the insulator becomes appreciable and the I_D will begin to decay. This combined with the very high trap density usually present in the a-Si films which negatively affects the observation of field effect in such devices may account for the descending portion of the curve. Indeed such leakage currents were observed in both a-Si and a-Si:H devices. But since the a-Si:H films contain an appreciably lesser number of trap sites, the drawing of electrons from the bulk of the semiconductor to the surface is comparatively easier.

The positive points of the present FETs are the following.

1. Using an interdigital finger structure for the source and drain electrodes, we were able to get an appreciable source drain current modulation even with an electrode separation of 0.15 cm and reasonable gate voltages. Thus we could avoid the photolithographic technique used to make the source and drain electrodes.

2. Europium oxide was used as the gate insulator. Usually the insulator used in a-Si:H FETs is electron beam gun evaporated or thermally grown SiO_2 . Europium oxide is comparatively easier to fabricate in the thin film form than SiO_2 .

3. Even, as deposited unhydrogenated films exhibited field effect. Hydrogenated samples generally exhibited more ordered and well shaped characteristics.

4. a-Si:H FETs with europium oxide thickness of 715 Å exhibited the maximum amplification factor.

5. Since the channel is essentially intrinsic in nature both electrons and holes contribute.

The main limitation of the present device was the low value of the gain-bandwidth product. Values as high as 6 MHz were reported for FETs fabricated with glow discharge

produced a-Si:H [26]. Maximum values obtained in the present case were around 4.8-5.0 kHz only. This can be improved by carefully optimizing the preparation conditions like the substrate temperature during Si deposition, hydrogenation conditions, insulator thickness and reducing the source-drain separation by better masking techniques.

REFERENCES

1. J.Bardeen and W.H.Brattain, Phys.Rev., **74** (1949) 230.
2. W.H.Brattain and J.Bardeen, Phys.Rev., **74** (1949) 231.
3. W.Shockley, The Bell System Technical Journal, **28** (1949) 435.
4. R.M.Ryder and R.J.Kircher, The Bell System Technical Journal, **28** (1949) 367.
5. Paul K.Weimer, "Handbook of Thin Film Technology", L.I.Maissel and R.Glang (Ed.) , McGraw-Hill Book Co., New York, (1970) 20-1.
6. J.C.Anderson, Thin Solid Films, **50** (1978) 25.
7. W.B.Pennebaker, Solid-State Electron., **5** (1965) 509.
8. V.L.Frantz, Proc.IEEE, **53** (1965) 760.
9. J.F.Skalski, Proc.IEEE, **53** (1965) 1792.
10. J.C.Anderson, Thin Solid Films, **36** (1976) 299.
11. J.C.Anderson, Thin Solid Films, **37** (1976) 127.
12. J.C.Anderson, Thin Solid Films, **38** (1976) 151.

13. W.E.Spear and P.G.LeComber, *J.Non-Cryst.Solids*, **8-10** (1972) 727.
14. A.Madan, P.G.LeComber and W.E.Spear, *J.Non-Cryst.Solids*, **20** (1976) 239.
15. P.G.LeComber, W.E.Spear and A.Ghaith, *Electron.Lett.*, **15** (1979) 179.
16. W.E.Spear and P.G.LeComber, *J.Non-Cryst.Solids*, **11** (1978) 153.
17. A.K.Malhotra and G.W.Neudeck, *Appl.Phys.Lett.*, **24** (1974) 557.
18. G.W.Neudeck and A.K.Malhotra, *J.Appl.Phys.*, **46** (1975) 239.
19. V.M.Koleshko and N.V.Babushkina, *Thin Solid Films*, **62** (1979) 1.
20. P.Singh and B.Baishya, *Indian J.Phys.*, **61A** (1987) 230.
21. P.Sing and B.Baishya, *Thin Solid Films*, **148** (1987) 203.
22. C.R.Dutta and K.Barua, *Thin Solid Films*, **100** (1983) 149.
23. C.R.Dutta and K.Barua, *Indian J.Phys.*, **57A** (1983) 338.
24. W.Shockley and G.I.Pearson, *Phys.Rev.*, **74** (1949) 230.

25. N.B.Goodman, *Phil Mag.B*, **45** (1982) 407.
26. K.D.Mackenzie, A.J.Snell, I.French, P.G.LeComber, W.E.Spear, *Appl.Phys.A*, **31** (1983) 8.
27. W.E.Spear and P.G.LeComber, "Topics in Applied Physics", Vol.55, J.D.Joannopoulos and G.Lucovsky (Ed.), Springer-Verlag, Berlin (1984) 63.

Chapter 6

CHARACTERIZATION OF CADMIUM SULPHIDE THIN FILMS PREPARED BY CHEMICAL BATH DEPOSITION METHOD

Abstract

Cadmium sulphide thin films are prepared by chemical bath deposition. Sulphur deficiency usually observed is mostly prevented by slightly modifying the deposition method. Instead of n-type, intrinsic films are obtained due to this modification. The films are found to be uniform, adhere tightly to the substrate and reproducible in electrical properties. From the d.c. and a.c. conductivity studies it is found that there exist two dominant trap levels near the midgap--most probably on either side of the Fermi level--with a very low density of states at the Fermi level proper. From the dielectric studies, ϵ is found to be independent of temperature upto 423K. From the frequency dependence of ϵ , the existence of monovalent impurities, vacancies and microvoids in the film are suggested.

6.00 Introduction

Cadmium sulphide is one of the extensively investigated materials. It is a typical example for a II-VI compound. Thin films of CdS in the thickness range 2-30 μm are usually used in the solar cells and various other applications such as piezoelectric transducers and photovoltaic devices [1-4]. The recent spurt in the interest in CdS thin films is mainly due to its suitability in the production of low cost solar panels for terrestrial applications.

A large number of techniques are employed for the deposition of CdS films, prominent among them are evaporation [5-14], sputtering [15,16], spray pyrolysis [17-19], molecular beam epitaxy [20], vapour phase epitaxy [21], chemical vapour deposition, screen printing [22,23], chemical bath deposition [24] and anodization [25]. Each of these methods has its own merits and demerits. For example, in the case of evaporation it is well known that some type of confinement of the evaporant vapour, like hot wall technique (HWT) is necessary to avoid a fast preferential loss of the high vapour pressure component (sulphur) from the depositing phase [26-29]. HWT contributes significantly to the preparation of thin films with bulk properties. It was also observed that vacuum evaporation yields very good uniformity in the film thickness.

Sputtering is a very suitable method for producing highly pure and defect free CdS films. But this method requires special sputtering targets. Screen printing is recently employed for the production of low cost CdS solar cells. However this method is not suitable for producing very thin layers and also the thickness uniformity of the film is very poor.

Chemical method by far is largely employed for the production of CdS thin films. Chemical method is preferred because it is cheaper and easier compared to the physical method. It will assume greater importance in the near future, if large scale manufacturing of low cost thin film solar cells is to be a reality for terrestrial applications. Among different chemical methods, spray pyrolysis comes first as far as the preparation of CdS thin films are concerned. Spray pyrolysis was used as early as 1910 to obtain transparent oxide films [30]. But it was in 1960, Chamberline et al. extended the technique to sulphide and selenide films [31-33]. This technique involves the spraying of an aqueous solution containing soluble salts of the constituent atoms of the desired compound on to a substrate maintained at elevated temperatures. The spray undergoes a pyrolytic decomposition at this temperature and forms a single crystallite or a cluster of crystallites of the product. To obtain CdS films, a dilute aqueous solution of a water-soluble cadmium salt and a sulpho-organic salt are

commonly used [34-35]. The most commonly used chemicals are cadmium chloride and thiourea. The spray deposited films are strongly adherent to the substrates. They are in general pin hole-free and stable with time and temperatures. However, the surface topography of the films is rough and depends on the spray conditions. At annealing temperatures above the spray temperatures, recrystallization increases the grain size and may produce some preferential orientation effects [36].

Chemical bath deposition is another chemical method which is gaining popularity due to the possibility of preparing highly uniform and adherent films. It is a form of solution growth technique pioneered by the works of Bode and co-workers [37-39]. The solution growth technique was first used in 1946 to prepare PbS films for infrared applications [40]. The chemical aspects of the solution growth is outlined below. According to the solubility product principle, in a saturated solution of a weakly soluble compound the product of the molar concentrations of its ions called the ionic product (IP) is a constant at a given temperature. For example, $\text{Cd}(\text{OH})_2$ when added to water will hydrolyze according to the reaction,



The ionic product (IP) is given by

$$\begin{aligned} [\text{Cd}^{2+}] \times [\text{OH}^-]^2 &= \text{Constant (solubility product SP)} \\ &= 2.2 \times 10^{-14} \quad (\text{at } 25^\circ\text{C}) \end{aligned}$$

There is no equilibrium if this relationship is not satisfied. If the IP exceeds SP precipitation occurs. When $IP < SP$ the solid phase will dissolve until the above relation is satisfied.

It is necessary to eliminate spontaneous precipitation in order to form a thin film by a controlled ion-by-ion reaction. This can be achieved by using a fairly stable complex of the metal ions. The concentration of the metal ions is controlled by adding an appropriate complexing agent in correct concentration. For producing CdS, ammonia solution acts as the complexing agent. If a high concentration of S^{2-} ions exists locally, such that the solubility product is exceeded, localized spontaneous precipitation of a sulphide can occur. This problem can be overcome by generating chalcogen ions slowly and uniformly throughout the volume of the solution. This is achieved by having thiourea in an alkaline aqueous solution. The kinetics of growth of a thin film in this process is determined by the ion-by-ion deposition of the chalcogenide on the nucleating sites of the immersed surfaces.

In the present studies, thin films of CdS are prepared by chemical bath deposition (CBD) in a manner described by Pavaskar et al. [24] with some modifications. The details are described in the subsequent section. Eventhough the structure, d.c.sd electrical conduction, photoconduction, and

photovoltaic effects of this material are well studied [24, 41-44], its a.c. conduction mechanisms and dielectric properties are not so extensively investigated. A detailed account of these properties of CdS thin films prepared by CBD is presented here. It is shown here that the modifications employed in the deposition method enabled to obtain intrinsic films with an entirely different distribution of the density of states in the energy gap.

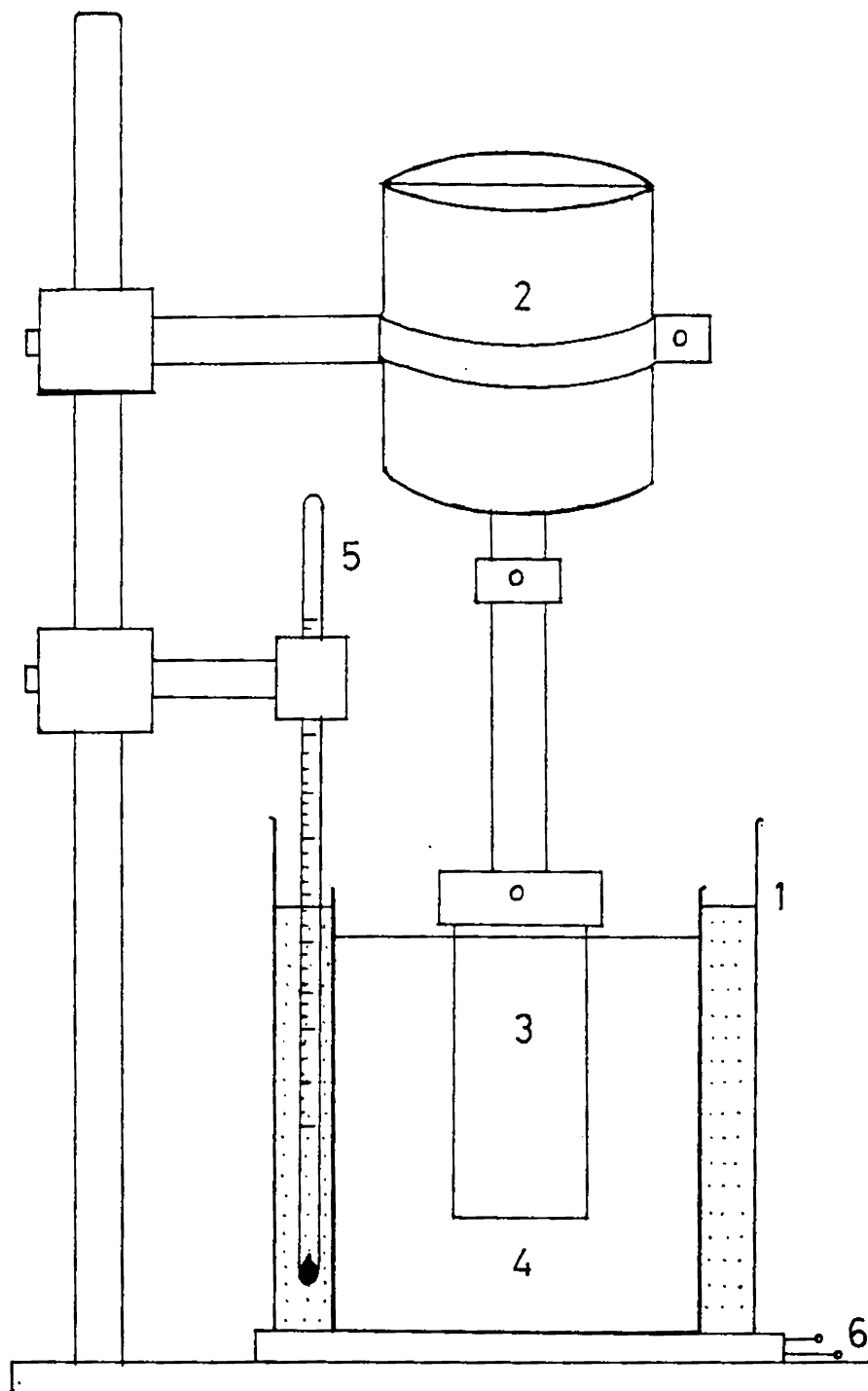
6.10 Method of preparation of cadmium sulphide

In this method, films are prepared by the reaction of thiourea with cadmium tetraammonium sulphate. The set up used here for the preparation is shown in Figure 6.10. It consists of an oil bath (1) whose temperature can be controlled using a variac. The temperature is monitored by a thermometer (5). The chemical solution taken in a 250 c.c. flask is placed in the oil bath. The cleaned glass slides on which the films are to be deposited are kept rotating inside the reaction solution using a small d.c. motor (2).

Freshly prepared distilled water is used to prepare the solutions. For each deposition 10 c.c. of 1 mole cadmium sulphate solution and 50 c.c. of 2 mole ammonia solution are mixed in a 250 c.c. beaker to form a complex compound. To

Fig.6.10

Schematic diagram of the set-up for the preparation of CdS thin films by chemical bath deposition



1. Oil bath
2. D.C. Motor
3. Substrate
4. Thiourea solution
5. Thermometer
6. Heater

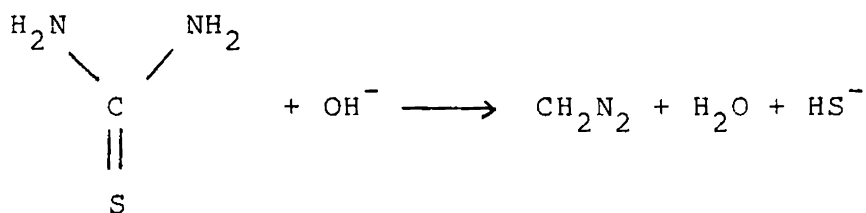
this solution is added 10 c.c. of 1 mole thiourea solution from a burette. The solution is heated to 80-90°C. The substrates are kept rotating inside this solution. The films formed are washed using distilled water, dried and subjected to measurements.

The mechanism of CdS formation as suggested by Pavaskar et al. [24] is given below:-

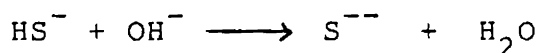
1. Cadmium salt reacts with ammonia to form the complex compound,



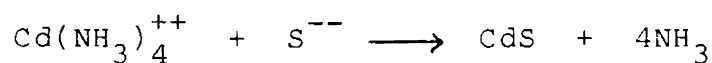
2. Diffusion of the complex ion, OH^- , and thiourea to the catalytic surface of CdS.
3. Dissociation of the thiourea on the CdS catalytic surface in an alkaline medium.



4. Formation of bivalent sulphide ions



5. Formation of CdS



The method described above is the standard chemical bath technique for the deposition of CdS films. But we made a slight deviation by rotating the glass slides inside the hot thiourea solution and adding cadmium tetraammonium sulphate from a burette. This enabled us to get better films by avoiding to a greater extent the sulphur deficiency in the films which is commonly observed in other chemical methods.

6.20 Experimental details and measurement techniques

The thickness of the films varied from 1000 to 1300 Å. The films were given silver electrodes in another coating chamber. For d.c. conductivity studies, electrodes were deposited in the planar structure. For capacitance measurements the glass slides were precoated with the first electrode before depositing CdS films. All the measurements were carried out by placing the films inside the metal cell described in Chapter 2. Current was measured using an electrometer amplifier (model EA 815 ECIL). For a.c. conductivity and dielectric measurements HP 4277 A LCZ bridge was used. A.C. conductivity was measured as a function of frequency from 10 kHz to 1 MHz.

Capacitance and loss factor measurements were carried out as a function of frequency and temperature in the range 350 kHz to 1 MHz and 300K to 458K respectively.

6.30 Results and discussion

6.31 D.C. conduction

From the current-voltage studies it was found that the conduction is ohmic upto an applied electric field of 4×10^3 V/cm above which upto a field of 9.5×10^3 V/cm the slope is 6.67 favouring a conduction mechanism controlled by deep traps (Figure 6.30). For fields above 10^4 V/cm the slope is 2.38 supporting a space charge limited conduction. The d.c. electrical conductivity (σ) of the films is $6.7 \times 10^{-10} \Omega^{-1} \text{cm}^{-1}$. The plot of $\ln \sigma$ vs. $10^3/T$ exhibits two slopes giving activation energies $E_1 = 1.55$ eV below 333K and $E_2 = 1.1$ eV above 350K (Figure 6.31). This is contrary to the usual observation of a low activation energy at lower temperature and a high activation energy at a higher temperature. But as explained in Chapter 2, such observations were reported earlier eventhough a satisfactory explanation was not presented. In all films studied here, the low activation energy occurred above ~ 333 K. From the values of the activation energies, we can conclude that the dominant trap levels lie around the middle of the energy gap.

Fig.6.30

I - V characteristic of Ag - CdS - Ag
structure

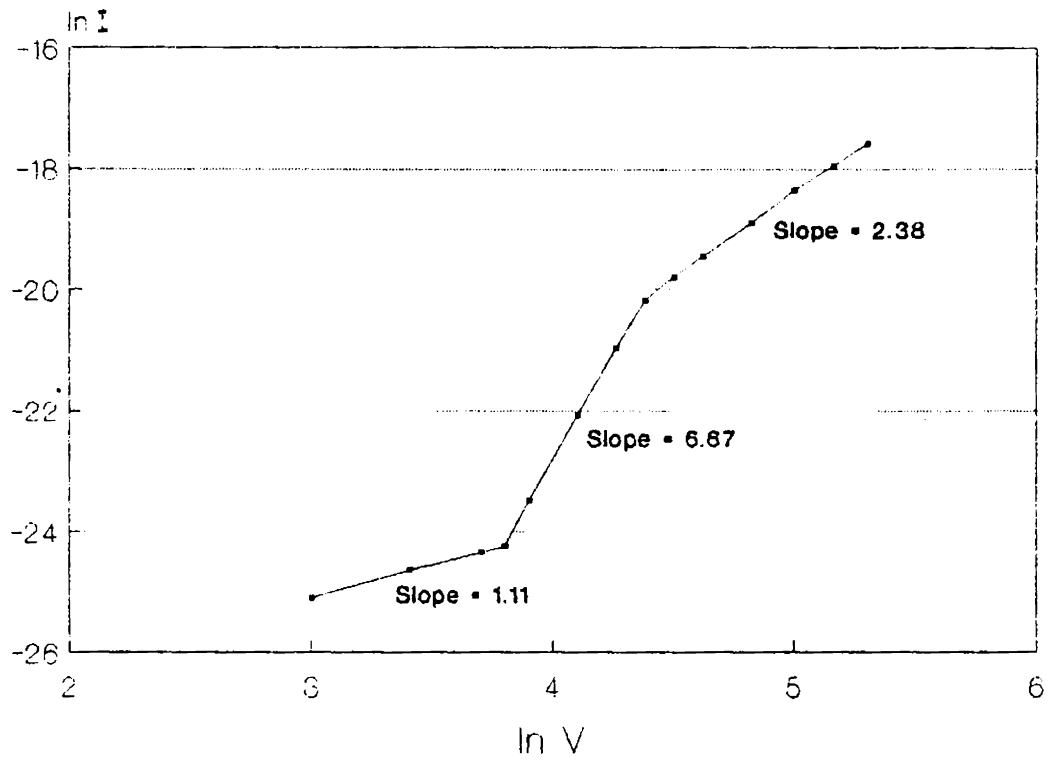
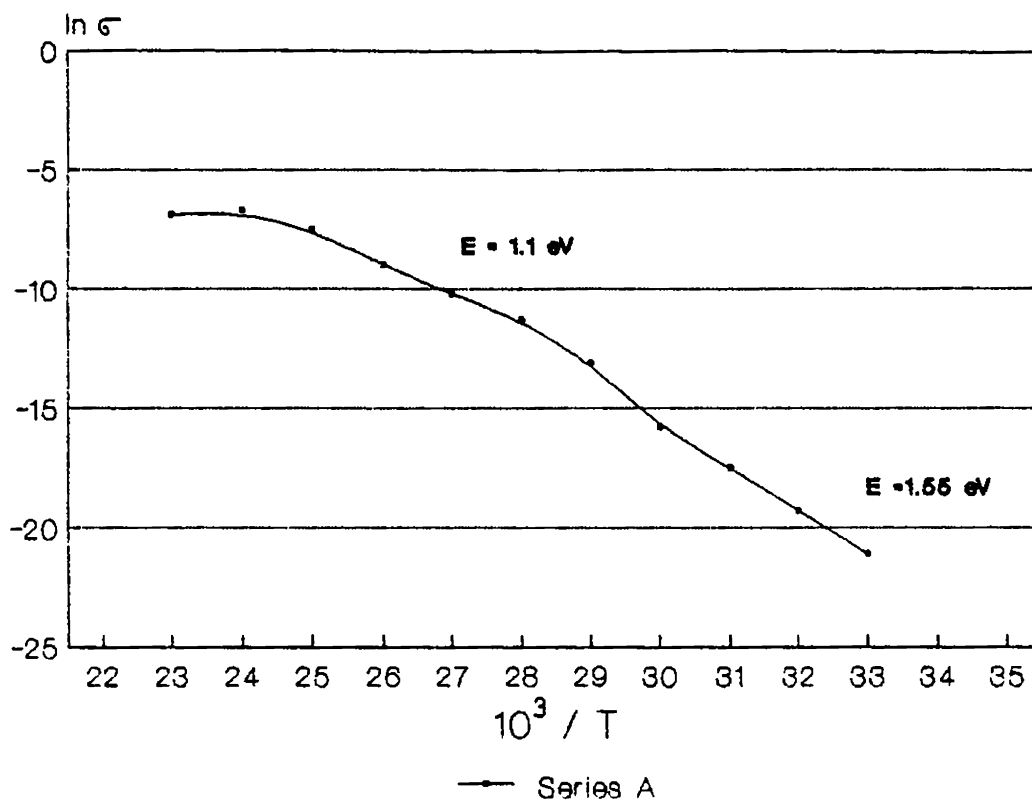


Fig.6.31

 $\ln \sigma$ vs $10^3 / T$ 

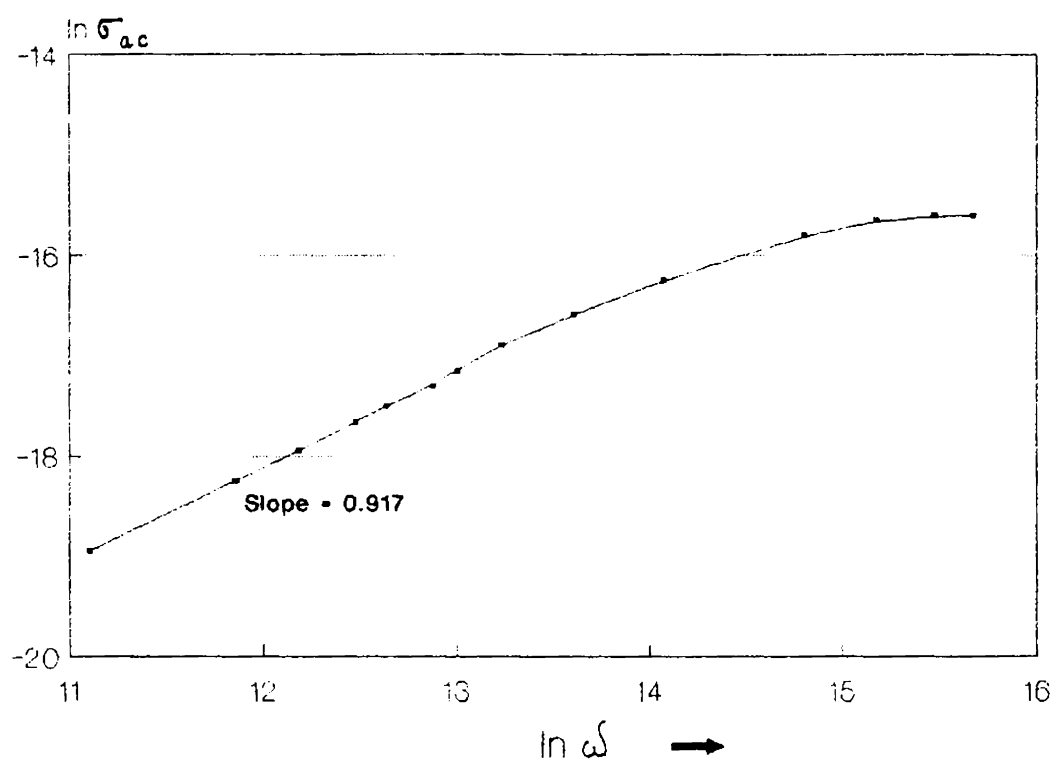
The CdS prepared by the spray pyrolysis and conventional chemical bath method are n-type because of the sulphur deficiency [24]. But in our method sulphur deficiency is not likely to occur. On the contrary, there is every possibility for the presence of excess of sulphur atoms making the films intrinsic if not slightly p-type. Though hot probe method suggests the films to be slightly p-type, it is not safe to draw such a conclusion for samples with very low conductivity. Hall effect measurements under strong photoexcitation could have confirmed these results. However the very low value of the conductivity ($\sim 10^{-10} \Omega^{-1} \text{cm}^{-1}$) demonstrates that the film is atleast intrinsic showing that the present method is suitable to reduce sulphur deficiency in CdS films.

6.32 A.C. conduction

A.C. conduction of the CdS films were analysed using Elliott's theory of a.c. conduction in chalcogenide glasses given in Chapter 2 [45,46]. A plot of $\ln \sigma_{a.c}$ vs. $\ln \omega$ shows that $\sigma_{a.c}$ increases with frequency (Figure 6.32) in the range at which measurements were carried out. At high frequencies (above 300 kHz), there is a levelling off of the curve which was repeatedly observed in all the measurements. This behaviour is due to semiconductor-metal contact effects at these frequencies. The slope (S) of the linear part of the curve is 0.0917.

Fig.6.32

Dependence of the a.c conductivity of CdS films on the measurement frequency



According to this theory, the frequency dependence of $\sigma_{a.c}$ is given by the relation

$$\sigma_{a.c} = \frac{\pi^2 N K}{24} \left[\frac{8e^2}{K W_M} \right]^6 \left[\frac{\omega^S}{\tau_0^\beta} \right] \quad (6.10)$$

where N is the density of defect states at the Fermi level, K is the dielectric constant, e is the electronic charge, ω is the frequency, W_M is the binding energy, which as a first approximation can be considered to be equal to the band gap energy and τ_0 is the bulk relaxation time which is of the order of an inverse phonon frequency ($\tau_0 \sim 10^{-13}$ sec.). β is equal to $6 kT/W_M$ where k is the Boltzmann constant and T is the absolute temperature. The relation between S and β is

$$S = (1 - \beta) \quad (6.20)$$

In the present study β was calculated to be equal to 0.0647 by assuming a band gap of 2.4 eV. Hence $S = 0.9353$. But from Figure 6.32 we get S as 0.917. This means that the approximation of W_M as the binding energy is not valid in this case. It seems that Elliott also faced a similar problem with another sulphur containing compound (As_2S_3) in comparing the calculated and measured values of S for certain chalcogens [45]. It is more appropriate to calculate W_M from the experimental value

of S . Using the experimental value of S we obtained β as 0.083 and W_M as 1.868. Using these values of s , β and W_M we calculated the density of defect states N at the Fermi level and obtained a value of $4.05 \times 10^{12} \text{ cm}^{-3} \text{ eV}^{-1}$. Even though this is a very low value compared to the reported values ($\sim 10^{19} - 10^{20}$) [24], it is not altogether improbable due to the following reasons:

1. Most of the reported values represent the density of states of n-type films with high sulphur deficiency. Present films are prepared by a slightly different method and they are essentially intrinsic.
2. By taking into account the very low value of the d.c. conductivity and the intrinsic nature of the films, we can consider the Fermi level to be just at the mid-gap ($\sim 1.2 - 1.3 \text{ eV}$). The activation energies obtained from the d.c. measurements indicate that the Fermi level is relatively free from traps while there are a large number of states on either side of it.
3. We have employed a.c. conductivity measurements to calculate N unlike the usual field effect method. Field effect method has always a tendency to over estimate N due to the surface states. There can be very large differences in the calculated values of N depending upon the methods of measurement [47].

Hence we can conclude that the value of N calculated in the present case indicates the more probable bulk value of the density of states at the Fermi level of the CdS films prepared by chemical bath deposition.

6.33 Dielectric measurements

The capacitance and loss factor of the films were measured as a function of frequency and temperature. From this the dependence of dielectric constant (ϵ) on frequency was found out. As the frequency was varied from 300 kHz to 1 MHz, ϵ varied from 16.5 to 10.31 in a step like fashion as shown in Figure 6.33. Usually the presence of monovalent impurities and vacancies in the film produce such a behaviour of ϵ . In the present case, since the glass substrates rotated inside the hot thiourea solution were precoated with silver electrodes, the inclusion of traces of silver into the CdS films cannot be ruled out. Moreover, the presence of microvoids and vacancies are common in the chemically prepared films. This explains the existence of different relaxation times which in turn cause the particular shape of the ϵ vs frequency curve. ϵ and $\tan \delta$ were more or less constants upto 423K above which ϵ decreased suddenly and reached a value of 4.12 at 448K. Above 423K $\tan \delta$ increased suddenly (Figure 6.34). The ionisation of traps together with the dominance of the chaotic thermal oscillations at high temperatures are perhaps the reasons for the sudden decrease of ϵ and increase of $\tan \delta$ above 423K.

Fig.6.33

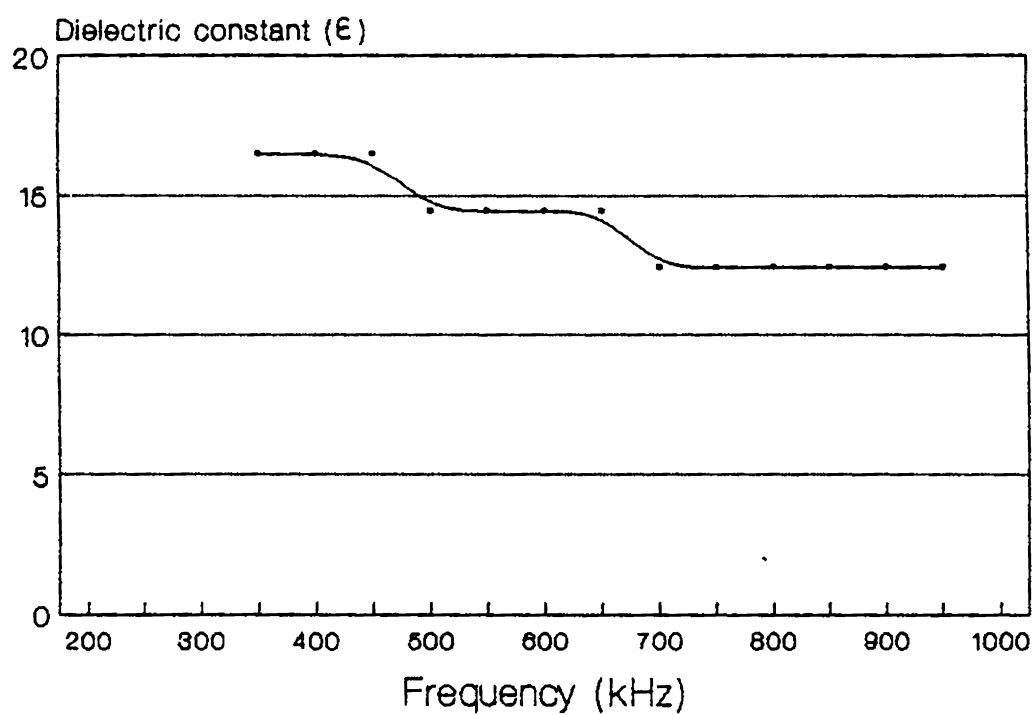
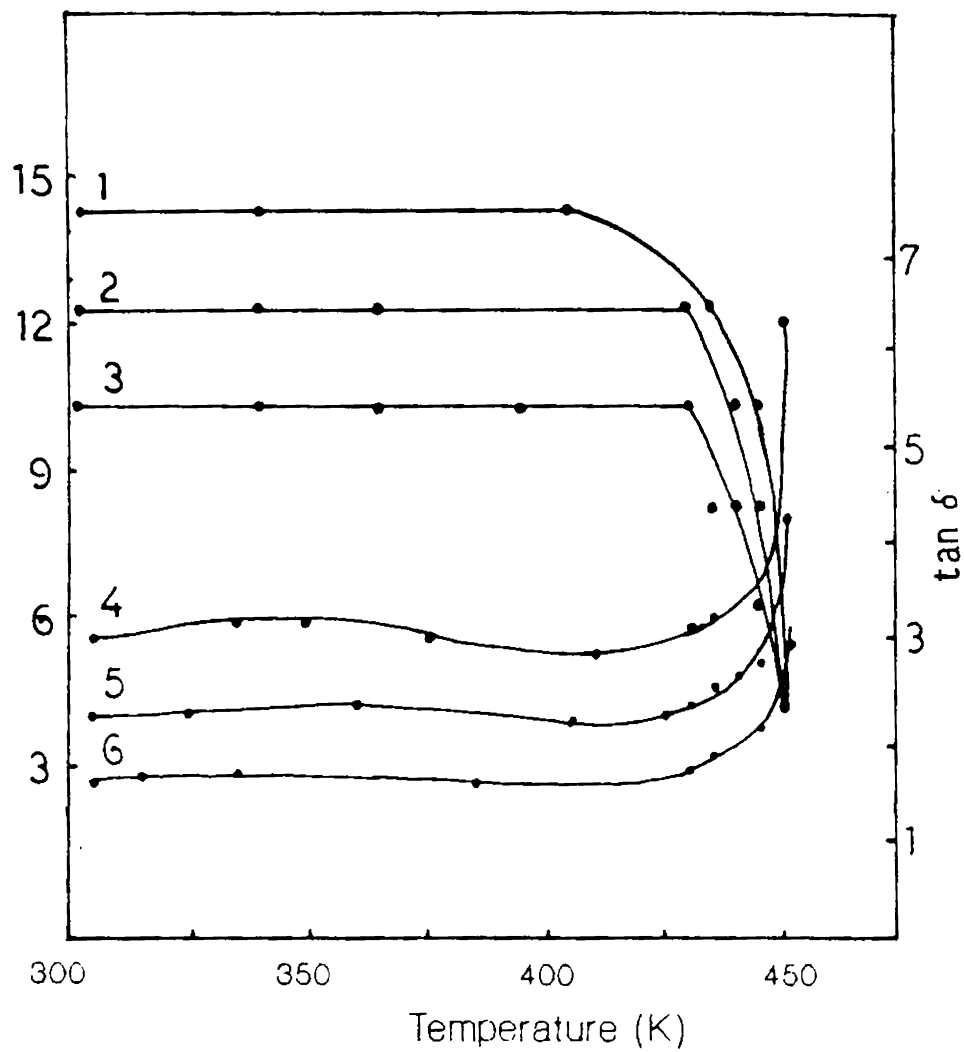
**Dielectric constant vs
Frequency**

Fig.6.34

**Dielectric constant & Loss factor vs
Temperature for CdS thin films**

Dielectric constant (ϵ)1, 2 & 3 - ϵ 4, 5 & 6 - $\tan \delta$

6.40 Conclusion

From the foregoing investigations it becomes clear that CdS films prepared by the chemical bath deposition technique are uniform, adhere tightly to the substrate and resist abrasion. They are reproducible in thickness and electrical properties. The important parameters of preparation are the temperature, concentration of the solution, speed of rotation of the slides and the time of reaction. From the d.c. and a.c. conductivity studies of CdS thin films thus prepared, it was found that there exist two dominant trap levels near the midgap--most probably on either side of the Fermi level--with a very low density of states at the Fermi level proper. From the dielectric studies ϵ was found to be independent of temperature upto 423K. From the frequency dependence of ϵ , the existence of monovalent impurities, vacancies and microvoids in the film are suggested.

REFERENCES

1. F.A.Shirland and E.F.Kelly, Adv.Energy Convers., **6** (1966) 201.
2. K.L.Chopra and S.R.Das, "Thin Film Solar Cells", Plenum Press, New York (1983), 295.
3. J.Daklerk and E.F.Kelly, Rev.Sci.Instrum., **36** (1965) 506.
4. L.M.Frass, W.P.Bleha, J.Grinberg and A.D.Jacobson, J.Appl. Phys., **47** (1976) 584.
5. N.Romeo, G.Sberveglieri and L.Terricone, Thin Solid Films, **55** (1978) 413.
6. N.G.Dhere and N.R.Parikh, Thin Solid Films, **60** (1979) 257.
7. L.C.Burton, T.L.Hemah and J.D.Meakin, J.Appl.Phys., **50** (1979) 6014.
8. A.Amith, J.Vac.Sci.Technol., **15** (1978) 353.
9. K.Mitchell, A.L.Fahrenbruch and R.H.Bube, J.Vac.Sci.Technol., **12** (1975) 909.
10. G.H.Hewig and W.H.Bloss, Thin Solid Films, **45** (1977) 1.
11. V.G.Bhide, S.Tatar and A.C.Rastogi, Pramana, **9** (1977) 399.

12. E.Khwaja and S.G.Tomlin, *J.Phys.D: Appl.Phys.*, **8** (1975) 581.
13. L.M.Frass, W.P.Bleha and P.Braatz, *J.Appl.Phys.*, **46** (1975) 491.
14. C.Wu and R.H.Babe, *J.Appl.Phys.*, **45** (1974) 648.
15. S.Durand, *Thin Solid Films*, **44** (1977) 43.
16. A.Piel and H.Murray, *Thin Solid Films*, **44** (1977) 65.
17. H.L.Kwok and W.C.Siu, *Thin Solid Films*, **61** (1979) 249.
18. R.S.Berg, R.D.Nasby and C.Lampkin, *J.Vac.Sci.Technol.*, **15** (1979) 359.
19. B.K.Gupta and O.P.Agnihotri, *Phil.Mag.*, **37** (1978) 631.
20. D.C.Cameron, W.Duncan and W.M.Tsang, *Thin Solid Films*, **58** (1979) 61.
21. K.Ito and T.Ohsawa, *Jpn.J.Appl.Phys.*, **16** (1977) 11.
22. N.Croitoru and S.Jacobson, *Thin Solid Films*, **56** (1979) 25.
23. Z.Parada and E.Sahabowska, *Thin Solid Films*, **66** (1980) 255.
24. N.R.Pavaskar, C.A.Manezes and A.P.B. Sinha, *J.Electrochem. Soc.*, **124** (1977) 743.
25. J.Vedel, M.Soubeyrand and E.Kastel, *J.Electrochem.Soc.*, **124** (1977) 177.

26. J.I.B.Wilson and J.Woods, *J.Phys.Chem.Solids*, **34** (1973) 171.
27. A.Lopez-Otero, *Thin Solid Films*, **49** (1978) 3.
28. M.E.Behrndt and S.C.Morenom, *J.Vac.Sci.Technol.*, **8** (1971) 494.
29. J.N.Zemel, *J.Lumin.*, **7** (1973) 524.
30. M.Foex, *Bull.Soc.Chim.*, **11** (1944) 6.
31. R.R.Chamberlin, WPAFB Contract No.AF-331657-7919 (1962).
32. J.E.Hill and R.R.Chamberlin, U.S.Patent 3 148084 (1964).
33. R.R.Chamberlin and J.S.Skarman, *J.Electrochem.Soc.*, **113** (1966) 86.
34. J.L.Vossen and W.Kern (Eds.), *Thin Film Process*, Academic Press, New York (1978).
35. F.Dutault and J.Lahaye, *Proc. 2nd EC Photovoltaic Solar Energy Conference, Berlin*, R.Van Overstracten and W.Palz (Eds.), Reidel, Holland (1979) 898.
36. E.Shanthi, A.Banerjee, V.Dutta and K.L.Chopra, *Thin Solid Films*, **71** (1980) 237.
37. D.E.Bode, *Proc.Natl.Elec.Conf.*, **19** (1963) 630.

38. D.E.Bode, T.H.Johnson and B.N.Maclian, *J.Appl.Optics*, **4** (1965) 327.
39. D.E.Bode, *Physics of Thin Films, Vol.3*, G.Hass and R.E.Thun (Eds.), Academic Press, New York (1966), 275.
40. R.J.Cashman, *J.Opt.Soc.Am.*, **36** (1946) 356.
41. K.L.Chopra and S.R.Das, *Thin Film Solar Cells*, Plenum Press, New York (1983).
42. G.Berote, D.Cossemant, E.Orben de Xevry, and J.M.Streydio, *Conf.Record of the 16th IEEE Photovoltaic Specialists Conference*, San Diego, CA, USA (1982) 872.
43. V.A.Shalpak, *Sov.Phys.-Semicond.(USA)*, **16** (1982) 785.
44. E.Vateva and D.Nesheva, *J.Non-Cryst.Solids*, **51** (1982) 381.
45. S.R.Elliott, *Phil.Mag.B*, **36** (1977) 1291.
46. S.R.Elliott, *Phil.Mag.B*, **37** (1978) 553.
47. J.D.Joannopoulos and G.Lucovsky (Eds.), *Topics in Applied Physics*, Springer-Verlag, **55** (1984) 82.

Chapter 7

CONCLUSIONS AND SUGGESTIONS FOR FUTURE RESEARCH

In this thesis it is established that vacuum evaporation of high purity silicon granules using tungsten baskets followed by hydrogen plasma annealing is a reliable and economical method for the production of hydrogenated amorphous silicon thin films. In the second chapter the experimental set-up for the production of hydrogenated and unhydrogenated amorphous silicon films are presented in detail.

The investigations presented in this thesis are mainly centred around the electrical properties of amorphous silicon and cadmium sulphide thin films. In chapter 3 a detailed analysis of the results of the investigations on d.c. and a.c. electrical conduction on a-Si and a-Si:H is presented. It has been proved that a-Si:H films prepared by the present method are very similar to the glow discharge produced films as far as the electrical properties are concerned. It is observed that generally d.c. electrical activation energies of a-Si films are very high compared to that of a-Si:H films. Intrinsic films with an activation energy $E_a = 0.75$ eV are obtained for hydrogen annealing temperature of 573K at a hydrogen partial pressure of 0.05 torr. The a.c. conductivity of a-Si:H films is measured as a function

of frequency, temperature and film thickness. It is found that $\sigma_{a.c}$ is proportional to ω^n where n varies from 0.7 to 1.5.

The investigations on the adsorbate induced d.c. conductivity changes in the a-Si and a-Si:H thin films have established the effect of donor type and acceptor type gases. The investigations have shown that by simply exposing a silicon film to hydrogen does not change its conductivity much. Similarly, the effects of N_2 , O_2 and H_2S are also negligible. An exposure of the films to CO_2 causes the conductivity to decrease by 60% of its original value. However, exposures to NH_3 gas and H_2O vapour cause the conductivities to increase dramatically, especially in the latter case in which σ increases to about 3000 times. The change is more pronounced in the first few hours and then σ remains almost a constant. This study establishes unambiguously how the presence of a very small amount of certain gases can change the electrical properties of a-Si and a-Si:H thin films. This also explains the diverse results obtained by various research groups in different laboratories and sometimes at the same laboratory at different preparation runs. Important differences are observed in the general shapes of the curves between the a-Si and a-Si:H films studied here.

Dielectric properties of the a-Si and a-Si:H films are measured as a function of frequency, temperature and film thickness. In the case of a-Si the dielectric constant (ϵ) increases with frequency. ϵ is also found to be independent of temperature in the measurement range studied. This rules out the presence of interfacial polarization. The most possible mechanism is suggested as due to the polarization resulting from imperfections, defects and microvoids in the films. Dangling bonds in the material are the most important defects in amorphous silicon films and they play an important role in the dielectric properties of these films. In a-Si:H films interfacial polarization is dominant. This is due to the passivation of dangling bonds by hydrogen which reduces their contribution to the polarization mechanism. The thickness dependence of ϵ is explained as the direct manifestation of the porosity of the films. The increase in the loss factor with frequency in the manner observed in these experiments indicates the role of electrode and lead resistance in the measurements. In brief it can be said that the dielectric properties of a-Si and a-Si:H are very much dependent upon the frequency, temperature and film thickness.

In chapter 5, the details of the successful fabrication and characterization of a-Si and a-Si:H field effect transistors are presented. It was possible to draw an

appreciable drain current by using an interdigitated finger structure for the source and drain electrodes. Instead of the usual SiO_2 films, vacuum evaporated europium oxide films are used as the gate insulator. This made the fabrication much easier. The maximum amplification ratio of 194 is observed for a gate insulator thickness of 715 \AA . It is also found that since the semiconductor is almost intrinsic in nature, both electrons and holes contribute to the conduction through the channel. The main limitation of the device is the low value of the gain-bandwidth product. This can be improved by a careful modification of the preparation conditions.

Finally in chapter 6, a detailed account of the preparation of CdS thin film by chemical bath technique and its characterization are presented. By this method it was possible to prepare nearly intrinsic CdS films. A.C.conduction through the films was measured and was analysed using Elliott's theory for a.c. conduction in chalcogenide glasses. The density of states at the Fermi level was calculated from this data and was found to be nearly seven orders less than the reported values. This is explained as due to the fact that most of the reported values represent n-type materials with very high sulphur deficiency. The films prepared by the present method are almost intrinsic

in nature. Also the difference may not be as high as it appears since most of the reported values are found out by the field effect method and it is a common fact that this method has a tendency to over estimate the density of states. From the dielectric studies ϵ is found to be independent of temperature upto 423K. From the frequency dependence of ϵ , the existence of monovalent impurities, vacancies and microvoids in the films is suggested.

SUGGESTIONS FOR FUTURE WORK

A careful examination of the various reviews on the properties of a-Si:H would reveal that it exhibits a variety of electrical properties making it one of the most important materials for device applications. Eventhough the material has been subjected to thorough investigations regarding its structural and electrical properties, so many questions still remain unanswered. Further studies on the precise relationships between defects, hydrogen content and dopants are required for a better understanding and control of the compositional and structural homogeneity of a-Si:H films. Conflicting evidences have been presented over the existence of steep gradients in hydrogen concentration. Also there are questions relating to the interfaces between a-Si:H and both metals and insulators. Of course

the most important application for which a-Si:H films are used is the production of low cost solar cells. In this field also there are still problems to be resolved, like the Staebler-Wronski instability, dependence of solar cell fill factor on film thickness etc. Similarly in the case of a-Si:H field effect transistors, the low value of the gain-bandwidth product is still a problem to be tackled.

The limitation to the efficiency of a-Si:H devices is mainly due to the high localized state density. A further decrease in the density of localized states will have to be obtained by improved deposition techniques and heat treatments. A significant increase in the mobility of the charge carriers has also to be achieved. If these targets can be attained, a-Si:H films can be used to produce thin film FETs, diodes and charge coupled devices successfully and economically.